

# The Investigation of Heavy Metal Adsorption on Modified Activated Carbon Materials

A Thesis submitted to the Committee on Graduate Studies  
in Partial Fulfillment of the Requirements for the Degree of Doctorate in Philosophy  
in the Faculty of Arts and Science

Trent University

Peterborough, Ontario, Canada

© Copyright by Kyle S. Fisher, 2024

Materials Science, PhD. Graduate Program

May 2024

# Abstract

The Investigation of Heavy Metal Adsorption on Modified Activated Carbon Materials

Kyle S. Fisher

This thesis describes the preparation, optimization, functionalization, and characterization of activated carbon materials sourced from a petroleum coke feedstock for the tailored removal of heavy metal species in contaminated waters. The goal of this work is to develop an understanding of the mechanisms that drive adsorption of heavy metals onto activated carbon surfaces. By determining the mechanisms that drive adsorption, activated carbon materials can be modified to increase the efficiency of the adsorption process. The novelty of this work comes from the use, modification, and functionalization of activated carbon derived from petroleum coke, a waste by-product of the oil-sands extraction process, a source not prevalent in current literature. The novelty also comes from the determination of the methods by which heavy metals are adsorbed onto the given adsorbate as literature does not focus on the mechanisms themselves. The work presented sheds light on the specific adsorption mechanisms, with the aim of elucidating how a given material's surface can be enhanced to target a specific analyte. This work focused on the use of microwave plasma atomic emission spectroscopy (MP-AES), x-ray photoelectron spectroscopy (XPS), and Brunauer-Emmett-Teller theory (BET) to obtain the necessary data required for the determination of adsorption mechanisms, adsorption capacities, and surface characterization of the materials. MP-AES is used for the determination of the adsorption capacity of the materials produced. Surface characterization of the materials was done using XPS, and surface area and pore

size distributions were determined using BET for surface area determination and nitrogen adsorption measurements following density functional theory for pore size distribution determination.

XPS of the activated carbon post-chromium and post-arsenic adsorption show a reduction of the metals from chromium (VI) to chromium (III) and from arsenic (V) to arsenic (III). By increasing the amount of hydroxyl functional groups on the AC surface through a simple thermal-treatment, the chromium adsorption was increased from 17.0 mg/g to 22.4 mg/g. By loading a reducing agent onto the activated carbon surface, an increased number of potential binding sites for the arsenic are loaded onto the AC surface and the adsorption of arsenic increased from 8.1% to 51%.

**Keywords:**

Activated Carbon, Petroleum Coke, Functionalization, Adsorption, Adsorption  
Mechanisms, Kinetics, Surface Characterization, Chromium, Arsenic.

# Acknowledgements

*To Dr. Andrew Vreugdenhil:*

I would like to thank you for your guidance and support over the years. Thank you for being a great supervisor, for never accepting mediocrity, and always pushing me to be better.

*To Dr. Aaron Slepko and Dr. Franco Gaspari:*

Thank you for being a part of my committee and sharing your suggestions and ideas with me throughout this process. I greatly appreciate the invaluable feedback you have provided.

*To Dr. Sathish Ponnurangam:*

I would like to thank you for taking the time out of your schedule to share your thoughts on the work I have done. I appreciate you joining the examining committee and taking an interest in the work that I have done.

*To the IMRL:*

Thank you for all of the advice and support that you have provided both in and out of the lab. The hours spent presenting work and asking questions, discussing theories, and sharing knowledge learned together was amazing and I couldn't have asked for a better group.

*To my family:*

You are the ones who taught me to strive for excellence and to set high goals and standards for myself. I can always count on you to be there when I need you and couldn't ask for a better support system. Thank you for making me who I am, encouraging me to push harder, and being the best support system there is.

*To my wife, Laurie:*

Putting into words how much you have supported me throughout this journey is not possible. Thank you for putting up with all the late nights, long hours, and unintelligible scientific rants I have put you through. You have stood by my side through every step and have always believed in me. You are my best friend and without your love and support, this achievement wouldn't have been possible. It doesn't matter where life takes us next, as long as I have you by my side.

# Table of Contents

<b>Keywords:</b> .....	<b>iv</b>
<b>Acknowledgements</b> .....	<b>v</b>
<b>Table of Contents</b> .....	<b>vi</b>
<b>List of Figures</b> .....	<b>x</b>
<b>List of Tables</b> .....	<b>xiii</b>
<b>List of Equations</b> .....	<b>xiv</b>
<b>List of Abbreviations</b> .....	<b>xv</b>
<b>List of Abbreviated Sample Names</b> .....	<b>xv</b>
<b>1. Chapter 1: Introduction to the Research</b> .....	<b>1</b>
1.1. <i>Background Information</i> .....	2
1.1.1. Oil Sands and Bitumen Extraction .....	3
1.1.2. Hard Rock Mining.....	5
1.2. <i>Current Literature</i> .....	6
1.3. <i>Activated Carbon as an Adsorbent</i> .....	8
1.4. <i>Objectives of this Study</i> .....	11
<b>2. Chapter 2: Experimental Procedures and Methods</b> .....	<b>12</b>
2.1. <i>Materials</i> .....	12
2.1.1. Chromium Study Materials .....	12
2.1.2. Arsenic Study Materials .....	13
2.1.3. Co-Adsorption Study Materials.....	13
2.2. <i>Activation and Functionalization Procedures</i> .....	13
2.2.1. Standard Activation Procedure.....	13
2.2.2. Ammonium Chloride-Water Refluxed AC .....	14
2.2.3. Ammonium Chloride-Dichloromethane Refluxed AC.....	15
2.2.4. Ammonium Chloride – Dry Mixture AC .....	15
2.2.5. Ammonium Chloride – Adsorbed AC.....	15
2.2.6. Thermally Treated Activated Carbon.....	16
2.2.7. Iron Loading of AC Surface .....	16
2.2.8. Manganese Loading of AC Surface .....	17
2.2.9. Iron-Manganese Loading of AC Surface .....	17
2.3. <i>Chromium (VI) Study</i> .....	17
2.3.1. Long-Term Adsorption Testing.....	18
2.3.2. Chromium (VI) Kinetics .....	18
2.4. <i>Arsenic (V) Study</i> .....	18
2.4.1. Efficacy Comparison.....	19
2.4.2. Arsenic (V) Kinetics.....	19
2.5. <i>Arsenic (III) Study</i> .....	19
2.5.1. Arsenic (III) Kinetics .....	20
2.6. <i>Co-Adsorption Study</i> .....	20

2.6.1.	Arsenic (V) Enhancement and/or Competition Investigation – Arsenic:Chromium Binary Mixtures .....	21
2.6.2.	Arsenic (V) Enhancement and/or Competition Investigation – Stepwise Adsorption .....	21
2.6.3.	Isotherm Modelling .....	22
2.6.4.	Kinetic Data .....	22
2.7.	<i>Microwave Plasma Atomic Emission Spectroscopy</i> .....	23
2.7.1.	MP-AES Analysis Operating Conditions for Chromium Study .....	23
2.7.2.	MP-AES Analysis Operating Conditions for Arsenic Study .....	24
2.7.3.	MP-AES Analysis Operating Conditions for Co-Adsorption Study .....	24
2.8.	<i>Surface Characterization</i> .....	25
2.8.1.	Nitrogen Adsorption Measurements .....	25
2.8.2.	X-ray Photoelectron Spectroscopy .....	26
<b>3.</b>	<b>Chapter 3: Chromium Study Published as: Adsorption of Chromium (VI) Using an Activated Carbon Derived from Petroleum Coke Feedstock .....</b>	<b>27</b>
	<i>Abstract</i> .....	28
	<i>Keywords:</i> .....	30
3.1.	<i>Introduction:</i> .....	31
3.2.	<i>Experimental Procedures and Methods</i> .....	34
3.3.	<i>Results and Discussion</i> .....	34
3.3.1.	Characterization of AC.....	34
3.3.2.	Chromium (VI) Kinetics .....	39
3.3.3.	Kinetic Modelling .....	43
3.3.4.	Proposed Adsorption Mechanism .....	48
3.4.	<i>Chromium Conclusions</i> .....	55
<b>4.</b>	<b>Chapter 4: Arsenic Study Published as: Metal Impregnated Petroleum Coke Derived Activated Carbon for the Adsorption of Arsenic in Acidic Waters .....</b>	<b>57</b>
	<i>Abstract</i> .....	58
	<i>Keywords:</i> .....	60
	<i>Synopsis:</i> .....	60
4.1.	<i>Introduction</i> .....	61
4.2.	<i>Experimental Procedure and Methods</i> .....	64
4.3.	<i>Results and Discussion</i> .....	64
4.3.1.	Nitrogen Adsorption Measurements .....	65
4.3.2.	As (V) Efficacy Comparison: Milligram per Gram Adsorption Comparison .....	68
4.3.3.	As (V) Efficacy Comparison: Normalized Surface Area Substrates .....	69
4.3.4.	As (V) Efficacy Comparison: Normalized Microporosity Substrates .....	71
4.3.5.	XPS Characterization of Metal Modified Activated Carbons Pre- and Post-Arsenic (V) Adsorption.....	73
4.3.6.	Energy-Dispersive X-Ray Spectroscopy (EDS).....	76
4.3.7.	Scanning Electron Microscope (SEM) Images .....	79
4.3.8.	Proposed Mechanisms: Iron-Based Arsenic Adsorption .....	81
4.3.9.	Proposed Mechanisms: Manganese-Based Arsenic Adsorption .....	83
4.3.10.	Arsenic Kinetics: As (V) Kinetics Curves.....	85
4.3.11.	Arsenic Kinetics: Arsenic (V) Kinetic Modelling .....	87

4.3.12.	Arsenic Kinetics: As (III) Kinetics Curves .....	91
4.3.13.	Arsenic Kinetics: As (III) Kinetic Modelling.....	92
4.3.14.	Literature Comparison.....	94
4.4.	<i>Conclusion</i> .....	96
<b>5.</b>	<b>Chapter 5: Binary Mixture As:Cr Study Published as: The Investigation of the Co-Adsorptive Relationship between Arsenic (V) and Chromium (VI) Using a Petroleum Coke Sourced Activated Carbon.....</b>	<b>97</b>
	<i>Abstract</i> .....	98
	<i>Keywords</i> .....	100
5.1.	<i>Introduction</i> .....	101
5.2.	<i>Experimental Procedure and Methods</i> .....	104
5.3.	<i>Results and Discussion</i> .....	105
5.3.1.	Nitrogen Adsorption Measurements .....	105
5.3.2.	Arsenic (V) Adsorption Enhancement and/or Competition Evaluation: Binary Mixture at pH 3.....	106
5.3.3.	Arsenic (V) Adsorption Enhancement and/or Competition Evaluation: Binary Mixture at pH 8.....	107
5.3.4.	Arsenic (V) Adsorption Enhancement and/or Competition Evaluation: Stepwise Adsorption at pH 3 .....	111
5.3.5.	Arsenic (V) Adsorption Enhancement and/or Competition Evaluation: Binary Mixture at pH 8.....	112
5.3.6.	Chromium (VI) Adsorption Enhancement and/or Competition Evaluation .....	114
5.3.7.	pH 3 Isotherm Data and Modelling.....	115
5.3.8.	pH 8 Isotherm Data and Modelling.....	118
5.3.9.	XPS Characterization: Standard AC Prior to Adsorption of Heavy Metals .....	122
5.3.10.	XPS Characterization: Post-Adsorption of Arsenic-Only Samples.....	123
5.3.11.	XPS Characterization: Post-Adsorption of Chromium-Only Samples.....	124
5.3.12.	XPS Characterization: Post-Adsorption of As:Cr Mixed Metal Samples .....	126
5.3.13.	Proposed Adsorption Mechanisms: Individual Adsorption Mechanisms.....	128
5.3.14.	Proposed Adsorption Mechanisms: Chromium and Arsenic Co-Adsorption.....	128
5.4.	<i>Conclusion</i> .....	133
	<b>Chapter 6 – Conclusions and Future Works .....</b>	<b>134</b>
6.1.	<i>Conclusions</i> .....	134
6.2.	<i>Future Studies</i> .....	136
	<b>Reference List .....</b>	<b>138</b>
	<b>Appendix A: Fe2p, Mn2p, and As2p Peak Deconvolution .....</b>	<b>148</b>
	<b>Appendix B: Elemental Distribution Mapping .....</b>	<b>150</b>
	<b>Appendix C: O1s Peak Deconvolution .....</b>	<b>153</b>
	<b>Appendix D: Kinetic Modelling for the Adsorption of As (V) .....</b>	<b>155</b>
	<b>Appendix E: Kinetic Modelling for the Adsorption of As (III) .....</b>	<b>157</b>
	<b>Appendix F: Freundlich Isotherm Modelling for pH 3 Chromium Adsorption .....</b>	<b>159</b>

**Appendix G: Langmuir Isotherm Modelling for pH 8 Chromium Adsorption.....160**

# List of Figures

<b>Figure 1:</b> (A) O1s XPS peak splitting of Commercial AC. (B) O1s XPS peak splitting of Standard AC. (C) O1s XPS peak splitting of Thermally-Treated AC. (D) O1s XPS peak splitting of $\text{NH}_4^+$ -Adsorbed AC. (E) O1s XPS peak splitting of $\text{NH}_4^+$ -Dry AC [67,68,69].	38
<b>Figure 2:</b> Kinetics curve of the produced activated carbons compared to the commercial AC. Results show 92% adsorption of total chromium (approximately 22 mg/g) in all activated carbons after two weeks with the exception of the standard AC which shows 64% total chromium adsorption (VI) (approximately 17 mg/g). Maximum possible adsorption (i.e., 100%) is $25 \pm 1$ mg/g.	40
<b>Figure 3:</b> Adsorption capacity of chromium (VI) activated carbons normalized to 1000 $\text{m}^2$ surface area.	42
<b>Figure 4:</b> Adsorption capacity of chromium (VI) for activated carbons normalized to 1 $\text{cm}^3$ pore volume and adjusted for microporosity percentage.	42
<b>Figure 5:</b> All kinetic modelling of ACs used for Cr (VI) adsorption. (A) Pseudo-first order kinetic modelling of Commercial AC. (B) Pseudo-second-order kinetic modelling of Commercial AC. (C) Pseudo-first order kinetic modelling of Standard AC. (D) Pseudo-second-order kinetic modelling of Standard AC. (E) Pseudo-first order kinetic modelling of $\text{NH}_4^+$ -Adsorbed AC. (F) Pseudo-second-order kinetic modelling of $\text{NH}_4^+$ -Adsorbed AC. (G) Pseudo-first order kinetic modelling of Thermally-Treated AC. (H) Pseudo-second-order kinetic modelling of Thermally-Treated AC.	47
<b>Figure 6:</b> Deconvolution of the Cr2p peak observed on the surface of the standard AC post-chromium adsorption.	49
<b>Figure 7:</b> Deconvolution of the Cr2p peak observed on the surface of the Thermally-Treated AC, post-chromium adsorption.	49
<b>Figure 8:</b> (A) O1s deconvolution of standard AC pre-exposure to chromium (VI). (B) O1s deconvolution of standard AC post-exposure to chromium (VI). (C) O1s deconvolution of thermally-treated AC pre-exposure to chromium (VI). (D) O1s deconvolution of thermally treated AC post-exposure to chromium (VI).	52
<b>Figure 9:</b> The adsorption schematic demonstrating the reduction of chromium (VI) in solution to chromium (III) hydroxide and the oxidation of alcohols to ketones on the activated carbon surface.	53
<b>Figure 10:</b> The Jones Oxidation reaction mechanism sourced from Organic Chemistry 2 <sup>nd</sup> Edition by Clayden et al.. Mechanism found on page 544.	54
<b>Figure 11:</b> Nitrogen adsorption isotherm and hysteresis plots of the Standard, Commercial, Fe-Loaded, Mn-Loaded, and FeMn-Loaded Activated Carbons.	67
<b>Figure 12:</b> Comparison of various activated carbons investigating the adsorption efficiency of arsenic (V) after a 6 hour exposure time.	69
<b>Figure 13:</b> Deconvolution of the Fe (top Left), Mn (Top Right), and As (Bottom) XPS peaks in the FeMn-Loaded AC, post-As exposure.	74
<b>Figure 14:</b> Elemental distribution mapping of carbon (Middle Left), oxygen (Middle Right), manganese (Bottom Left), and iron (Bottom Right) present within the FeMn-Loaded Activated Carbon. A layered distribution map of the surface's elemental composition is shown in the top figure.	77
<b>Figure 15:</b> SEM imaging (Magnification x15000) of the Standard Activated Carbon to show the smallest pore size visible with the SEM images obtained.	80
<b>Figure 16:</b> SEM imaging (Magnification x5000) of the Standard (top left), Fe-Loaded (top right), Mn-loaded (bottom left), and FeMn-loaded Activated Carbons used in this study.	81

<b>Figure 17:</b> <b>A)</b> Shows the iron physisorbed to the surface of the activated carbon. <b>B)</b> Shows the two iron products, FeOOH, and the Intermediate FeO-O-AsH <sub>2</sub> O <sub>3</sub> , formed as a result of the exposure to arsenic. <b>C)</b> Shows the reduced As (III), as a result of the electron flow from the activated carbon through the iron, physisorbed to the iron-loaded surface through Hydrogen Bonding. ....	83
<b>Figure 18:</b> <b>A)</b> Shows the redox reaction between As (V) and Mn (II) where As (V) is reduced to As (III) and Mn (II) is oxidized to Mn (III). <b>B)</b> Shows the redox reaction between As (V) and Mn (II) where As (V) is reduced to As (III) and Mn (II) is oxidized to Mn (IV). ....	84
<b>Figure 19:</b> <b>A)</b> Shows the product of reaction (1) where MnO is oxidized to MnOOH. <b>B)</b> Shows the product of reaction (2) where MnO is oxidized to MnO <sub>2</sub> . As (III) is physisorbed to the Mn-Loaded AC surface through Hydrogen Bonding. ....	85
<b>Figure 20:</b> Kinetics curves of As (V) adsorption for the various activated carbons investigated. Arsenic adsorption is given in percent adsorption with a maximum adsorption (i.e. 100%) of 25 mg/g. ....	87
<b>Figure 21:</b> Pseudo First- (Left) and Pseudo Second- (Right) Order kinetic modelling of the As (V) adsorption using the FeMn-Loaded AC. ....	91
<b>Figure 22:</b> Kinetics curves of the As (III) adsorption using the FeMn-Loaded, Standard, and Commercial Activated Carbons. ....	92
<b>Figure 23:</b> Typical nitrogen adsorption isotherm and hysteresis plots of the activated carbon used in this study. ....	106
<b>Figure 24:</b> Arsenic adsorption enhancement effect as observed by changing the initial concentration of chromium in solution at pH 3 with 50 ppm arsenic. ....	107
<b>Figure 25:</b> Arsenic adsorption enhancement effect as observed by changing the initial concentration of chromium in solution at pH 8 with 50 ppm arsenic. ....	108
<b>Figure 26:</b> This shows the enhancement of arsenic adsorption as a function of the changing chromium concentration in the system. The x-axis is presented as the amount of leftover chromium in solution (C <sub>e</sub> ) rather than the initial starting concentration of chromium in the solution. ....	109
<b>Figure 27:</b> This graph shows the arsenic adsorption enhancement phenomenon at the various starting concentrations of chromium over multiple stir times. The maximum arsenic adsorption occurs at lower starting concentrations of chromium as the stir times decrease. ....	110
<b>Figure 28:</b> Arsenic adsorption comparison for the arsenic only adsorption, the step-wise adsorption, and the binary mixture at pH 3. ....	112
<b>Figure 29:</b> Arsenic adsorption comparison for the arsenic only, the step-wise adsorption, and the binary mixture adsorption at pH 8. Note that the concentration of chromium is presented in parts per million as it is the concentration of chromium in solution while the arsenic adsorption is presented in mg/g as this is expressing the mg of arsenic adsorbed per gram of activated carbon added to the solution. ....	113
<b>Figure 30:</b> Isotherm data of chromium adsorption in the individual and mixed solutions at pH 3. ....	116
<b>Figure 31:</b> Langmuir isotherm modelling for the adsorption of chromium at pH 3. ....	118
<b>Figure 32:</b> Isotherm data of chromium adsorption in the individual and mixed solutions at pH 8. ....	119
<b>Figure 33:</b> Freundlich isotherm modelling for the adsorption of chromium at pH 8. ....	121
<b>Figure 34:</b> XPS deconvolution of the O1s peak for the Standard AC before adsorption of chromium or arsenic [67]. ....	123
<b>Figure 35:</b> XPS deconvolution of the O1s peak for the activated carbon after arsenic-only adsorption [67]. ....	124
<b>Figure 36:</b> XPS deconvolution of the O1s peak for the activated carbon after chromium-only adsorption [67]. ....	125

<b>Figure 37:</b> As <sub>2p</sub> peak deconvolution (left) and Cr <sub>2p</sub> peak deconvolution (right) for the AC exposed to the 50 ppm:200 ppm As:Cr solution [71,72,92,93].	127
<b>Figure 38:</b> Possible formation and structure of a chromium complex containing an arsenic ligand in the mixed metal solution.	129
<b>Figure A1:</b> XPS deconvolution of the Fe <sub>2p</sub> (left) and Mn <sub>2p</sub> (right) peaks in the FeMn-Loaded AC pre-arsenic exposure.	148
<b>Figure A2:</b> XPS deconvolution of the Fe <sub>2p</sub> (left) and As <sub>2p</sub> (right) peaks in the Fe-Loaded AC post-arsenic exposure.	149
<b>Figure A3:</b> XPS deconvolution of the Mn <sub>2p</sub> (left) and As <sub>2p</sub> (right) peaks in the Mn-Loaded AC post-arsenic exposure.	149
<b>Figure B1:</b> Elemental distribution mapping of the carbon (bottom left), and oxygen (bottom right) present within the Standard AC at 500x magnification. A layered distribution map of the surface's elemental composition is shown at the top.	150
<b>Figure B2:</b> Elemental distribution mapping of carbon (middle left), oxygen (middle right), and iron (bottom) present within the Fe-Loaded activated carbon at 500x magnification. A layered distribution map of the surface's elemental composition is shown at the top.	151
<b>Figure B3:</b> Elemental distribution mapping of carbon (middle left), oxygen (middle right), and manganese (bottom) present within the Mn-loaded activated carbon at 500x magnification. A layered distribution map of the surface's elemental composition is shown at the top.	152
<b>Figure C1:</b> XPS deconvolution of the O <sub>1s</sub> peak for the Fe-Loaded AC.	153
<b>Figure C2:</b> XPS deconvolution of the O <sub>1s</sub> peak for the Mn-Loaded AC.	154
<b>Figure C3:</b> XPS deconvolution of the O <sub>1s</sub> peak for the FeMn-Loaded AC.	154
<b>Figure D1:</b> Pseudo First- (left) and Pseudo Second- (right) Order kinetic models for the adsorption of As (V) using the Standard AC.	155
<b>Figure D2:</b> Pseudo First- (left) and Pseudo Second- (right) Order kinetic models for the adsorption of As (V) using the Commercial AC.	155
<b>Figure D3:</b> Pseudo First- (left) and Pseudo Second- (right) Order kinetic models for the adsorption of As (V) using the Fe-Loaded AC.	156
<b>Figure D4:</b> Pseudo First- (left) and Pseudo Second- (right) Order kinetic models for the adsorption of As (V) using the Mn-Loaded AC.	156
<b>Figure E1:</b> Pseudo First- (left) and Pseudo Second- (right) Order kinetic models for the adsorption of As (III) using the Standard AC.	157
<b>Figure E2:</b> Pseudo First- (left) and Pseudo Second- (right) Order kinetic models for the adsorption of As (III) using the Commercial AC.	157
<b>Figure E3:</b> Pseudo First- (left) and Pseudo Second- (right) Order kinetic models for the adsorption of As (III) using the FeMn-Loaded AC.	158
<b>Figure F1:</b> Freundlich isotherm modelling of the chromium adsorption for the pH 3 isotherm data.	159
<b>Figure G1:</b> Langmuir isotherm modelling of the chromium adsorption for the pH 8 isotherm data.	160

# List of Tables

<b>Table 1:</b> MP-AES operating conditions for the analysis of chromium (VI). .....	24
<b>Table 2:</b> Detection wavelengths for arsenic (V) and chromium (VI) used in the high and low concentration calibration curve ranges. ....	25
<b>Table 3:</b> XPS atom percent surface composition of activated carbon. ....	35
<b>Table 4:</b> Oxygen atom percent speciation from deconvolution of the XPS O1s peak for the various activated carbons investigated [67,68,69].....	36
<b>Table 5:</b> The number of days required for various activated carbons to effectively remove chromium (VI) from solution while comparing their surface area and pore size distributions. ....	39
<b>Table 6:</b> Summary of the activated carbon adsorption capacities after 2 weeks normalized to grams (mg/g), surface area (mg/1000 m <sup>2</sup> ), and microporosity (mg/cm <sup>3</sup> micropores). ....	43
<b>Table 7:</b> A summary of the pseudo-first and pseudo-second-order kinetic modelling for each of the activated carbons that underwent kinetics experiments. ....	44
<b>Table 8:</b> Chromium atom percent speciation from deconvolution of the XPS Cr2p 3/2 peak post-chromium adsorption [68,69,71,72]. ....	50
<b>Table 9:</b> Oxygen atom percent speciation from deconvolution of the XPS O1s peak pre- and post-chromium adsorption for the species involved in the adsorption process [67,68,69]. ....	50
<b>Table 10:</b> Pore size distribution information obtained from nitrogen adsorption measurements. ....	66
<b>Table 11:</b> Arsenic (V) adsorption capacity comparisons normalized to surface area. ....	70
<b>Table 12:</b> Arsenic (V) adsorption capacities comparison normalized to microporosity. ....	72
<b>Table 13:</b> XPS species summary for metal-loaded activated carbons. [68,90,91,92,93,94,95]. ....	75
<b>Table 14:</b> XPS survey scan breakdown for the various activated carbon materials.....	75
<b>Table 15:</b> O1s deconvolution of the metal-loaded activated carbons [67,68].....	79
<b>Table 16:</b> A summary of the Pseudo First- and Pseudo Second-Order kinetic modelling for the activated carbons used for arsenic (V) adsorption. ....	88
<b>Table 17:</b> A summary of the Pseudo First- and Pseudo Second-Order kinetic modelling for the activated carbons used for the arsenic (III) adsorption. ....	93
<b>Table 18:</b> Comparison of petroleum coke derived activated carbons for As (V) and As (III) adsorption with other studies in the literature. ....	95
<b>Table 19:</b> XPS deconvolution summary of the relevant species in the O1s, Cr2p, and As2p peaks post-exposure to the mixed metal solution [67,71,93].....	126

# List of Equations

<b>Equation 1:</b> Pseudo-first-order kinetic modelling linear equation based on Langmuir adsorption kinetics.....	43
<b>Equation 2:</b> Pseudo-second-order kinetic modelling linear equation based on Langmuir adsorption kinetics.....	44
<b>Equation 3:</b> Non-linear isotherm modelling equation for the Langmuir isotherm model. ....	114
<b>Equation 4:</b> Non-linear isotherm modelling equation for the Freundlich isotherm model.....	115

## List of Abbreviations

AC	Activated Carbon
BET	Brunauer-Emmett-Teller
DFT	Density Functional Theory
EDS	Energy Dispersive x-ray Spectroscopy
MP-AES	Microwave Plasma Atomic Emission Spectroscopy
OSPW	Oil Sands Process-affected Water
PC	Petroleum Coke
PFO	Pseudo First-Order
PSO	Pseudo Second-Order
SEM	Scanning Electron Microscopy
Tris base	Tris(hydroxymethyl)aminomethane
WHO	World Health Organization
XPS	X-ray Photoelectron Spectroscopy

## List of Abbreviated Sample Names

NH <sub>4</sub> <sup>+</sup> -H <sub>2</sub> O-Reflux AC	Ammonium Chloride – Water Refluxed AC
NH <sub>4</sub> <sup>+</sup> -C <sub>2</sub> H <sub>2</sub> -Reflux AC	Ammonium Chloride – Dichloromethane Refluxed AC
NH <sub>4</sub> <sup>+</sup> -Dry AC	Ammonium Chloride – Dry Mixture AC
NH <sub>4</sub> <sup>+</sup> -Adsorbed AC	Ammonium Chloride – Adsorbed AC
Fe-Loaded AC	Iron Loaded Activated Carbon
Mn-Loaded AC	Manganese Loaded Activated Carbon
FeMn-Loaded AC	Iron and Manganese Loaded AC

# Chapter 1: Introduction to the Research

In five sections, this dissertation will describe the mechanisms through which heavy metals are adsorbed onto activated carbon materials and the co-adsorptive nature observed between arsenic and chromium in a binary-metal system.

The first section, chapters 1 and 2, provides an introduction to the work that will be presented and background information relevant to the studies that were performed. It also provides the methodology and the materials used in the studies that were conducted.

The second section, chapter 3, describes the main adsorption mechanism through which chromium (VI) is adsorbed onto the surface of a petroleum coke sourced activated carbon. This section also investigates the efficacy of a thermally treated activated carbon material and nitrogenated activated carbon materials to determine the optimal surface properties for chromium (VI) adsorption. The results of this study were published in the International Journal of Molecular Science's special issue "Adsorption Materials and Adsorption Behavior" as "Adsorption of Chromium (VI) Using an Activated Carbon Derived from Petroleum Coke Feedstock" [1].

The third section, chapter 4, describes the main adsorption mechanism through which arsenic (V) is adsorbed onto the surface of petroleum coke sourced activated carbon. This section also investigates the efficacy of adsorption using activated carbon surfaces functionalized with metal species. This work focused on determining how the metal species on the surface play a role in increasing the adsorption of arsenic. This work

was published in ACS Omega as “Metal Impregnated Petroleum Coke Derived Activated Carbon for the Adsorption of Arsenic in Acidic Waters” [2].

The fourth section, chapter 5, describes the co-adsorptive or competitive relationship observed between chromium (VI) and arsenic (V) in a binary system. This study investigates how arsenic adsorption is enhanced by the presence of chromium in low concentrations and how competition begins to affect this enhancement phenomenon at higher concentrations of chromium. This study also focuses on how the presence of arsenic enhances the adsorption of chromium under neutral conditions but competes with chromium for binding sites under acidic conditions. The results from this study are pending publication under the title “Investigation of the Co-Adsorptive Relationship between Arsenic (V) and Chromium (VI) Using a Petroleum Coke Sourced Activated Carbon” [3].

The final section, chapter 6, provides a conclusion to the works conducted and a summary of relevant findings from the works presented in the previous chapters.

This dissertation will present the works conducted and results obtained for the individual adsorption capacities of these metal species, as well as the co-adsorptive and/or competitive relationship that they have. Adsorption mechanisms of the analytes onto the activated carbon materials will be presented so that a thorough understanding of the interactions that occur during the adsorption processes are obtained.

## ***1.1. Background Information***

The works presented in this thesis focus on the functionalization, modification, and use of an adsorbent material derived from petroleum coke, a waste by-product of the

refining process of oil sands bitumen, as a tool for the environmental remediation of heavy metals in water supplies. Heavy metals are introduced to water supplies from sources such as household plumbing, electronic manufacturers, cement plants, and mining operations [4]. In Canada, the mining industry is a critical part of the economy, contributing \$125 billion to the national gross domestic product (GDP) in 2021, 5% of Canada's total GDP, and is responsible for 22% of Canada's total domestic exports [5]. As one of the largest industries in the Canada, the mining industry produces copious amounts of water contaminated with heavy metals that are in need of environmental remediation. One of the largest mining sectors in Canada is the extraction of oil from oil sands.

### **1.1.1. Oil Sands and Bitumen Extraction**

Oil sands are naturally occurring mixtures of sand, clay, water, and bitumen where the bitumen is extracted to produce oil products such as petroleum jelly, gasoline, and jet fuel. The Alberta Oil Sands in Canada represents the third-largest proven oil reserve in the world and contains approximately 97% of Canada's proven oil reserves with an estimated 166 billion barrels of recoverable oil reserves [6,7]. The extraction process to remove the bitumen from the tar sands and to refine the bitumen into useable oil products uses approximately 20 barrels of water for every 1 barrel of oil produced; and with a production rate of 1 million barrels of oil per day, the amount of wastewater produced is constantly growing [8]. The waste water produced from the extraction process becomes alkaline and contaminated with both organic contaminants such as naphthenic acids, and inorganic contaminants such as heavy metals, clays, and un-extracted bitumen [9,10]. These contaminated waters are then stored in tailings ponds that currently cover over 220

square kilometers in Alberta [11]. Due to the high concentration of contaminants, leeching of the tailings ponds into the nearby Athabasca River and other groundwater supplies is a growing concern.

Several studies suggest that tailings ponds water seeps into groundwater sources and contaminates groundwater and river systems [12,13,14,15]. An article by Li et al. [16] summarizes the composition and toxicity of oil sands process-affected water (OSPW) from active Suncor Energy Inc. mines in 2009. Metals present in the OSPW included Al, As, Ba, Cd, Co, Cr, Cu, Fe, Hg, Mn, Mo, Ni, Pb, Sb, Se, Sr, U, V, and Zn. The concentration of all metals present in the OSPW was above the Canadian Council of Ministers of the Environment (CCME) guidelines [16]. The works presented in this thesis focus on the adsorption of chromium (VI), arsenic (V) and arsenic (III). Chromium (VI) and arsenic were chosen for this study due to their high concentrations in the OSPW compared to the CCME guidelines (2 to 400 ppm in OSPW compared to 1 ppm listed by the CCME for chromium (VI); 1 to 33 ppm in OSPW compared to 5 ppm listed by the CCME for arsenic), as well as their risk to human health and environmental wellbeing.

Hexavalent chromium species are considered carcinogenic to humans through inhalation. Chromium (VI) exposure through inhalation can lead to lung, sinus, and throat cancer while chromium (VI) exposure through drinking water can lead to stomach and intestinal cancer. Acute health effects include respiratory irritation, nosebleeds, skin burns, and dermatitis. Chronic health effects also include kidney and liver damage, lesions, conjunctivitis, or gingivitis [17]. As a result of these major health concerns, chromium contributes towards the overall acute and/or chronic OSPW toxicity [16].

Arsenic (III) is predominant in reducing conditions while arsenic (V) is predominant in oxidizing conditions. Due to its high mobility in groundwater and sediment, arsenic (III) is considered to be the most toxic form of arsenic. Arsenic ingested through drinking water can lead to skin, bladder, lung, and kidney cancer. Acute arsenic poisoning includes vomiting, abdominal pain, and diarrhoea while chronic arsenic effects include skin lesions, hard patches on the hands and feet (hyperkeratosis), pulmonary disease, cardiovascular disease, and developmental delays [18]. Arsenic contamination in groundwater supplies is known in 21 countries with Bangladesh and West Bengal being the highest risk areas for arsenic exposure to humans [16]. Due to its extensive health concerns, arsenic in OSPW contributes to the overall toxicity of the OSPW.

### **1.1.2. Hard Rock Mining**

Hard rock mining is the process of ore extraction to remove non-fuel metals and minerals (i.e. materials that are not used for the purposes of releasing energy as opposed to fuel materials such as oil, gas, coal, uranium, and plutonium) from solid ore deposits [19]. The extraction process for the extraction of these metals and minerals involves the use of water and reagents to grind the large rocks containing the minerals to smaller pieces of debris that can be easily separated through physical or chemical separation techniques [20]. The wastewaters produced from this process contain a mixture of water and finely ground rock particulate that are contaminated with heavy metals, oils, and total dissolved solids that are typically acidic in nature [21]. An article by Fashola et al. identifies various heavy metal contaminants found in gold mine tailings including: Ca, Zn, Pb, Cr, Ni, As, Co, and Hg [22]. Due to the high concentrations of these heavy

metals, leaching of the wastewater from the tailings ponds into nearby groundwater supplies is a growing concern.

## ***1.2. Current Literature***

There are many methods for the removal of metal ions from different matrices. While techniques such as ion exchange, coagulation, flocculation, nanofiltration, and chemical precipitation are all used, adsorption has become the preferred method due to its simplicity, cost-effectiveness, and versatility [23,24]. Adsorption of analytes can occur through either physisorption or chemisorption mechanisms. Physisorption occurs when adsorbate molecules are adsorbed onto a materials surface through intermolecular forces such as van der Waals forces, or hydrogen bonding, while chemisorption occurs when adsorbate molecules are adsorbed onto the surface through intramolecular forces or chemical bonds [25].

A review article by Tolkou et al. [26] compares the use of many adsorbents for both arsenic and chromium removal from water. Some adsorbents for arsenic removal discussed in this review included hydrous nanostructure iron (III) – titanium (VI) binary oxides, iron (III) – copper (II) binary oxides, hierarchically porous CeO<sub>2</sub>-ZrO<sub>2</sub> nanospheres, graphene oxide-ferric hydroxide composites, and magnetite Fe<sub>3</sub>O<sub>4</sub>-reduced graphite oxide-MnO<sub>2</sub> nanocomposites. The iron (III) – copper (II) binary oxide prepared by Zhang et al. [27] showed high adsorption capacities for the removal of arsenic (V) and arsenic (III), reaching 83 and 122 mg/g, respectively. A study by Jauckowicz-Sobala et al. [28] recently showed that arsenic (III) removal using these iron-copper oxides occurs in a two-step mechanism, where the arsenic undergoes oxidation before being adsorbed to the

surface of the material. Other materials, such as the porous  $\text{CeO}_2\text{-ZrO}_2$  nanospheres prepared by Xu et al. [29] showed much lower adsorption capacities of 27 and 9 mg/g for the removal of arsenic (V) and arsenic (III), respectively. A study by Mahato and Krithiga [30] used solvent free synthesized  $\text{Fe}_2\text{O}_3/\text{AISBA-15}$  adsorbent for the adsorption of arsenic and chromium in waste water. Their study showed adsorption capacities of 2.02 mg/g for arsenic (V) in a single model system and 2.25 mg/g in a binary model system when chromium was present. The adsorption capacities of materials reported in the literature range significantly depending on the type of adsorbent used, the pH of adsorption, the initial concentration of arsenic present in solution, and other components within the matrix of the sample.

Similarly, a Tolkou et al. [26] review article presents adsorbents such as NiO nanoparticles, graphene oxide functionalized with magnetic cyclodextrin-chitosan, reductive and magnetic graphene/ $\text{Fe}_3\text{O}_4$  composites, and poly-pyrrole graphene oxide nanocomposites for the removal of chromium (VI) from waters. Similar results to those of the arsenic adsorption are observed with chromium adsorption in the fact that adsorption capacities presented in the literature range so drastically. Mahato and Krithiga [30] report adsorption capacities of 1.53 mg/g in the single model and 1.3 mg/g in the binary model containing arsenic using the solvent free synthesized  $\text{Fe}_2\text{O}_3/\text{AISBA-15}$  adsorbent while Setshedi et al. [31] obtained an adsorption capacity of 625 mg/g using the poly-pyrrole graphene oxide nanocomposite.

While the studies above mostly investigate the use of nanomaterials or graphene oxide nanocomposites, there are many other adsorbents that can be used. Common adsorbents include titanium dioxide, iron oxides/hydroxides, zeolites, activated alumina,

silica and silica activated carbon composites, biomass, and activated carbons [32,33]. Neisan et al. [32] review the use of several resin and fiber adsorbents for the removal of arsenic in water such as N-methyl-D-glucamine functionalized resins, and amine-doped acrylic ion-exchange fibers. These resins and fibers showed comparable adsorption capacities to the nanocomposites mentioned above, with both high adsorption capacities and low adsorption capacities depending on the conditions of adsorption and the adsorbent material itself. Several studies have also shown the use of biochar as an adsorbent for heavy metal removal. Chatzimichailidou et al. [34] compared the use of biochars derived from rice by-products for the adsorption of arsenic and chromium. Their review compared arsenic adsorption presented in the literature with the use of rice-straw biochar, magnetic biochar, and Fe-Al bimetallic oxide biochar, showing adsorption capacities of biochars ranging from less than 1 mg/g to 34 mg/g. Their review also compared chromium adsorption with other feedstocks such as apple wood, shrimp shell, and corn cobs with adsorption capacities ranging from less than 1 mg/g to 435 mg/g. Some studies have shown the use of minerals, such as zeolite, for adsorption purposes. For example, a study by Pinedo-Torres et al. [35] uses chabazite for the adsorption of arsenic, lead, cadmium, and chromium ions with their study showing an increase in the arsenic (V) adsorption by up to 79% but a decrease in the lead, cadmium, and chromium adsorption of between 33 and 67%.

### ***1.3. Activated Carbon as an Adsorbent***

Activated carbon (AC) is a carbon material specifically treated to have a high surface area (500 to 3000 m<sup>2</sup>/g) and porosity that can be used as an adsorbent material for the removal of contaminants from simple or complex matrices [36,37]. Activated carbons

can be made from any raw material that has high carbon content or that can be processed to have high carbon content, such as sawdust, wood chips, charcoal, coconut shells, tar, and grass ash [38]. As such, many studies use activated carbons for adsorption of heavy metals. A study by Cho et al. [39] have shown the use of granular activated carbon made from lignite modified by cationic polymer as an adsorbent for nitrate and chromium. A study by Narayanan and Ganesan [40] used granular activated carbon derived from jackfruit peels treated with  $H_2SO_4$  for the removal of chromium from wastewaters. A study by Taiwo and Chinyere [41] used activated carbon derived from Nigerian bamboo for the adsorption of cadmium, nickel, lead, chromium, copper, and zinc; and a study by Gong et al. [42] used coal-based mesoporous activated carbon for the removal of arsenic (III) and (V) in low concentrations and in a binary arsenic-chromium (VI) system.

While the literature shows many feedstocks can be used to make activated carbon, the work described in this thesis focuses on the use of petroleum coke as a feedstock for the preparation of activated carbon. Petroleum coke was chosen as the feedstock source for the activated carbons in this study for two main reasons. The first reason is because of petroleum coke's naturally high initial carbon content. Feedstocks such as sawdust or coconut husks have initial carbon contents of 45 to 60% and need to be carbonized or processed before the activation step [43,44]. Feedstocks such as charcoal have initial carbon contents of between 68 and 82% which either does not undergo a carbonization step, at the expense of the activated carbon yield, or must undergo a carbonization step to increase the carbon content [45,46,47,48]. Petroleum coke has a naturally high initial carbon content of between 90 and 97% meaning that there is very little cost associated

and resources dedicated to the preparation of the raw material before the activation step [49]. This allows for a lower cost material that can still be made with a high yield.

The second reason that petroleum coke was chosen as the feedstock for the preparation of the activated carbons in this study is due to its abundance. During the bitumen extraction process in oil sands mining, 15 to 30% of each barrel of oil sands bitumen becomes petroleum coke [50]. This is a natural by-product of the cracking process used to fragment the hydrocarbons into smaller pieces [51]. As a waste by-product, the Alberta Oil Sands produces approximately 10 million metric tons of petroleum coke per year. Due to its high sulfur content, between 1 and 10% w/w, the uses of petroleum coke in industry can be limited [52]. As such, 5 million metric tons of this petroleum coke is consumed by the coal industry and other industries per year, however the other 5 million metric tons is stored in stock piles and not consumed. As of 2011, the Alberta Oil Sands had nearly 80 million metric tons of petroleum coke waste stockpiled [50]. Due to the fact that petroleum coke is produced on site, any activated carbon that is produced from the petroleum coke would already be in close proximity to the tailings ponds that need treated. This would effectively eliminate any transportation costs associated with moving the material as the material is already on location. This presents a unique opportunity to use this abundant, high carbon waste by-product to produce a more valuable product. By efficiently activating and functionalizing petroleum coke, it can be used as an adsorbent for the heavy metal contamination in mining wastewaters, effectively turning a waste product of the mining process into a tool for environmental remediation of the wastewaters of the mining process.

### ***1.4. Objectives of this Study***

- 1) To functionalize or modify a petroleum coke sourced activated carbon to produce an effective adsorbate to be used for environmental remediation of heavy metals in mining wastewaters.
- 2) To determine the adsorption mechanisms through which heavy metals are effectively adsorbed onto the surface of an activated carbon material.
- 3) To investigate the surface functionality of the activated carbon materials before and after adsorption to understand how the surface of the material changes with exposure to the chosen analytes.
- 4) To investigate the forces which drive adsorption through modelling of the kinetic data obtained.
- 5) To investigate the adsorption behaviour (competition or co-adsorption) of heavy metals in mixed solutions through isotherm modelling of the activated carbon material.

## **Chapter 2: Experimental Procedures and Methods**

### ***2.1. Materials***

The feedstock petroleum coke was obtained from an active oil sands mine in Canada and compared to a commercially available activated carbon obtained from Strem Chemicals [53]. ACS reagent grade potassium hydroxide ( $\geq 85\%$ ) pellets used for the activation process were obtained from Sigma-Aldrich, St. Louis, Missouri, USA, and ACS reagent grade hydrochloric acid used for the acid wash of the activated carbon was obtained from VWR Chemicals, Radnor, Pennsylvania, USA.

#### **2.1.1. Chromium Study Materials**

Laboratory grade, 99.5% purity chromium (VI) oxide was purchased from Acros Organics, New Jersey, USA and was used for all chromium solutions and standards. Reagent grade, 99.5% purity, ammonium chloride was purchased from Saint-Léonard, Québec, Canada, and was used for all functionalizations requiring ammonium chloride doping. 48% w/w aqueous solution hydrobromic acid was purchased from Alfa Aesar, Haverhill, Massachusetts, USA, and used for the bromination of the activated carbon material. Tris(hydroxymethyl)aminomethane (more commonly referred to as tris base) was obtained from Fisher BioReagents, Waltham, Massachusetts, USA, and used as the buffering agent in all pH 8.0 samples.

### **2.1.2. Arsenic Study Materials**

MQ100 quality (under ISO 9001 qualifications) 97% arsenic (V) oxide hydrate with a degree of hydration of approximately 3 was purchased from Sigma Aldrich (St. Louis, Missouri, United States) and was used for all arsenic (V) solutions and standards. Arsenic (III) oxide, 99.5% purity (metals basis) was produced from Alfa Aesar (Haverhill, Massachusetts, United States) and used for all arsenic (III) solutions and standards. Reagent grade potassium permanganate and iron (III) chloride were purchased from Caledon Laboratory Chemicals (Georgetown, Ontario, Canada) and Ward's Science (Rochester, New York, United States), respectively, and used for all functionalizations requiring iron and/or manganese doping.

### **2.1.3. Co-Adsorption Study Materials**

Chromium (VI) oxide and tris base buffer were previously obtained for the chromium study and arsenic (V) oxide hydrate was obtained previously for the arsenic study. The materials previously purchased for the chromium and arsenic studies were also used in the co-adsorption study.

## ***2.2. Activation and Functionalization Procedures***

### **2.2.1. Standard Activation Procedure**

The activation procedure follows that provided by the three published papers listed herein by Fisher et al. and the published work by Strong et al. [1,2,3,54] To prepare the standard activated carbon used in the following experiments, petroleum coke (PC) was ground to passing 0.58 mm mesh and underwent preliminary heating in air at 400°C

for 1 hour. After cooling, the heated PC was mixed with solid KOH at a 1:1 ratio (w/w) and heated under nitrogen from room temperature to 900°C and held at 900°C for 5 minutes before cooling to room temperature before exposure to air. The resulting activated carbon was ground with a mortar and pestle and washed with 10 mL of deionized water for every 1 gram of initial feedstock used. Washing was done by stirring the slurry at 200 rpm for 1 hour at 80°C. The product was vacuum-filtered and rinsed with 10 mL of 0.1 M HCl for every 1 gram of initial feedstock used before being dried at 110°C overnight. The final product was labeled as “Standard AC” and was used as the starting material for all experimental studies.

### **2.2.2. Ammonium Chloride-Water Refluxed AC**

To prepare one version of the nitrogenated activated carbon, 15 g of Standard AC was placed in a round bottom flask with 300 mL of “constant boiling” hydrobromic acid (aqueous solution containing 47.6% HBr by mass to form what is referred to as a constant-boiling mixture [37]) and refluxed for 1 hour before being filtered and washed with acetonitrile. The resulting brominated activated carbon was then mixed with dry ammonium chloride ( $\text{NH}_4\text{Cl}$ ) and deionized water in a 1:1:10 by mass ratio, respectively, and then refluxed for 1 hour. The resulting solids were filtered, rinsed, and dried at 110°C overnight and labeled as “ $\text{NH}_4^+$ -H<sub>2</sub>O-Reflux AC.” This activated carbon was used specifically in the chromium study.

### **2.2.3. Ammonium Chloride-Dichloromethane Refluxed AC**

To prepare another version of the nitrogenated activated carbon for comparison, 15 g of Standard AC was placed in a round bottom flask with 300 mL of “constant boiling” hydrobromic acid and refluxed for 1 hour before being filtered and washed with acetonitrile. The resulting brominated activated carbon was then mixed with dry  $\text{NH}_4\text{Cl}$  and dichloromethane in a 1:1:10 by mass ratio, respectively, and refluxed for 1 hour. The resulting solids were filtered, rinsed, and dried at  $110^\circ\text{C}$  overnight and labeled as “ $\text{NH}_4^+$ - $\text{CH}_2\text{Cl}_2$ -Reflux AC.” This activated carbon was used specifically in the chromium study.

### **2.2.4. Ammonium Chloride – Dry Mixture AC**

To prepare a third version of nitrogenated activated carbon for comparison, Standard AC was mixed with dry ammonium chloride at a 1:1 mass ratio and thermally treated under flowing nitrogen at  $550^\circ\text{C}$  for 30 minutes. Once cooled, the activated carbon was washed and dried at  $110^\circ\text{C}$  overnight and was labeled as “ $\text{NH}_4^+$ -Dry AC”. This activated carbon was used specifically in the chromium study.

### **2.2.5. Ammonium Chloride – Adsorbed AC**

To prepare a final version of the nitrogenated activated carbon, Standard AC was mixed with dry ammonium chloride and deionized water in a 1:1:2 by mass ratio. The slurry was allowed to stir for 24 hours before being vacuum filtered and dried at  $110^\circ\text{C}$  overnight. The resulting solids were then thermally treated under flowing nitrogen at  $550^\circ\text{C}$  for 30 minutes. Once cooled, the activated carbon was washed and dried at  $110^\circ\text{C}$

overnight and labeled “NH<sub>4</sub><sup>+</sup>-Adsorbed AC”. This activated carbon was used specifically in the chromium study.

### **2.2.6. Thermally Treated Activated Carbon**

As a comparison to the NH<sub>4</sub><sup>+</sup>-Adsorbed AC, a non-nitrogenated activated carbon underwent the same thermal treatment as the NH<sub>4</sub><sup>+</sup>-Adsorbed AC. The Standard AC was mixed with deionized water in a 1:2 by mass ratio and allowed to stir for 24 hours before vacuum filtration and drying at 110°C. The resulting solids were then thermally treated at 550°C for 30 minutes under flowing nitrogen so that a comparison of a thermal-treatment activated carbon both with and without the addition of nitrogen could be compared. This activated carbon was labeled as “Thermally-Treated AC” and was used specifically in the chromium study.

### **2.2.7. Iron Loading of AC Surface**

An activated carbon with an iron-loaded surface was prepared using 0.15 M iron chloride solution. 100 mL of 0.15 M iron (III) chloride was added to 5 grams of Standard AC and the pH of the slurry was brought to 2.8 by addition of 1 M HCl. The slurry was stirred for 30 minutes and sonicated for 30 minutes before vacuum filtration. The product was rinsed with 400 mL deionized water for every 1 gram of initial activated carbon used and the resulting solids were dried at 110°C overnight. Once dried, the product was thermally treated at 400°C for 2 hours under flowing nitrogen and washed with 400 mL of deionized water for every 1 gram of initial activated carbon used. The resulting activated carbon was labeled “Fe-Loaded AC” and used specifically in the arsenic study.

### **2.2.8. Manganese Loading of AC Surface**

The above procedure for iron loading (section 2.2.7) was also used for manganese loading. A solution of 0.15 M potassium permanganate was added to the AC. Procedure 2.2.7 was followed; however the solution of 0.15 M iron (III) chloride was replaced with 0.15 M potassium permanganate. The resulting activated carbon was labeled “Mn-Loaded AC” and was used specifically in the arsenic study.

### **2.2.9. Iron-Manganese Loading of AC Surface**

In the mixed loading procedure, a mixed solution containing 0.15 M iron (III) chloride and 0.15 M potassium permanganate was used and procedure 2.2.7 was followed using the mixed solution in place of the 0.15 M iron (III) chloride. This activated carbon was labeled “FeMn-Loaded AC” and used specifically in the arsenic study.

## **2.3. *Chromium (VI) Study***

A 1000 ppm stock solution of chromium (VI) in deionized water was prepared from chromium (VI) oxide. All samples and standards were prepared by serial dilution from the 1000 ppm stock solution. All samples were prepared to a concentration of 50 ppm chromium (VI) with a final volume of 50 mL using 0.1 M tris base buffer to dilute the samples. Tris base buffer was used to ensure that the pH of the chromium solution did not shift after the addition of the activated carbon, but stayed between 7.0 and 8.0.

### **2.3.1. Long-Term Adsorption Testing**

A comparison of the efficiency of each activated carbon was conducted through long-term adsorption testing at a solution pH of 8. To evaluate the efficiency of the activated carbon to remove chromium from the solution, 0.1 g of activated carbon was added to the samples, in triplicate. Samples were allowed to sit until the solution color was nearly colorless (i.e., a slight tinge of yellow remaining). Once solutions became nearly colorless, the sample was filtered using a 0.45  $\mu\text{m}$  filter and analyzed using MP-AES for chromium quantitation.

### **2.3.2. Chromium (VI) Kinetics**

Adsorption kinetics of the chromium (VI) were obtained using the Standard AC,  $\text{NH}_4^+$ -Adsorbed AC, Thermally-Treated AC, and Commercial AC. Times of 5 min, 10 min, 30 min, 1 h, 2 h, 6 h, 24 h, 48 h, 72 h, 1 week, and 2 weeks were tested. 0.1 g of activated carbon was added, in triplicate, to samples and samples were allowed to stir on a shaker table for their respective time at a stirring speed of 150 rpm before being filtered using a 0.45  $\mu\text{m}$  filter. The filtrate was analyzed on the MP-AES for chromium quantitation.

## **2.4. Arsenic (V) Study**

A 1000 ppm stock solution of arsenic (V) was prepared in deionized water using arsenic pentoxide ( $\text{As}_2\text{O}_5$ ). All samples and standards were prepared by serial dilution from the 1000 ppm stock solution. Samples were prepared to a concentration of 50 ppm

arsenic (V) with a final volume of 50 mL using deionized water to dilute the samples. 1 M HCl was used to bring the pH of the samples to 3.0.

#### **2.4.1. Efficacy Comparison**

Samples were prepared in triplicate to a concentration of 50 ppm then 0.1 g of activated carbon was added to each sample. Samples were allowed to stir on a shaker table for 6 hours at 150 rpm. All samples were filtered using a 0.45  $\mu\text{m}$  filter and analyzed on the MP-AES. Comparisons of the efficacy of the activated carbons were done by investigating the adsorption capacity of the material: per gram (mg/g), normalized to a surface area of 1000  $\text{m}^2$  (mg/1000 $\text{m}^2$ ), and per  $\text{cm}^3$  of micropores present in the material (mg/ $\text{cm}^3$  micropores).

#### **2.4.2. Arsenic (V) Kinetics**

Adsorption kinetics of the arsenic (V) were obtained for the Standard AC, Fe-loaded AC, Mn-loaded AC, FeMn-loaded AC, and Commercial AC. Stir times of 5, 10, 30, 45, 60, 120, and 360 minutes were investigated. Samples were prepared in triplicate and 0.1 g of activated carbon was added to each sample. Samples were allowed to stir on the shaker table for their respective time at 150 rpm before being filtered with a 0.45  $\mu\text{m}$  filter. The filtrate was then analyzed using MP-AES analysis for arsenic quantitation.

### **2.5. Arsenic (III) Study**

A 500 ppm stock solution of As (III) was prepared in deionized water using arsenic trioxide ( $\text{As}_2\text{O}_3$ ). All samples and standards were prepared by serial dilution from the 500 ppm stock solution. Samples were prepared to a concentration of 50 ppm arsenic (III)

with a final volume of 50 mL using deionized water to dilute the samples. 1 M HCl was used to bring the pH of the sample to 3.0.

### **2.5.1. Arsenic (III) Kinetics**

Adsorption kinetics of the Commercial AC, Standard AC, and best performing metal-loaded activated carbon (FeMn-loaded AC) for As (V) adsorption was obtained for arsenic (III) at times of 5 minutes, 10 min, 30 min, 45 min, 1 hour, 2 hr, 6 hr, 24 hr, 48 hr, 72 hr, 1 week, and 2 weeks. 0.1 g of the particular activated carbon was added to the 50 mL, 50 ppm As (III) samples and allowed to stir on a shaker table for their respective times at 150 rpm before being filtered using a 0.45  $\mu\text{m}$  filter. The Filtrate was then analyzed using MP-AES analysis.

## **2.6. *Co-Adsorption Study***

1000 ppm stock solutions of chromium (VI) and arsenic (V) were prepared individually in both deionized water (for the pH 3 studies) and in tris base buffer (for the pH 8 studies). Chromium (VI) stock solutions were prepared using chromium (VI) oxide and arsenic (V) stock solutions were prepared using arsenic (V) pentoxide. All samples and standards were prepared from these stock solutions. Samples were prepared by serial dilution in water or tris base buffer and were prepared to contain varying concentrations of chromium (VI) and arsenic (V) with a final volume of 100 mL (for pH 3 study) or 50 mL (for pH 8 study), depending on the sample set.

Arsenic (V) adsorption was monitored under several conditions: binary mixtures of arsenic-chromium at pH 3, binary mixtures of arsenic-chromium at pH 8, stepwise adsorption analysis at pH 3, and stepwise adsorption analysis at pH 8.

### **2.6.1. Arsenic (V) Enhancement and/or Competition Investigation – Arsenic:Chromium Binary Mixtures**

To investigate how arsenic adsorption is affected by chromium in solution, binary mixtures of arsenic and chromium were prepared. Arsenic (V) concentrations were held constant at 50 ppm while chromium concentrations were varied at concentrations of 0, 1, 5, 10, 25, 50, 100, 150, 200, and 250 ppm. For the pH 3 study, binary mixtures of arsenic:chromium were prepared in triplicate in deionized water to a final volume of 100 mL. 0.05 g of petroleum coke derived activated carbon was added to each sample and samples were allowed to stir at 150 rpm for 1 week. For the pH 8 study, binary mixtures of arsenic:chromium were also prepared in triplicate in tris base buffer to a final volume of 50 mL. 0.1 g of petroleum coke derived activated carbon was added to each sample and samples were allowed to stir at 150 rpm for 1 week. All samples were filtered using 0.45  $\mu$ m filters and analyzed using MP-AES.

### **2.6.2. Arsenic (V) Enhancement and/or Competition Investigation – Stepwise Adsorption**

To investigate if the arsenic adsorption enhancement/competition occurs due to a stepwise process:

Step 1: Chromium (VI) solutions were prepared at 1, 5, 10, 25, 50, 100, 150, 200, and 250 ppm in 100 mL (pH 3) or 50 mL (pH 8) total volume. 0.05 g (pH 3) or 0.1 g (pH 8) of petroleum coke-derived activated carbon was added to each sample and samples were allowed to stir for 1 week at 150 rpm. Samples were vacuum filtered and the filtrate analyzed by MP-AES to determine chromium adsorption. The activated carbon filtered

from the samples was dried at 110°C overnight and kept for Step 2 of the stepwise adsorption evaluations.

Step 2: Arsenic (V) solutions were prepared at 50 ppm in 100 mL (pH 3) or 50 mL (pH 8) and the chromium-containing activated carbon from Step 1 was added to the arsenic solutions. These samples were allowed to stir for 1 week at 150 rpm and filtered using 0.45 µm filters before being analyzed using the MP-AES.

### **2.6.3. Isotherm Modelling**

The investigations outlined in sections 2.6.1 and 2.6.2. also provided the necessary data for isotherm modelling of the chromium (VI) species. Isotherm modelling of the chromium species in the binary mixtures, and the chromium-only solution from Step 1 of the stepwise study investigated under both the Langmuir Isotherm Model and Freundlich Isotherm Model. Isotherms from the chromium-only and the binary mixture were compared to determine if the arsenic in solution caused enhancement or competition to the chromium adsorption.

### **2.6.4. Kinetic Data**

Kinetic data of the chromium and arsenic species in the pH 3 binary mixtures was obtained at each concentration ratio at stir times of 5 min, 10 min, 30 min, 1 hr, 2 hrs, 6 hrs, 24 hrs, 48 hrs, 72 hrs, and 1 week. This data was used to investigate the arsenic adsorption enhancement phenomenon at various starting concentrations of chromium over multiple stir times.

While the kinetic data obtained does provide the necessary experimental data required to perform kinetic modelling of the systems, kinetic modelling was not performed in this study. Revellame et al. [55] discuss the consequences of data transformation to a linear dataset and how the data transformation tends to favor the pseudo second-order model if the majority of the data points are close to equilibrium. If a dataset is near equilibrium, linear data transformation to the pseudo first-order model will result in a non-linear curve and thus eliminate the pseudo first-order model. If a dataset is near equilibrium, data transformation to the pseudo second-order model will result in a perfect correlation coefficient ( $R^2$ ). As such, the kinetic modelling in this study would be too near equilibrium and provide results that are biased towards the pseudo second-order model.

## ***2.7. Microwave Plasma Atomic Emission Spectroscopy***

In this study, the Agilent Technologies 4200 MP-AES was used for all MP-AES analyses. MP-AES analysis used a cyclonic single-pass spray chamber, background correction set to “auto”, a linear calibration fit constructed to 10% calibration error, an acceptable linearity ( $R^2$ ) of  $\geq 0.9900$ , an ignition gas of argon, and a carrier gas of nitrogen.

### **2.7.1. MP-AES Analysis Operating Conditions for Chromium Study**

Chromium (VI) calibration standards of 1, 2, 5, 10, 25, and 75 ppm were prepared in 0.1 M tris base buffer to construct calibration curves used during MP-AES analysis. Operating conditions are given in Table 1, below.

**Table 1:** MP-AES operating conditions for the analysis of chromium (VI).

<b>Instrument Parameter</b>	<b>Operating Condition</b>
Spray Chamber	Cyclonic single-pass
Sample Uptake (s)	30
Stabilization (s)	15
Read Time (s)	10
Number of Replicates	3
Background Correction	Auto
Wavelength (nm)	425.433
Ignition Gas	Argon
Carrier Gas	Nitrogen
Carrier Gas Flow Rate (L/min)	0.70
Calibration Fit	Linear
Acceptable Tolerance	Linear $\geq 0.9900$
Calibration Error	10%

### **2.7.2. MP-AES Analysis Operating Conditions for Arsenic Study**

Arsenic (V) and arsenic (III) calibration standards of 1, 2, 5, 10, 25, 50, and 100 ppm were prepared in deionized water to construct calibration curves used during MP-AES analysis. All operating conditions are identical to those found in Table 1, with the exception of the wavelength used for detection. Arsenic emission was detected at 188.979 nm.

### **2.7.3. MP-AES Analysis Operating Conditions for Co-Adsorption Study**

Chromium (VI) calibration standards were prepared in deionized water to produce a high concentration calibration curve and a low concentration calibration curve in order to accurately measure the concentration of the high and low concentration levels of the

analyte in solution. Standard solutions containing concentrations of 1, 2, 5, 10, 25, and 50 ppm Cr (VI) were used to produce the low concentration calibration curve range. Standard solutions containing concentrations of 50, 100, 150, 200, and 250 ppm were prepared for the high concentration calibration curve range. Arsenic (V) calibration standards were prepared at concentrations of 1, 2, 5, 10, 25, and 50 ppm.

MP-AES analysis operating conditions are identical to those listed in Table 1. Information regarding the wavelengths used for analyte detection is presented in Table 2.

**Table 2:** Detection wavelengths for arsenic (V) and chromium (VI) used in the high and low concentration calibration curve ranges.

Analyte:	Wavelength (nm)	
	Low Concentration Calibration Curve	High Concentration Calibration Curve
Arsenic	200.334	Not applicable
Chromium	425.433	540.979

## 2.8. Surface Characterization

### 2.8.1. Nitrogen Adsorption Measurements

Surface characterization nitrogen adsorption measurements were carried out using gas phase nitrogen adsorption on a Tristar II plus (Micromeritics, Norcross, Georgia, U.S.A.). The AC samples were analyzed using N<sub>2</sub> adsorption at 77 K with points monitoring adsorption between 0.0065 p/p<sup>0</sup> and 0.995 p/p<sup>0</sup> and 52 points desorption between 0.995 p/p<sup>0</sup> and 0.104 p/p<sup>0</sup>. All surface areas were reported using BET surface area analysis with pore size distributions that were developed using DFT with slit geometry modeling 2D-NLDFT (two dimensional non-local density functional theory) with N<sub>2</sub> carbon finite pores.

### **2.8.2. X-ray Photoelectron Spectroscopy**

Measurements of the XPS spectra were carried out on an AXIS Supra spectrometer (Kratos, Spring Valley, New York, NY, U.S.A.). A monochromatic AlK $\alpha$  source (15mA, 15kV) was used with the instrument work function calibrated to give a binding energy (BE) of 83.96 eV for the Au4f<sub>7/2</sub> line for metallic gold. The spectrometer dispersion was adjusted to give a BE of 932.62 eV for the Cu2p<sub>3/2</sub> line of metallic copper. The Kratos charge neutralizer system was used on all specimens and survey scan analyses were carried out with an analysis area of 300 x 700 microns with a pass energy of 160 eV. A pass energy of 20 eV with an analysis area of 300 x 700 microns was carried out for high-resolution analyses. Fitting of peaks was conducted using CASA XPS (version 2.31) with the spectra being corrected to the main line of the carbon 1s spectrum at 284.8 eV.

# **Chapter 3: Chromium Study**

## **Published as: Adsorption of Chromium (VI) Using an Activated Carbon Derived from Petroleum Coke Feedstock**

Type: Original Research Article

Submitted to: International Journal of Molecular Science

Status: Published, Dec. 18, 2022

Authors: Kyle S. Fisher<sup>1</sup> and Andrew J. Vreugdenhil<sup>1,2</sup>

<sup>1</sup> Materials Science Graduate Program, Trent University, Peterborough, Ontario, Canada, 1600 W Bank Drive, K9L 0G2.

<sup>2</sup> Department of Chemistry, Trent University, Peterborough, Ontario, Canada, 1600 W Bank Drive, K9L 0G2.

## ***Abstract***

This study aims to determine the main adsorption mechanism by which chromium (VI) is adsorbed onto the surface of a petroleum-coke sourced activated carbon, a feedstock not prevalent in current literature. The study also aims to produce an activated carbon adsorbent that is both cost-effective and efficient for the removal of chromium (VI) in neutral waters. The efficacy of thermally-treated petroleum coke activated carbon and nitrogenated petroleum coke activated carbon using ammonium chloride is compared to the efficacy of commercially available activated carbon. X-ray photoelectron spectroscopy of the activated carbons was obtained both before and after exposure to chromium (VI) for characterization of the materials and confirmation of chromium adsorption. The thermally-treated and nitrogenated activated carbons showed significant enhancement of chromium (VI) removal compared to the non-treated petroleum coke activated carbon (22.4 mg/g, 21.9 mg/g, and 17.0 mg/g, respectively). However, there was no significant difference observed between the thermally-treated and nitrogenated materials. This indicates that nitrogenation of the surface does not improve the adsorption capacity of the activated carbon, but rather the thermal-treatment itself. X-ray photoelectron spectroscopy showed a significant increase in the alcohol functional groups on the surface of the activated carbon material as a result of the heat-treatment process; from 21.7 atomic percent in the non-treated activated carbon to 29.2 atomic percent in the thermally-treated activated carbon. The alcohol functional groups present on the surface allow for chromium (VI) to undergo reduction to chromium (III) under a similar mechanism to the well-known Jones Oxidation Reaction where the reduced chromium (III) species are then physisorbed to the surface of the activated carbon. XPS results are

consistent with this as the chromium species present on the surface of the adsorbent is primarily  $\text{Cr}(\text{OH})_3$  (85.6% in the standard AC and 82.5% in the thermally-treated AC). Pseudo-first order and pseudo-second order kinetic modelling of the adsorbents indicate that they follow a pseudo-second order reaction where the rate limiting step is the chemical sorption of the adsorbate itself.

***Keywords:***

Adsorption; chromium (VI); activated carbon; adsorption mechanism; nitrogenation; functionalization; thermal treatment

### **3.1. Introduction:**

Representing one of the largest oil deposits in the world, in 2020 the Alberta oil sands in Canada produced approximately 2.98 million barrels, where 1 barrel is approximately 159 L, of crude bitumen per day [56]. The Government of Canada estimates that reserves of 166.3 billion barrels of bitumen are held in the Alberta oil sands; accounting for approximately 10% of the world's proven oil reserves [7]. Vast quantities of water are required for the bitumen extraction process; a single barrel of oil requires 19.7 barrels of water for the extraction and refining process: 16.4 barrels of recycled water and 3.3 barrels of new water. As the industrial operation is adjacent to the Athabasca River, water is imported from the river for the refining process [57]. As a result of the extraction of bitumen, the resulting processed water becomes alkaline and contaminated with organic acids and heavy metals. Oil sand companies store processed wastewater on-site in tailings ponds that exist at a pH of approximately 8.0. As of 2017, the Government of Alberta reported that tailings ponds cover an area of 220 square kilometers [11]. Due to the large amounts of water used in the process and the resulting contamination, concerns over these tailings ponds have increased over the years. Heavy metal contamination is particularly prominent with metals such as aluminum, arsenic, chromium, nickel, and vanadium [12]. The Government of Canada has documented that the average concentration of *total* chromium in uncontaminated adjacent surface waters is generally below 1 µg/L [58]. The Alberta oil sands report chromium (VI) concentrations in the tailings ponds water reaching up to 2000 µg/L [57]. As chromium (VI) is more toxic than chromium (III) and as tailing ponds waters are contaminated by chromium (VI)

species rather than chromium (III) species, this study focuses only on the removal of chromium (VI) species as the more acute need.

Chromium (VI) is highly toxic to both plant and animal life. It is also a widely recognized carcinogen [59]. Toxic effects of chromium show reduced growth in plants, smaller root systems, damage to cell membranes, a decrease or inhibition of seed germination, delayed growth, wilting, and death. In the human body, the excretion of Cr(VI) is very slow due to accumulation in the tissues. This results in the observation of elevated concentrations even decades after exposure has stopped. Toxic effects on humans and animals include developmental issues, promotion of carcinogenesis, as well as damage to the skin, respiratory, reproductive, and digestive systems [60].

Although there are many methods for the removal of metal ions from different matrices; such as ion exchange, coagulation, flocculation, nanofiltration, and chemical precipitation; adsorption has become the preferred method due to its simplicity, cost-effectiveness, and versatility [23,24]. A 2006 review article by Mohan and Pittman [61] provides an extensive review of various adsorbents used for Cr (III) and Cr (VI) adsorption. A 2018 study by Yang et al. [62] investigates the use of cassava sludge sourced activated carbon; a 2020 study by Wang et al. [63] investigates the use of granular activated carbon for mechanisms and modeling of Cr (VI) adsorption, and a 2022 article by Alvarez-Galvan et al. [64] investigates Cr (VI) adsorption using seaweed-sourced activated carbon. Activated carbon sourced from many different feedstocks is investigated in the literature; however, to our knowledge, petroleum coke-sourced activated carbon has only been mentioned as an alternative feedstock proposed for the preparation of activated carbons in Mohan and Pittman's review article. This research

focuses on petroleum coke-sourced activated carbon as a potentially viable, cost-effective, and efficient feedstock, rather than just an alternative feedstock.

Petroleum coke, also known as petcoke, is a waste by-product of the bitumen extraction process from oil sands ore. As of 2011, the processing of oil sands in Alberta produced nearly 10 million tons of petcoke per year. The coal industry and other industries have a total consumption of nearly 5 million tons of petcoke per year. The stockpile of petcoke at the end of the year in 2011 in Alberta was approximately 72 million metric tons of petcoke. Since approximately 15 to 30 percent of a barrel of tar sands bitumen can end up as petcoke [50], this creates an opportunity to use the petcoke produced as a feedstock for a more valuable product by way of efficient activation and effective chemical or thermal tailoring of the surface chemistry to generate economically viable and environmentally valuable activated carbon for environmental remediation.

In this work, petcoke was used to produce an activated carbon using chemical activation with KOH as the activating agent. While the KOH from activation has been shown to be recoverable [49], for this research we have investigated intentionally minimal amounts of KOH to reduce overall cost and the environmental impact to generate a commercially viable and highly effective adsorbent from oil sands processing waste materials. All activated carbons used in this study were produced using a 1:1 KOH to petcoke (*w/w*) ratio. In the literature, the nitrogenation of an adsorbent's surface has been shown to enhance the adsorption of chromium (VI) [65,66]. As such, we have investigated the role that nitrogen functionalization of low KOH petroleum coke-sourced activated carbon has on chromium (VI) adsorption. This research provides an avenue for valuable use of waste petcoke and a means of reducing chromium (VI) contamination in mining process water using a cost-effective and efficient material.

Chromium (VI) adsorption was evaluated using this array of petcoke-sourced, low chemical input activated carbons to determine the optimal formulation conditions for Cr (VI) adsorption and to demonstrate in the literature the likely mechanism by which chromium (VI) is adsorbed onto the surface of a given material. A commercially available activated carbon was also used for adsorption and compared as an external benchmark. Evaluation of the remediation materials focused on post-treatment methods of the activated carbons, long-term testing of the efficacy of the activated carbon for chromium (VI) removal, and kinetics evaluation of each activated carbon.

### ***3.2. Experimental Procedures and Methods***

Please refer to Chapter 2 for all experimental procedures and methods.

### ***3.3. Results and Discussion***

#### **3.3.1. Characterization of AC**

The surface composition of the activated carbon and its modification was identified using XPS and is summarized in Table 3. Long-term adsorption testing of the activated carbons proved that simply adding more nitrogen to the surface does not increase Cr (VI) adsorption. This is shown for example in the  $\text{NH}_4^+$ -Dry AC that needed 29 days to adsorb ~90% Cr (VI) and had a nitrogen content of 3 atomic percent compared to the  $\text{NH}_4^+$ -Absorbed AC and Thermally-Treated AC that had a nitrogen content of less

than 1 atomic percent and adsorbed ~90% Cr (VI) in 16 and 20 days, respectively (Table 5).

**Table 3:** XPS atom percent surface composition of activated carbon.

<b>Sample</b>	<b>Atom % C</b>	<b>Atom % O</b>	<b>Atom % N</b>	<b>Atom % Si</b>	<b>Atom % S</b>	<b>Atom % Br</b>
Standard AC:	77.63	17.04	0.39	2.17	0.42	0.00
NH <sub>4</sub> <sup>+</sup> -H <sub>2</sub> O-Reflux:	88.64	9.30	0.62	0.85	0.60	0.15
NH <sub>4</sub> <sup>+</sup> -CH <sub>2</sub> Cl <sub>2</sub> - Reflux:	86.43	10.29	0.95	1.51	0.56	0.14
NH <sub>4</sub> <sup>+</sup> -Dry:	80.35	11.36	3.12	3.70	0.78	0.00
NH <sub>4</sub> <sup>+</sup> -Adsorbed:	88.86	8.03	1.64	0.84	0.63	0.00
Thermally-Treated AC:	80.60	16.29	0.67	1.87	0.00	0.00
Commercial AC:	85.26	14.74	0.00	0.00	0.00	0.00

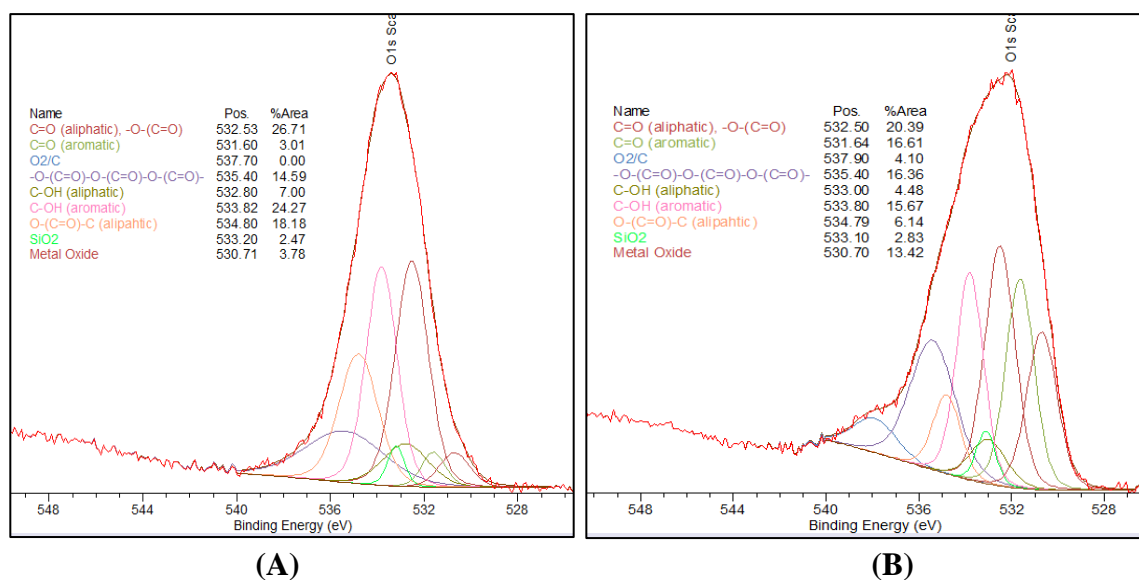
The Cr (VI) adsorption is more likely driven by oxygen speciation on the AC surface. The XPS high-resolution O1s peak for each AC sample was fit with synthetic components corresponding to the different oxygen species on the surface. The percent area of the O1s peak for each oxygen species are presented in Table 4.

**Table 4:** Oxygen atom percent speciation from deconvolution of the XPS O1s peak for the various activated carbons investigated [67,68,69].

Species	Binding Energy (eV)	Standard AC (Percent Integrated Peak Area)	NH <sub>4</sub> <sup>+</sup> -Dry AC (Percent Integrated Peak Area)	NH <sub>4</sub> <sup>+</sup> -Adsorbed AC (Percent Integrated Peak Area)	Thermally-Treated AC (Percent Integrated Peak Area)	Commercial AC (Percent Integrated Peak Area)
C=O (Aliphatic), -O-(C=O)	532.50	20.39	31.70	8.21	5.70	26.71
C=O (Aromatic)	531.60	16.61	9.41	11.94	10.81	3.01
O2/C	537.70	4.10	1.94	3.79	7.70	0.00
-O-(C=O)-	535.60	16.36	12.97	15.47	18.14	14.59
O-(C=O)-	532.80	4.48	5.99	18.14	13.20	7.00
O-(C=O)-	533.80	15.67	18.24	10.83	16.03	24.27
C-OH (Aliphatic)	534.80	6.14	3.79	10.95	8.97	18.18
C-OH (Aromatic)	533.20	2.83	5.51	3.81	1.51	2.47
O-(C=O)-C (Aliphatic)	530.70	13.42	10.67	16.86	17.93	3.78
SiO <sub>2</sub>						
Metal Oxide						

In particular, similarities in the total C-OH can be seen for the Commercial AC,  $\text{NH}_4^+$ -Adsorbed AC, and Thermally-Treated AC. The amounts of C-OH species are increased in these activated carbons compared to the Standard AC.

Figure 1 shows the XPS spectra of the O1s peak deconvolution for the activated carbon materials that are summarized in Table 4. The C-OH functionality can provide a binding site for the oxophilic chromium. As there is a lower percentage of this oxygen species in the Standard AC, it is expected that the adsorption capacity in the Standard AC is lower. Similarly, for the  $\text{NH}_4^+$ -Dry AC, this species has more C-OH than what is observed in the Standard AC, but is significantly lower than that observed for the other activated carbon materials. The importance of this speciation is consistent with the fact that the long-term testing results show that  $\text{NH}_4^+$ -Dry AC is more effective with respect to Cr (VI) adsorption than the Standard AC but less effective than the other activated carbons.



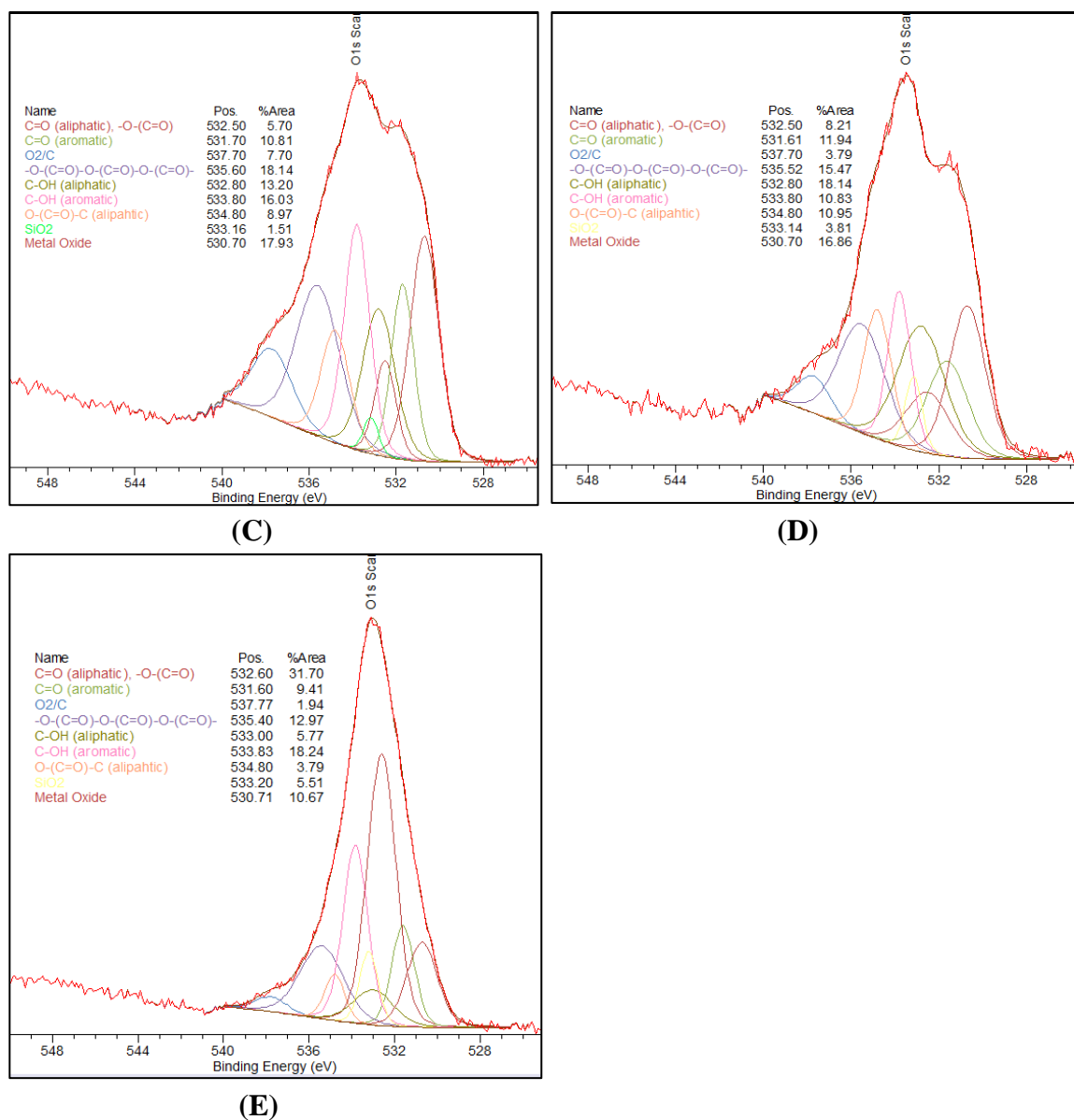


**Figure 1:** (A) O1s XPS peak splitting of Commercial AC. (B) O1s XPS peak splitting of Standard AC. (C) O1s XPS peak splitting of Thermally-Treated AC. (D) O1s XPS peak splitting of  $\text{NH}_4^+$ -Adsorbed AC. (E) O1s XPS peak splitting of  $\text{NH}_4^+$ -Dry AC [67,68,69].

Long-term testing of the activated carbons showed no correlation between the amount of nitrogen loaded on the surface and the time required to achieve 90% adsorption. Long-term testing results, including pore size distributions and surface areas of each activated carbon evaluated, can be found in Table 5. Based on the long-term testing results, the two functionalized petroleum coke-activated carbons that were the

most effective for chromium adsorption were the  $\text{NH}_4^+$ -Adsorbed AC, and the Thermally-Treated AC. As such, these two activated carbons were used in the solution phase adsorption kinetics experiments, along with the Standard AC and the Commercial AC comparators.

**Table 5:** The number of days required for various activated carbons to effectively remove chromium (VI) from solution while comparing their surface area and pore size distributions.

Activated Carbon	Number of Days to Adsorb 90% Total Cr(VI) in Solution	Surface Area ( $\text{m}^2/\text{g}$ )	Pore Size Distribution (Total Pore Volume: Micropore Volume) ( $\text{cm}^3/\text{g}:\text{cm}^3/\text{g}$ )
Standard AC	100 <sup>1</sup>	900 ± 34	0.383:0.302
$\text{NH}_4^+$ -H <sub>2</sub> O-Reflux	29	1020 ± 23	0.467:0.319
$\text{NH}_4^+$ -CH <sub>2</sub> Cl <sub>2</sub> -Reflux	55	860 ± 15	0.364:0.276
$\text{NH}_4^+$ -Dry	29	930 ± 39	0.406:0.301
$\text{NH}_4^+$ -Adsorbed	16	1100 ± 48	0.445:0.330
Thermally-Treated	20	1050 ± 35	0.444:0.337
Commercial AC	16	1350 ± 40	0.480:0.270

### 3.3.2. Chromium (VI) Kinetics

The adsorption kinetics of chromium (VI) using the four different activated carbon materials chosen from the long-term testing was evaluated. Adsorption kinetics over a 2-week time period was determined for the Thermally-Treated AC,  $\text{NH}_4^+$ -Adsorbed AC, Standard AC, and Commercial AC. Chromium (VI) adsorption equilibrium for each activated carbon system was achieved within the 2-week time period. The final adsorption capacities of the Thermally-Treated,  $\text{NH}_4^+$ -Adsorbed and Commercial ACs were all approximately 92% of the total chromium in solution while the Standard AC was only able to achieve 64% total chromium adsorption after the 2-week period (Figure 2).

<sup>1</sup> After 100 days, 90% adsorption was still not achieved and it was concluded that adsorption had reached equilibrium and would not increase further.

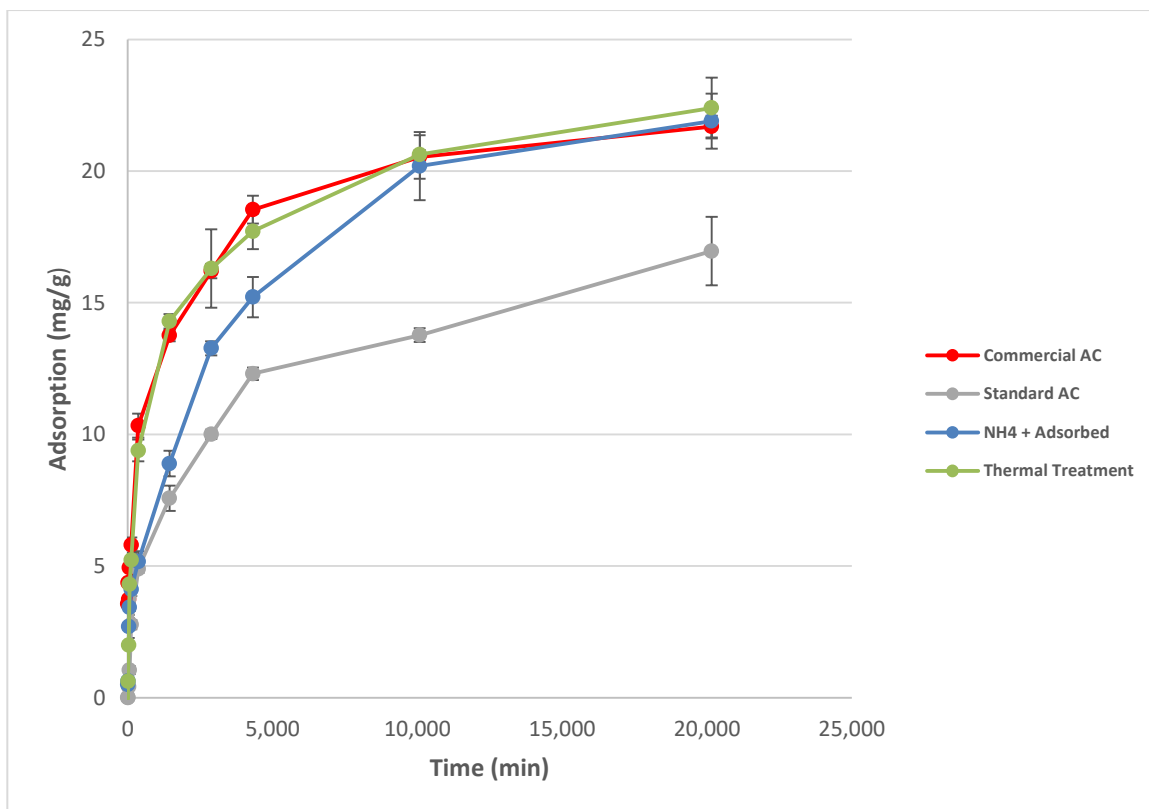


**Figure 2:** Kinetics curve of the produced activated carbons compared to the commercial AC. Results show 92% adsorption of total chromium (approximately 22 mg/g) in all activated carbons after two weeks with the exception of the standard AC which shows 64% total chromium adsorption (VI) (approximately 17 mg/g). Maximum possible adsorption (i.e., 100%) is  $25 \pm 1$  mg/g.

The kinetics are consistent with the previous observation that the post-activation treatment does increase the adsorption capacity of the treated activated carbon materials. As described in Section 3.3.1, this is likely due to the changes in the oxygen functional groups on the surface as a result of the thermal treatment. This also indicates that, since there is no significant change in the adsorption capacities between the Thermally-Treated and the  $\text{NH}_4^+$ -Adsorbed ACs, a simple thermal treatment is just as effective for increasing the adsorption capacity as an ammonium chloride functionalization since the ammonium addition is not causing the increase in the adsorption capacity. Chromium (VI) adsorption kinetics for each of the produced activated carbons indicate that, despite lower surface

areas compared to the commercial AC, a petroleum coke-activated carbon with a post-activation thermal treatment matches the adsorption capabilities of the commercial activated carbon on a milligram per gram basis. To remove the dependence of adsorption kinetics on total surface area and isolate the influence of surface functional groups, the adsorption capacity of the activated carbons was also investigated on a milligram of chromium (VI) adsorbed normalized to 1000 m<sup>2</sup> material surface area.

When adsorption results are normalized to 1000 m<sup>2</sup>, the petroleum coke-based activated carbons that were produced showed higher adsorption capacities than the commercially available activated carbon in units of mg Cr (VI) adsorbed/1000m<sup>2</sup> surface area (Figure 3). This indicates that the surface chemistry of the activated carbons plays a more important role in the adsorption than the surface area of the activated carbon as similar adsorption results can be achieved with activated carbons of lower surface area by simply changing the surface chemistry.

To investigate whether pore size plays a significant role in adsorption, normalization to micropore volume was also carried. Microporosity of the commercial activated carbon makes up 56% of the total pore volume while microporosity of the Standard AC, NH<sub>4</sub><sup>+</sup>-Adsorbed, and Thermally-Treated are 79%, 74%, and 76%, of the total porosity, respectively. The adsorption capacities of the activated carbons in terms of microporosity relative to 1 cm<sup>3</sup> total pore volume shown in Figure 4 indicates that the more microporous samples have higher adsorption capacities per micropore area (Table 6).

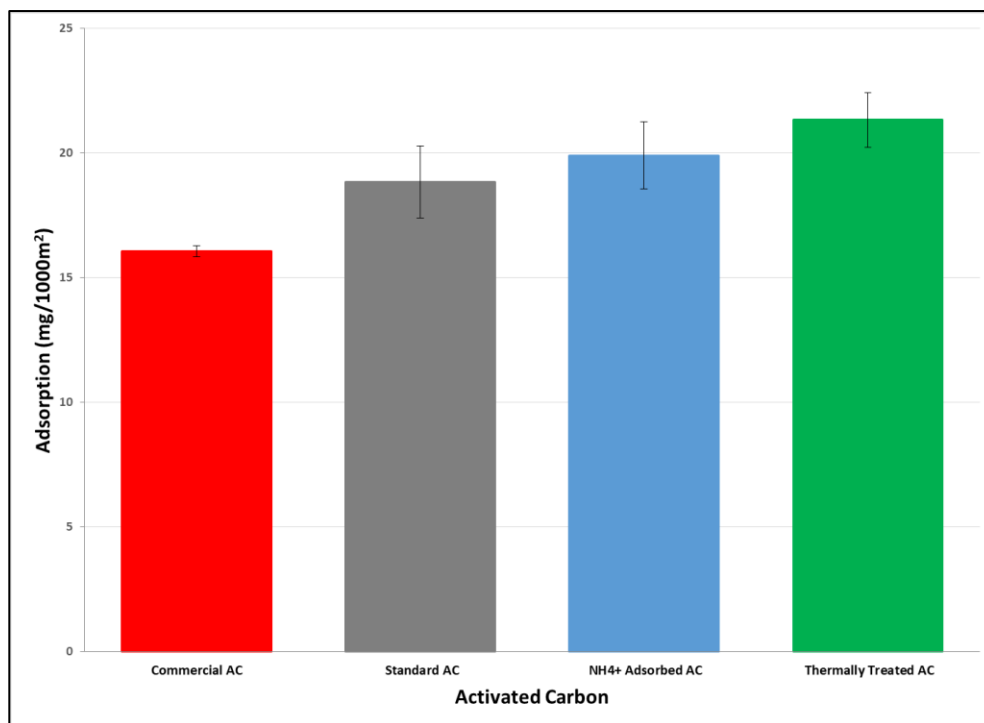


**Figure 3:** Adsorption capacity of chromium (VI) activated carbons normalized to 1000 m<sup>2</sup> surface area.

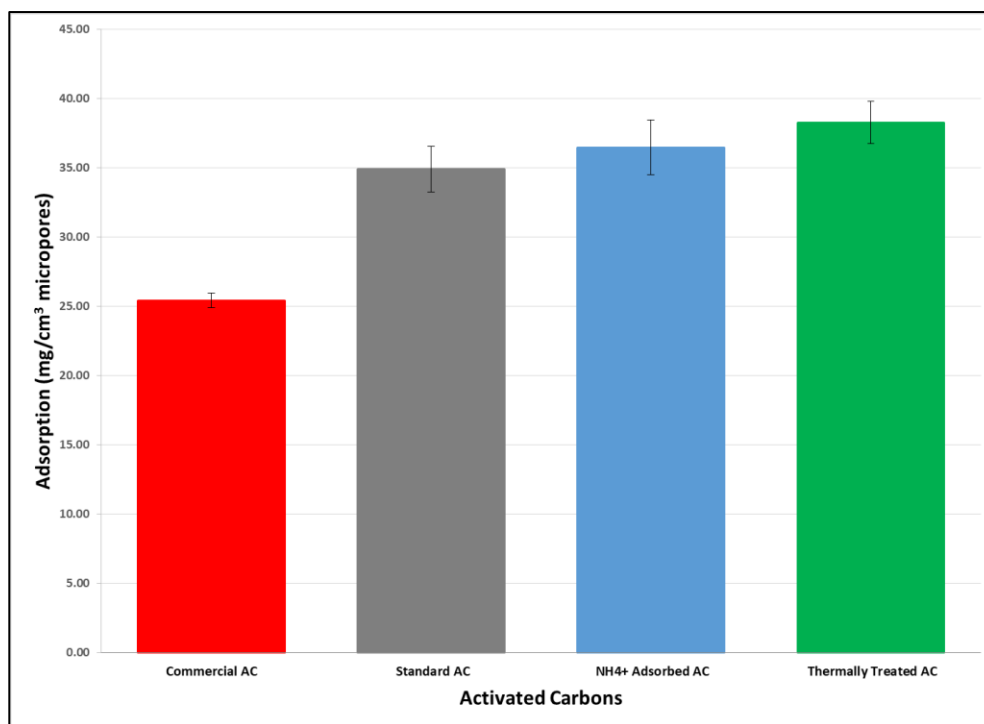


**Figure 4:** Adsorption capacity of chromium (VI) for activated carbons normalized to 1 cm<sup>3</sup> pore volume and adjusted for microporosity percentage.

**Table 6:** Summary of the activated carbon adsorption capacities after 2 weeks normalized to grams (mg/g), surface area (mg/1000 m<sup>2</sup>), and microporosity (mg/cm<sup>3</sup> micropores).

Activated Carbon	Adsorption Capacity (mg/g)	Surface Area (m <sup>2</sup> /g)	Adsorption (mg/1000 m <sup>2</sup> )	Micropore Percentage	Adsorption (mg/cm <sup>3</sup> Micropores)
Standard AC	16.96 ± 1.30	900 ± 34	18.85 ± 1.44	79%	34.92 ± 1.65
NH <sub>4</sub> <sup>+</sup> - Adsorbed AC:	21.90 ± 1.48	1100 ± 48	19.91 ± 1.34	74%	36.49 ± 1.99
Thermally-Treated AC:	22.39 ± 1.16	1050 ± 35	21.33 ± 1.10	76%	38.29 ± 1.52
Commercial AC:	21.69 ± 0.29	1350 ± 40	16.07 ± 0.22	56%	25.42 ± 0.52

The findings from sections 3.3.2. indicate that the adsorption capacity of the activated carbon is not restricted by surface area or by the pore size, but rather, the adsorption capacity is a result of the surface functionality where we are reaching an equilibrium point between the chromium and the functional groups present on the surface before we are reaching the saturation of the activated carbon surface itself.

### 3.3.3. Kinetic Modelling

Pseudo-first and pseudo-second-order kinetic modelling was performed for each of the activated carbons following Langmuir adsorption kinetics using the information from the kinetics curve found in Figure 2. A review article by Revellame et al. and Tran et al. [55,70] shows how pseudo-first-order kinetic modelling should be linear with respect to Equation 1:

$$\ln[q_e - q(t)] = -k_1 t + \ln(q_e) \quad (1)$$

**Equation 1:** Pseudo-first-order kinetic modelling linear equation based on Langmuir adsorption kinetics.

where  $q(t)$  and  $q_e$  are the amount (in mg/g) of adsorbate adsorbed at any given time,  $t$ , and at equilibrium, respectively, and where  $k_1$  is the rate constant for the pseudo-first-order kinetic model. Pseudo-second-order kinetic modelling was shown to be linear with respect to Equation 2:

$$\frac{t}{q(t)} = \left(\frac{1}{q_e}\right)t + \frac{1}{k_2 q_e^2} \quad (2)$$

**Equation 2:** Pseudo-second-order kinetic modelling linear equation based on Langmuir adsorption kinetics.

where  $q(t)$  and  $q_e$  are the amount (in mg/g) of adsorbate adsorbed at any given time,  $t$ , and at equilibrium, respectively, and where  $k_2$  is the rate constant for the pseudo-second-order kinetic model. Table 7 shows the summary of the kinetic modelling for each of the activated carbons.

**Table 7:** A summary of the pseudo-first and pseudo-second-order kinetic modelling for each of the activated carbons that underwent kinetics experiments.

Activated Carbon:	PFO or PSO Model	Model Equation	Linearity ( $R^2$ ) of the Model	$k$ Value	
				1 <sup>st</sup> order units (1/s)	$q_e$ value (mg/g)
Commercial AC	First	$y = -2.53 \times 10^{-4}x + 2.6744$	0.9801	$2.53 \times 10^{-4}$	14.50
	Second	$y = 0.0459x + 18.688$	0.9970	$1.13 \times 10^{-4}$	21.79
Standard AC	First	$y = -2.35 \times 10^{-4}x + 2.7477$	0.9627	$2.35 \times 10^{-4}$	15.61
	Second	$y = 0.0573x + 81.984$	0.9882	$4.01 \times 10^{-5}$	17.45
NH <sub>4</sub> <sup>+</sup> -Absorbed AC	First	$y = -2.63 \times 10^{-4}x + 2.9657$	0.9985	$2.63 \times 10^{-4}$	19.41
	Second	$y = 0.0445x + 42.561$	0.9848	$4.65 \times 10^{-5}$	22.47
Thermally-Treated AC	First	$y = -2.54 \times 10^{-4}x + 2.8393$	0.9783	$2.54 \times 10^{-4}$	17.10
	Second	$y = 0.0441x +$	0.9966	$7.08 \times 10^{-5}$	22.68

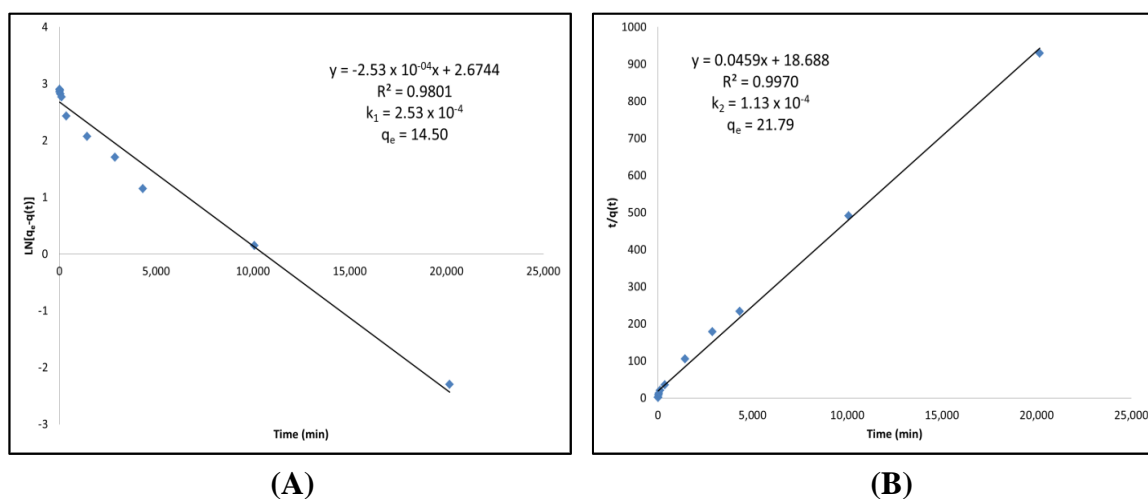
If the activated carbon adsorption kinetics follows a pseudo-first-order model, it indicates that the adsorption behaves as a first-order reaction where one reactant is present in excess. If the activated carbon adsorption kinetics follows a pseudo-second-order model, it indicates that the rate-limiting step is the chemical adsorption itself, in other words, the adsorption rate is dependent on the adsorption capacity of the adsorbent not on the concentration of the adsorbate.

For the Commercial AC, the pseudo-second-order modeling fits the data better with a linear correlation ( $R^2$ ) of 0.9970, compared to the pseudo-first-order modeling with an  $R^2$  of 0.9801. This can clearly be seen as the linear relationship is higher in the second-order model. This is also consistent with the  $q_e$  value that is calculated using this model. The  $q_e$  value obtained using this model was 21.8 mg/g while the kinetics curve for the commercial AC showed equilibrium adsorption after 2 weeks to be 21.7 mg/g. It is also clear by the adsorption rate constant,  $k$ , that the commercial AC follows the pseudo-second-order kinetic model because the adsorption rate constant  $k_2$  is lower than  $k_1$  from the pseudo-first-order model.

The Standard AC also fits well with the pseudo-second-order modeling. It can be shown that  $R^2$  value is higher using a pseudo second-order relationship compared to the pseudo first-order model (0.9882 compared to 0.9627). The calculated  $q_e$  for the pseudo-second-order model is 17.5 mg/g, which is also similar to the experimental equilibrium of 17.0 mg/g obtained from the kinetics curve after 2 weeks. Finally, the rate constant  $k_2$  was also calculated to be lower than the rate constant  $k_1$ , indicating that the rate is limited to the pseudo-second-order model.

The  $\text{NH}_4^+$ -Adsorbed AC shows better linearity for the pseudo first-order model ( $R^2$  of 0.9985) compared to the pseudo second-order model ( $R^2$  of 0.9848); however, both the  $q_e$  and  $k$  values for the pseudo-second-order model show that the second-order model is a better fit. The  $q_e$  value calculated under the pseudo-second-order model is much closer to that which was determined in the kinetics experiments, and the  $k_2$  adsorption rate constant is lower than the  $k_1$  adsorption rate constant, indicating that the adsorption rate is dependent on the chemical sorption itself, rather than the excess concentration of a reactant.

Finally, the Thermally-Treated AC follows a pseudo second-order model more accurately than the pseudo first-order model. The linearity in the pseudo second-order model is much greater ( $R^2$  of 0.9966) than the pseudo first-order model ( $R^2$  of 0.9783), the  $q_e$  value calculated from the model is more accurate than that which was determined in the kinetics experiment, and the  $k_2$  adsorption rate constant is lower than the  $k_1$  as determined from the pseudo-first-order model. Figure 5, below, provides the modelling of the activated carbons.



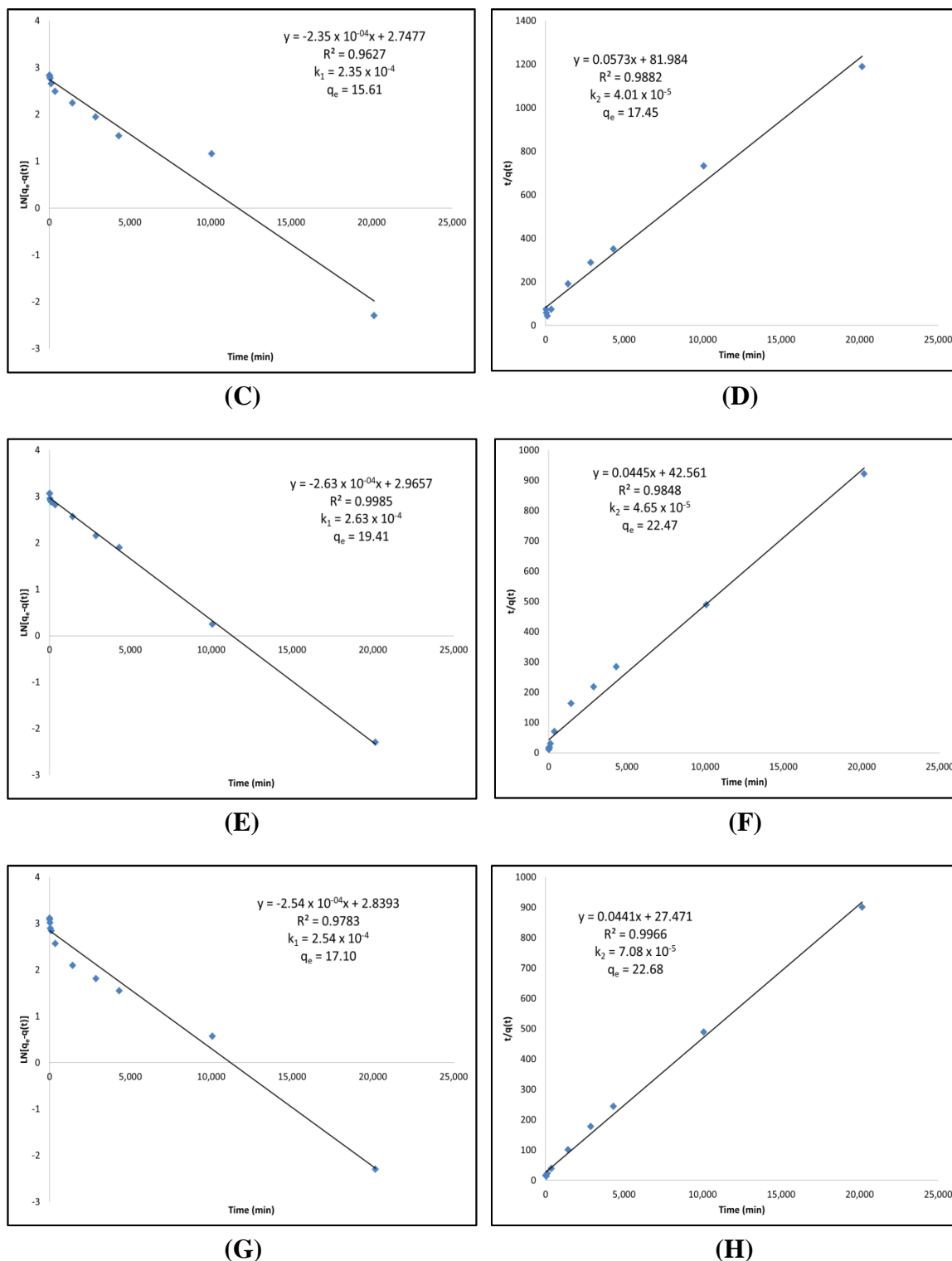


**Figure 5:** All kinetic modelling of ACs used for Cr (VI) adsorption. (A) Pseudo-first order kinetic modelling of Commercial AC. (B) Pseudo-second-order kinetic modelling of Commercial AC. (C) Pseudo-first order kinetic modelling of Standard AC. (D) Pseudo-second-order kinetic modelling of Standard AC. (E) Pseudo-first order kinetic modelling of  $\text{NH}_4^+$ -Adsorbed AC. (F) Pseudo-second-order kinetic modelling of  $\text{NH}_4^+$ -Adsorbed AC. (G) Pseudo-first order kinetic

modelling of Thermally-Treated AC. (H) Pseudo-second-order kinetic modelling of Thermally-Treated AC.

### **3.3.4. Proposed Adsorption Mechanism**

XPS spectra were obtained of the chromium species present on the activated carbon materials following exposure to chromium (VI) containing aqueous solutions. The deconvolution of the Cr2p spectral region is presented in Figure 6 and Figure 7 for the standard AC and Thermally-Treated AC, respectively. XPS spectra of the activated carbon before exposure to chromium showed no peak in the 572 to 584 eV binding energy region. This confirms that chromium adsorption is occurring as a peak in this region is present after the activated carbons' exposure to chromium. The deconvolution, species assignments, and the percent of total peak area of the Cr2p XPS signal for each chromium species observed on the standard AC and the Thermally-Treated AC samples are presented in Table 8.

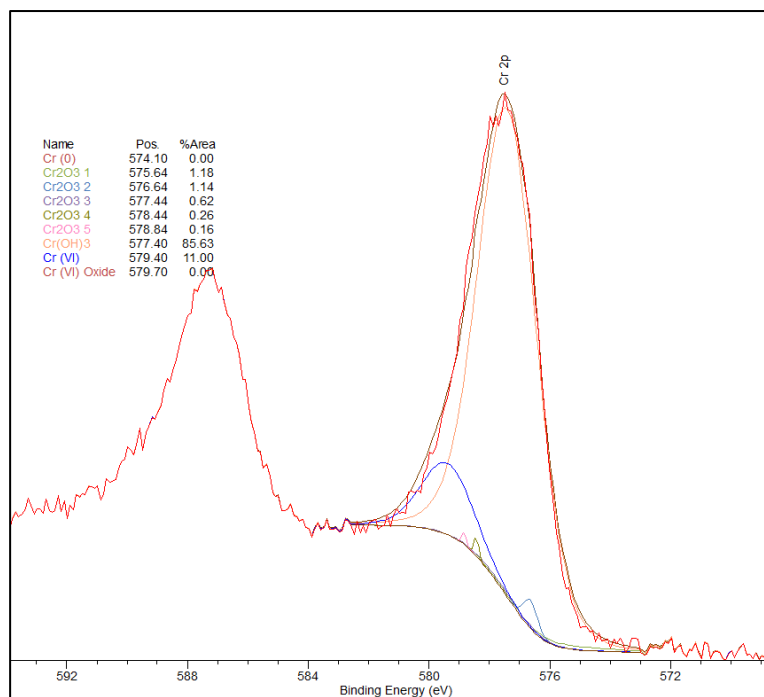


**Figure 6:** Deconvolution of the Cr2p peak observed on the surface of the standard AC post-chromium adsorption.

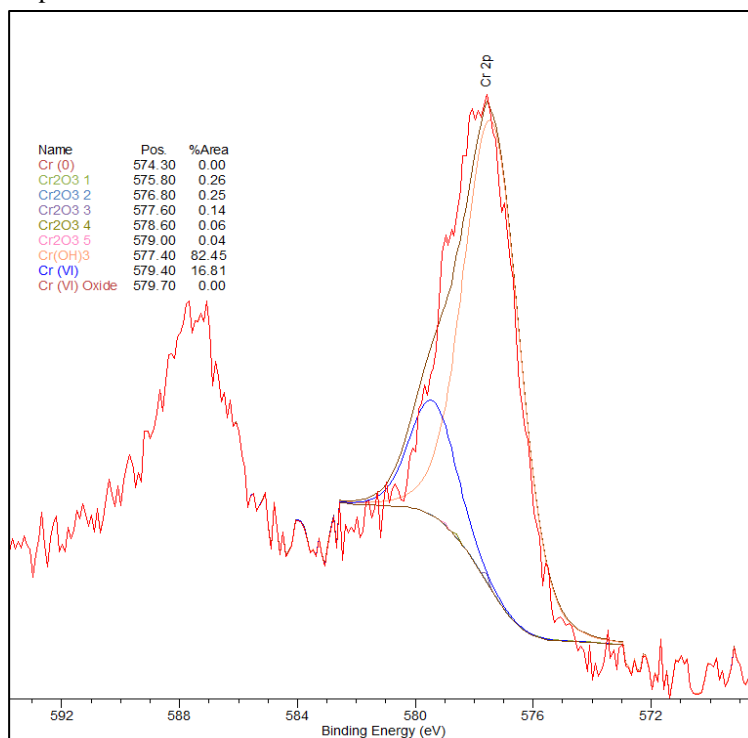


**Figure 7:** Deconvolution of the Cr2p peak observed on the surface of the Thermally-Treated AC, post-chromium adsorption.

**Table 8:** Chromium atom percent speciation from deconvolution of the XPS Cr2p 3/2 peak post-chromium adsorption [68,69,71,72].

Species	Binding Energy (eV)	Standard AC (Percent Integrated Peak Area)	Thermally-Treated AC (Percent Integrated Peak Area)
Cr <sub>2</sub> O <sub>3</sub>	575.60, 576.60, 577.40, 578.40, 579.20	3.36	0.75
Cr(OH) <sub>3</sub>	577.20	85.63	82.45
Cr (VI) mixed species	579.40	11.00	16.81

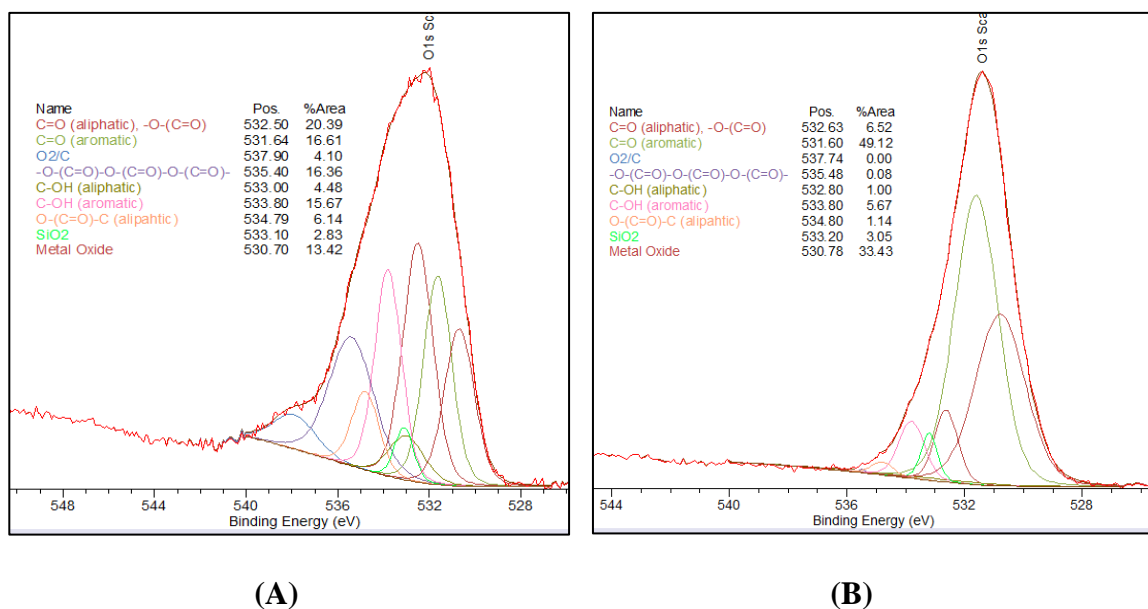
As shown in Table 8 the chromium species on the AC substrates are predominantly chromium hydroxide (Cr(OH)<sub>3</sub>) for both surfaces. Note that the Cr<sub>2</sub>O<sub>3</sub> species identification is made more complex by the well-known XPS multiplet splitting for this and similar species as described by Biesinger, et al. [72] in their XPS study of chromium compounds. Most importantly, the chromium VI species to which the AC surface was exposed are extensively converted to chromium (III) following adsorption. In addition, chromium adsorption is dependent on the surface functionality of the carbon. The thermal treatment of activated carbon substrates results in an increase in the number of C-OH functional groups on the carbon surface as shown in Table 9. Thermal treatment of the activated carbon substrate results in a substantial increase in the total C-OH functionality from 21.7% to 29.2% of the O1s peak area. This increase, in turn, results in an increase in the adsorption of chromium species onto the surface as presented in the kinetics of adsorption displayed previously in Figure 2 with a maximum total chromium adsorption of 64% for the standard AC and 93% for the thermally treated AC.

**Table 9:** Oxygen atom percent speciation from deconvolution of the XPS O1s peak pre- and post-chromium adsorption for the species involved in the adsorption process [67,68,69].

	C=O (aliphatic)	C=O (aromatic)	C-OH (aliphatic)	C-OH (aromatic)
Standard AC Pre-Cr	20.39	16.61	4.48	15.67

Adsorption: Standard AC Post-Cr	6.52	49.12	1.00	5.67
Adsorption: Thermally-Treated AC	5.70	10.81	13.20	16.03
Pre-Cr Adsorption: Thermally-Treated AC	39.82	35.47	0.00	7.83
Post-Cr Adsorption:				

Upon chromium adsorption, a substantial decrease in the C-OH functionality is observed from 20.2% to 6.7% and 29.2% to less than 7.8% for the Standard AC and Thermally Treated AC, respectively. An increase in carbonyl functionality is also detected for the Standard AC and Thermally Treated AC species following chromium exposure. Figure 8 shows the O1s peak deconvolution of the Standard AC and the Thermally-Treated AC both before and after exposure to Cr (VI).



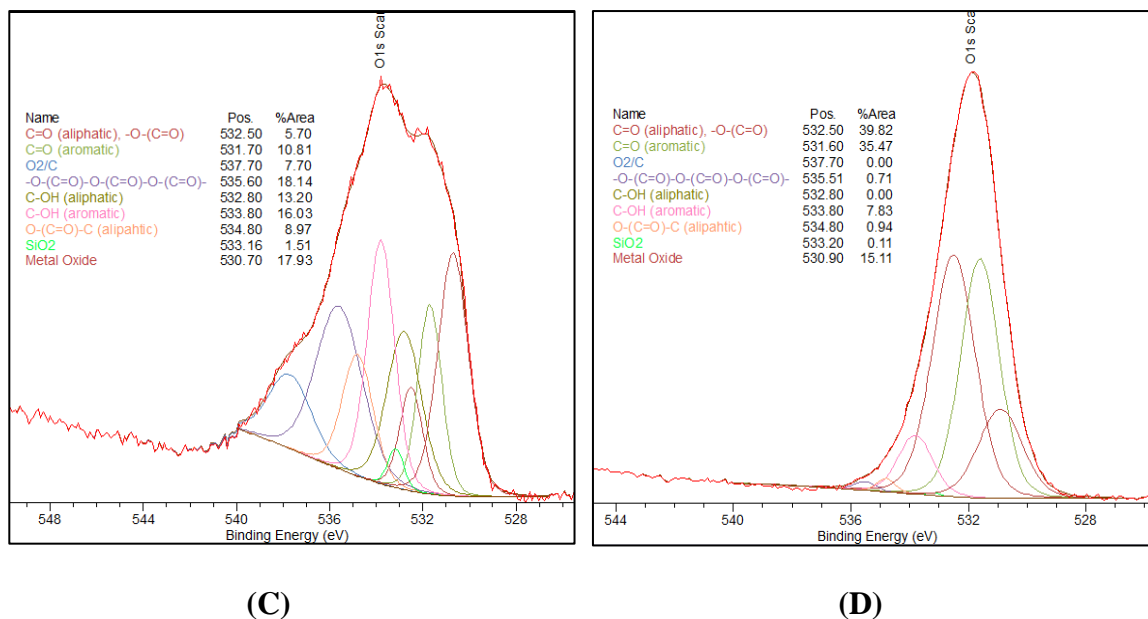


**Figure 8:** (A) O1s deconvolution of standard AC pre-exposure to chromium (VI). (B) O1s deconvolution of standard AC post-exposure to chromium (VI). (C) O1s deconvolution of thermally-treated AC pre-exposure to chromium (VI). (D) O1s deconvolution of thermally treated AC post-exposure to chromium (VI).

Based on these observed changes in oxidation states and the effect of thermal treatment of the carbon, we propose a redox adsorption process as shown in Figure 9. This process is similar to the known organic Jones Oxidation reaction mechanism for the reaction of  $\text{HCrO}_4^-$  with an alcohol where  $\text{HCrO}_4^-$  reacts with an alcohol to form a ketone and an unstable chromium (VI) species,  $\text{CrO}(\text{OH})_2$ . Further reactions then reduce this chromium (VI) species to Cr (III) [73].

Speciation of chromium (VI) at pH 8.0 is predominantly chromate ions ( $\text{CrO}_4^{2-}$ ) [74]. As such, we propose that chromate ions ( $\text{CrO}_4^{2-}$ ) react with the OH species on the surface of the activated carbon materials to form ketones on the carbon surface and the unstable  $\text{CrO}(\text{OH})_2$  species. This unstable species is then reduced to  $\text{Cr}(\text{OH})_3$  which is adsorbed onto the activated carbon materials. This mechanism shows how an increase in the alcohol functional groups on the surface can increase the adsorption of chromium by

providing more sites at which this mechanism can occur. The proposed adsorption mechanism for chromium adsorption is shown in Figure 9.

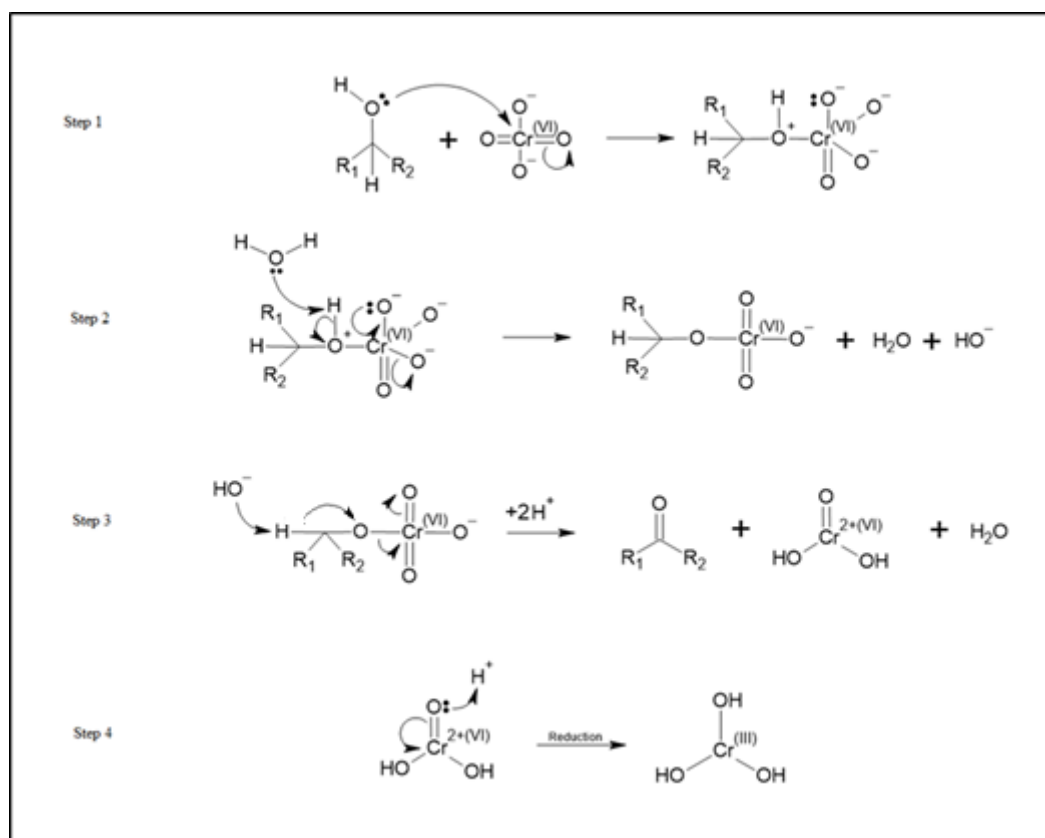


**Figure 9:** The adsorption schematic demonstrating the reduction of chromium (VI) in solution to chromium (III) hydroxide and the oxidation of alcohols to ketones on the activated carbon surface.

As previously mentioned, the proposed reaction above is very similar to the well-known Jones Oxidation reaction. The Jones Oxidation reaction mechanism is shown in Figure 10. When comparing these two mechanisms, steps 1 and 2 found in Figure 9 are very similar to step 1 found in Figure 10. The resulting product of these steps is a chromate ester. Similarly, step 3 found in Figure 9 is very similar to step 2 of Figure 10 where the result of the reaction is a ketone and the chromium (VI) species, CrO(OH)<sub>2</sub>. Finally, step 4 of Figure 9 is consistent with the “further steps” portion of the Jones

Oxidation reaction found in Figure 10 where Cr (VI) is reduced to Cr (III). It is important to note that the Jones Oxidation reaction is an organic mechanism that focuses on the formation of ketone from alcohol. While the transformation of alcohol to a ketone is important, this study is more focused on the reduction of chromium (VI) to chromium (III).

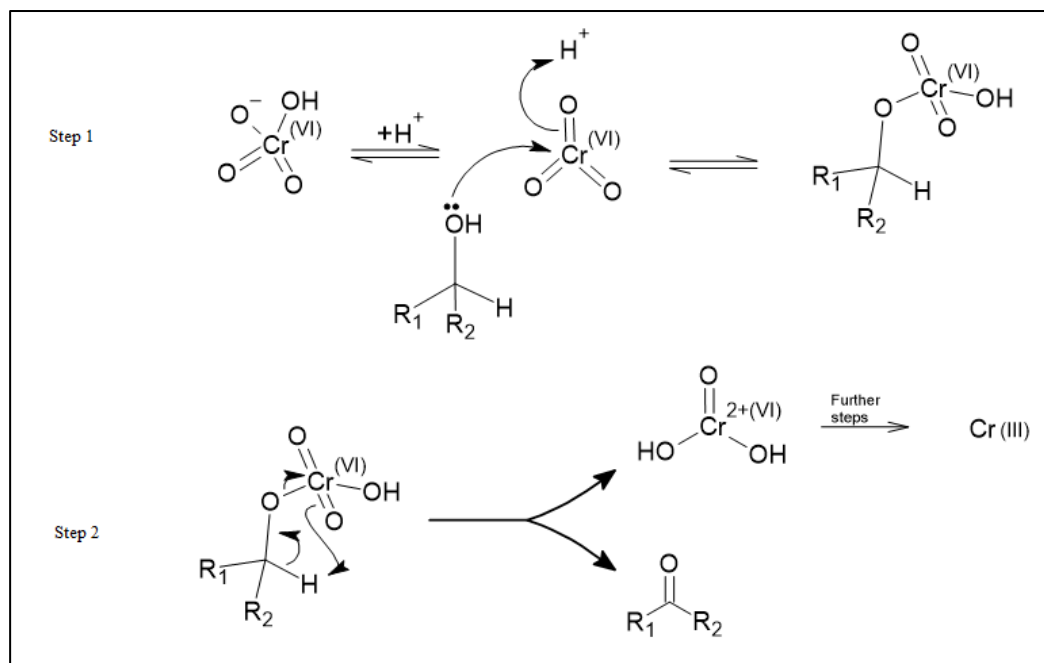


**Figure 10:** The Jones Oxidation reaction mechanism sourced from Organic Chemistry 2<sup>nd</sup> Edition by Clayden et al.. Mechanism found on page 544.

The net result of this process is the reduction of the chromium (VI) species to chromium (III) and the conversion of the OH to a carbonyl species on the surface. In our proposed mechanism, the  $\text{Cr}(\text{OH})_3$  species is then physisorbed onto the activated carbon surface through hydrogen bonding between the hydrogen atoms on the  $\text{Cr}(\text{OH})_3$  species and the electron-rich oxygen centers of the carbonyl functional groups of the activated carbon.

### ***3.4. Chromium Conclusions***

An efficient, cost-effective activated carbon that can be produced on a large scale was produced for chromium (VI) adsorption using a simple thermal treatment on petroleum coke-derived activated carbon. Thermal-treatment of the activated carbons produced in the lab resulted in a shift in the oxygen speciation that allowed for increased adsorption capabilities, equivalent to that of commercial activated carbon material. Adsorption capacity comparisons normalized to surface area and pore volume basis showed that functionality of the activated carbons and higher microporosity percentages increased the adsorption capacities and that these factors are more beneficial than having a high surface area. Kinetics studies of the activated carbons produced in the lab compared to that of the commercial activated carbon showed varying degrees of chromium (VI) adsorption during the initial kinetics with no significant difference observed at kinetics periods after one week in all but the Standard AC. Kinetic modeling shows that the adsorbents follow a pseudo-second-order kinetic model indicating that the adsorption rate is dependent on the sorption itself [70,55]. It was also determined that the addition of the ammonium chloride was not the cause of the increased adsorption observed but rather the shift in the oxygen speciation. XPS of the activated carbons shows that the main factor in the increased adsorption is a change in the oxygen speciation as a result of the post-activation thermal treatment. By increasing the alcohol functional groups through the thermal treatment, we provide more sites for which chromate ions can undergo a similar mechanism to the well-known Jones Oxidation mechanism where

alcohol reacts with chromium (VI) species to form ketones and reduce the chromium (VI) to chromium (III) [73]. In this case, the increased alcohol functionality on the activated carbon surface allows chromate ions to be reduced to  $\text{Cr(OH)}_3$  where it is subsequently adsorbed to the ketone-rich surface of the activated carbon through physical adsorption, mainly hydrogen bonding.

## **Chapter 4: Arsenic Study**

### **Published as: Metal Impregnated Petroleum Coke Derived Activated Carbon for the Adsorption of Arsenic in Acidic Waters**

Type: Original Research Article

Submitted to: ACS Omega

Status: Published, July 31, 2023

Authors: Kyle S. Fisher<sup>1</sup> and Andrew J. Vreugdenhil<sup>1,2</sup>

<sup>1</sup> Materials Science Graduate Program, Trent University, Peterborough, Ontario, Canada, 1600 W Bank Drive, K9L 0G2.

<sup>2</sup> Department of Chemistry, Trent University, Peterborough, Ontario, Canada, 1600 W Bank Drive, K9L 0G2.

## ***Abstract***

The efficacy of metal-impregnated petroleum coke activated carbon for the adsorption of arsenite and arsenate in acidic waters is investigated in this study. Unmodified petroleum coke activated carbon, FeCl<sub>3</sub>-loaded activated carbon, KMnO<sub>4</sub>-loaded activated carbon, and a mixed FeCl<sub>3</sub>-KMnO<sub>4</sub>-loaded activated carbon were evaluated. Surface characteristics of the activated carbons before and after arsenic adsorption were analyzed by X-ray Photoelectron Spectroscopy (XPS). Arsenate adsorption was significantly improved by the addition of an iron-manganese-loaded activated carbon; increasing adsorption from 8.1% to 50.9% of an approximately 25 mg/g maximum adsorption. Oxidation-reduction reactions are proposed based on the observed arsenic 2p 3/2, iron 2p 3/2, and manganese 2p 3/2 XPS peaks. While iron in the iron-loaded activated carbon is not acting as the reducing agent, it is acting as a conductor for the flow of electrons from the activated carbon to the arsenic for reduction to take place prior to physisorption of the arsenic. In the manganese-loaded activated carbon, manganese acts as the reducing agent for arsenic prior to arsenic adsorption to the surface through physisorption. XPS of the post-arsenic (V) exposure samples showed that the Fe<sub>2</sub>O<sub>3</sub> species was reduced from 32.2% to 1.7% in the FeMn-loaded sample while FeOOH species were increased from 53.2% to 81.7%. This is consistent with the proposed mechanism. Similarly, MnO in the FeMn-loaded activated carbon dropped from 26.8% to 15.4% while MnOOH and MnO<sub>2</sub> increased from 40.0% and 33.2% to 44.0% and 40.6%, respectively. This is consistent with the proposed mechanism. The adsorption of arsenite was also evaluated to show that the modification of the activated carbon

adsorbed not only the arsenic (V) species, but also the more toxic arsenic (III) species without the need for oxidation of the arsenic prior to adsorption.

***Keywords:***

Adsorption, Arsenic, Activated Carbon, Functionalization, Metal Impregnation

***Synopsis:***

Arsenic contamination from hard rock mining sources seep into drinking water and ground water supplies in the environment. This study focuses on the mechanisms through which arsenic adsorption occurs on modified activated carbon materials so that contamination can be cleaned at the source.

## ***4.1. Introduction***

As one of the twentieth most abundant elements in the Earth's crust, arsenic can be found in no fewer than 245 mineral species. The most common of these minerals is arsenopyrite, a mineral often found alongside high deposits of gold and, when oxidized, produces arsenic and sulfur oxiacids (e.g.  $\text{H}_3\text{AsO}_3$ ,  $\text{H}_3\text{AsO}_4$ ,  $\text{H}_2\text{SO}_4$ ) [75,76,77]. During the mining processes, arsenic is released into acid mine drainage when sulfide bearing materials are exposed to atmospheric water and oxygen. The Society for Mining, Metallurgy, and Exploration (SME) notes that mining activities, especially sulfide mining, increases the rate of arsenic released from minerals that are exposed to weathering during the excavation process [78]. Closed in 2004, the Giant Mine located in Yellowknife, NT, Canada produced 237, 000 tons of arsenic trioxide dust in its 52 year operation. Seepage from the chambers containing this arsenic trioxide is evident as concentrations of arsenic in some mine waters exceed 4000 ppm [77]. Treating these tailings is an important step in mitigating the chances of seepage or tailings spills that would result in elevated levels of arsenic in nearby groundwater and drinking water supplies.

Arsenic contamination in water supplies is already a widespread problem in a number of countries worldwide. Existing in valence states of As (III) under reducing conditions and As (V) under oxidizing conditions, arsenic contamination affects over 140 million people across 50 countries that have drinking water with higher arsenic concentrations than the World Health Organization's (WHO's) acceptable level of 10  $\mu\text{g/L}$  [79,80]. The majority of arsenic contamination can be found in South Asian

countries such as Bangladesh, Cambodia, and India; however, several Latin American countries including Argentina, Bolivia, and Mexico have been identified to contain waters with arsenic concentrations above 50  $\mu\text{g/L}$  [79,80]. In Bangladesh alone, the WHO reported 19 million people exposed to arsenic concentrations above the national standard of 50  $\mu\text{g/L}$  and 39 million people exposed to arsenic concentrations above the WHO's guideline of 10  $\mu\text{g/L}$  [79,80].

Although there are many methods for the removal of metal ions from different matrices; such as ion exchange, coagulation, flocculation, nanofiltration, and chemical precipitation; adsorption has become the preferred method due to its simplicity, cost-effectiveness, and versatility [23,24]. Many studies in the literature have already shown the possibility of using adsorbent materials for the removal of arsenic in contaminated waters. A study by Byambaa et al. showed high adsorption capacities using an adsorbent derived from acid mine drainage sludge. The maximum adsorption capacity found in this study was 50.4 mg/g, compared to the 29.1 mg/g that was obtained when using a commercially available granular ferric hydroxide adsorbent [81]. Another study by Singh et al. used a graphene oxide functionalized with a zirconium-based metal-organic framework nanocomposite for the removal of arsenic and through isotherm modelling obtained a maximum adsorption capacity of nearly 150 mg/g [82]. Studies in the literature investigate the adsorption of arsenic using many types of adsorbents; some include: modified saxaul ash, magnetite nanoparticles, functionalized diatom silica shells, and activated carbons [83,84,85,86]. Adsorption mechanisms can vary depending on the feedstock material being used. For example, the magnetite nanoparticles investigated by Liu et al. show arsenic adsorption occurring through redox reactions while the

functionalized diatom silica shells investigated by Zhang et al. show arsenic adsorption occurring through either chemisorption exchanges between oxygen groups on the arsenic and thiol groups or through surface complexation between As (III), protonated nitrogen, and hydroxyl groups [84,85].

In the literature, petroleum coke (or petcoke) has been proven to be an effective adsorbent for trace metals. A study by Pourrezaei et al. used zero valent iron enhanced petroleum coke to adsorb vanadium, manganese, nickel, and molybdenum in oil sands process water [87]. Another study by Karimi et al. use activated carbon prepared by CO<sub>2</sub> activation from a petroleum coke feedstock to adsorb metallic ions from oil sands tailings water. Their study provided adsorption data using their material on metals such as calcium, magnesium, strontium, sodium, and potassium; however, it did not provide data on arsenic adsorption [88]. To our knowledge, little work has been done on the adsorption of arsenic using petroleum coke derived activated carbons [89]. Petroleum coke has been chosen as the feedstock of choice in this study for two main reasons. Petroleum coke is a waste by-product of the bitumen extraction process from oil sands ore. As of 2011, the oil sands in Alberta produced nearly 10 million metric tons of petroleum coke per year. The coal industry and other industries have a total consumption of 5 million metric tons of petcoke per year. The remaining petcoke is stockpiled in large quantities and at the end of 2011, Alberta contained stockpiles of petcoke weighing nearly 72 million metric tons [50]. Therefore, the first reason this study focuses on the use of a petroleum coke feedstock is due to the sheer abundance of the feedstock material allowing for the opportunity to use the waste petcoke as feedstock for a more valuable product. The second reason that petcoke was chosen as the feedstock material is due to its naturally

high carbon content. Activated carbons can be made from any raw material that has a high carbon content or that can be processed to contain a high carbon content. Feedstocks include sawdust, wood chips, charcoal, coconut shell, tar, and grass ash [37]. These feedstocks can vary significantly in the initial carbon content they contain. Sawdust contains approximately 60% carbon, wood chips contain between 45 and 50% carbon, and charcoal contains 68 to 82% carbon [38,43,44,45,46]. These feedstocks often need elaborate preparation methods before the activation process because of their lower carbon content. This is not required for the use of petroleum coke as a feedstock because of its naturally high carbon content of between 90 and 97% [45,48]. This means that there is little cost associated and resources dedicated to the preparation of the raw material before activation.

This study will therefore focus on the use of petroleum coke derived activated carbon and the modification of the activated carbon surface for the removal of arsenic (III) and arsenic (V) from acidic waters. This work describes the novel development of a highly effective adsorbent derived from the oil sands waste product, petroleum coke, its application in environmental remediation of arsenic species, and specifically, the mechanisms by which arsenic adsorption occurs on the modified activated carbon surface.

## ***4.2. Experimental Procedure and Methods***

Please refer to chapter 2 for all experimental procedures and methods.

## ***4.3. Results and Discussion***

### 4.3.1. Nitrogen Adsorption Measurements

The standard activated carbon follows both a type I and a type II nitrogen adsorption isotherm with a large increase of adsorbate adsorbed in the microporous region and a small increase in adsorbate adsorbed in the higher pressure region. This indicates a highly microporous sample. Desorption seems to follow a type H4 hysteresis, however, the desorption isotherm does not fully close to the adsorption isotherm. The Fe-Loaded, Mn-Loaded, and Commercial Activated Carbon materials follow a mixture of type I and type II nitrogen adsorption isotherms, similar to what is seen with the standard AC. The quantity of nitrogen adsorbed is less than that observed in the standard AC in the Fe-Loaded, Mn-Loaded, and Commercial AC indicating a smaller pore volume in these materials. The isotherms for these samples also show a steeper curve near the saturation point indicating a higher percentage of mesopores and macropores. These materials follow a type H4 hysteresis. Unlike the other activated carbon materials, the FeMn-loaded AC follows a type II adsorption isotherm where there is very little adsorption in the micropore region and a very larger increase in the adsorption at higher relative pressures. The FeMn-loaded AC follows H3 hysteresis. The majority of the adsorption is occurring at the higher relative pressures indicating that the majority of the pore volume is made of mesopores and macropores. The FeMn-loaded AC shows the biggest difference due to blocking of the micropores and should show the most significant decrease in the micropore percentage. A summary of the pore information obtained from the nitrogen adsorption measurements is provided in Table 10. Figure 11 shows the nitrogen isotherm plots of the activated carbons used within this study.

**Table 10:** Pore size distribution information obtained from nitrogen adsorption measurements.

<b>Activated Carbon Material:</b>	<b>BET Surface Area (m<sup>2</sup>/g)</b>	<b>Total Pore Volume (cm<sup>3</sup>/g)</b>	<b>Micropore Percentage</b>	<b>Average Pore Width (nm)</b>
Commercial AC	1329 ± 38	0.5011 ± 0.0440	53.3 ± 2.7	4.82 ± 0.11
Standard AC	975 ± 19	0.4143 ± 0.0086	76.7 ± 0.4 <sub>4</sub>	3.60 ± 0.03 <sub>5</sub>
Fe-Loaded AC	748 ± 13	0.3349 ± 0.0098	67.4 ± 0.5 <sub>5</sub>	3.95 ± 0.05 <sub>6</sub>
Mn-Loaded AC	487 ± 15	0.2494 ± 0.0142	58.9 ± 0.7 <sub>5</sub>	6.35 ± 0.13
FeMn-Loaded AC	397 ± 11	0.3479 ± 0.0190	31.1 ± 1.1	9.60 ± 0.21

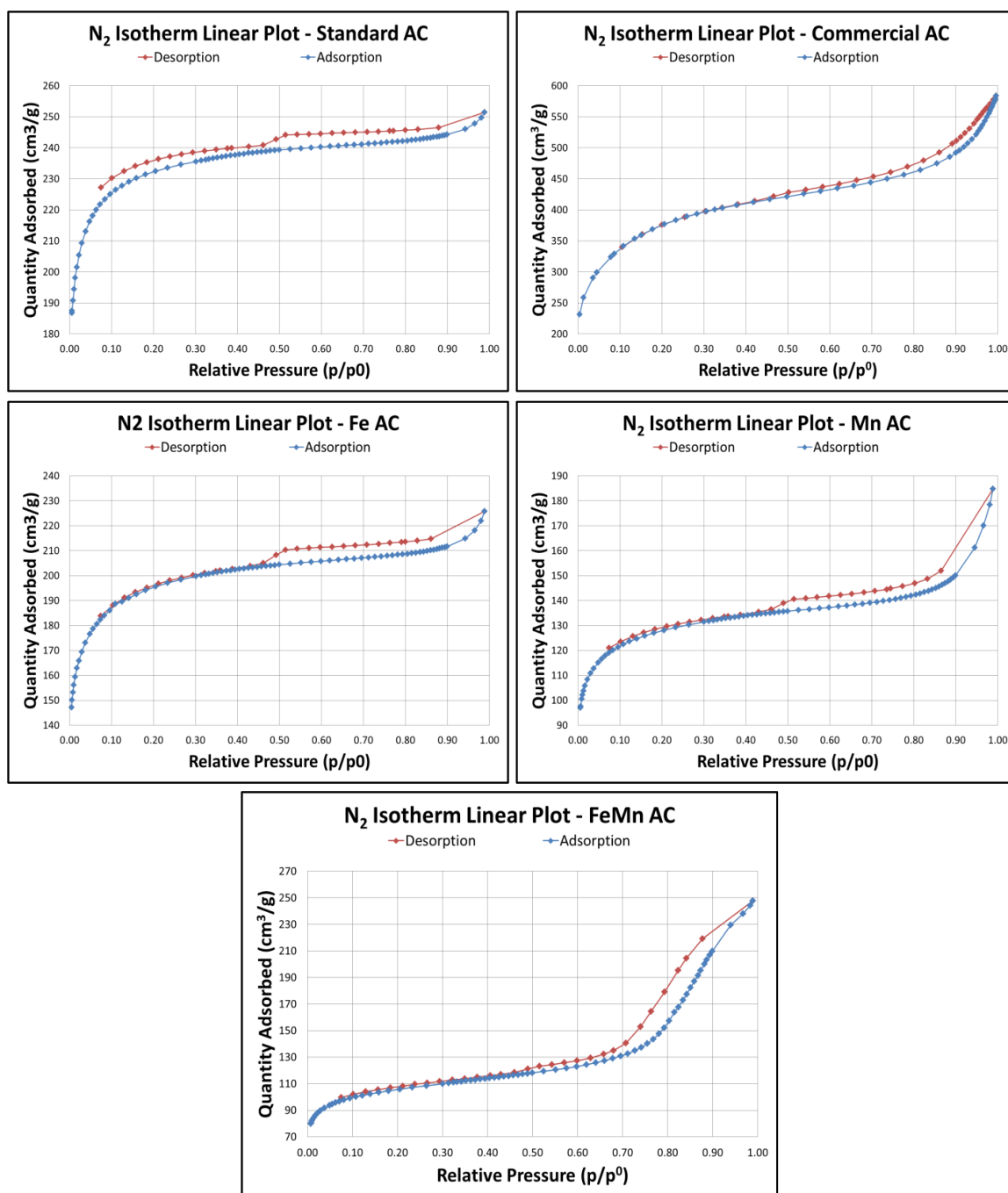


**Figure 11:** Nitrogen adsorption isotherm and hysteresis plots of the Standard, Commercial, Fe-Loaded, Mn-Loaded, and FeMn-Loaded Activated Carbons.

#### **4.3.2. As (V) Efficacy Comparison: Milligram per Gram Adsorption Comparison**

To compare the efficacy of the various activated carbons for arsenic (V) adsorption, 0.1 g of activated carbon was added to 50 mL samples of 50 ppm arsenic (V). Samples were stirred at 150 rpm for 6 hours then filtered before elemental analysis of the filtrate.

To compare the efficacy of the different activated carbon substrates, adsorption with respect to the amount of activated carbon added was compared in milligrams of arsenic (V) adsorbed per gram of activated carbon (mg/g). As shown in Figure 12, there was a dramatic improvement in the adsorption of arsenic after functionalization with the iron, manganese and iron/manganese together. All of the metal-modified activated carbons showed increased adsorption of arsenic (V) compared to the unmodified activated carbon. The single-metal loaded activated carbons showed adsorptions of  $4.9 \pm 0.2$  mg/g and  $6.0 \pm 0.2$  mg/g for iron-loaded and manganese-loaded activated carbons, respectively, while the Standard AC showed an adsorption of  $2.1 \pm 0.1$  mg/g. By loading the combination of iron and manganese onto the surface, the adsorption efficiency is even more dramatically improved with arsenic adsorption reaching  $12.9 \pm 0.6$  mg/g.

The Commercial AC was also tested after functionalization with the iron-manganese mixture. An improvement in the adsorption capacity was observed from  $8.5 \pm 0.3$  mg/g to  $15.6 \pm 1.1$  mg/g. This shows that surface functionalization plays a key role in adsorption and that the adsorption capacity of a material with a high surface area can be improved by modification of the surface functionalization even at the cost of a decrease in the specific surface area. Since this study aims to focus on the modification of the

petroleum coke activated carbon, the functionalization of the Commercial AC will not be investigated further.

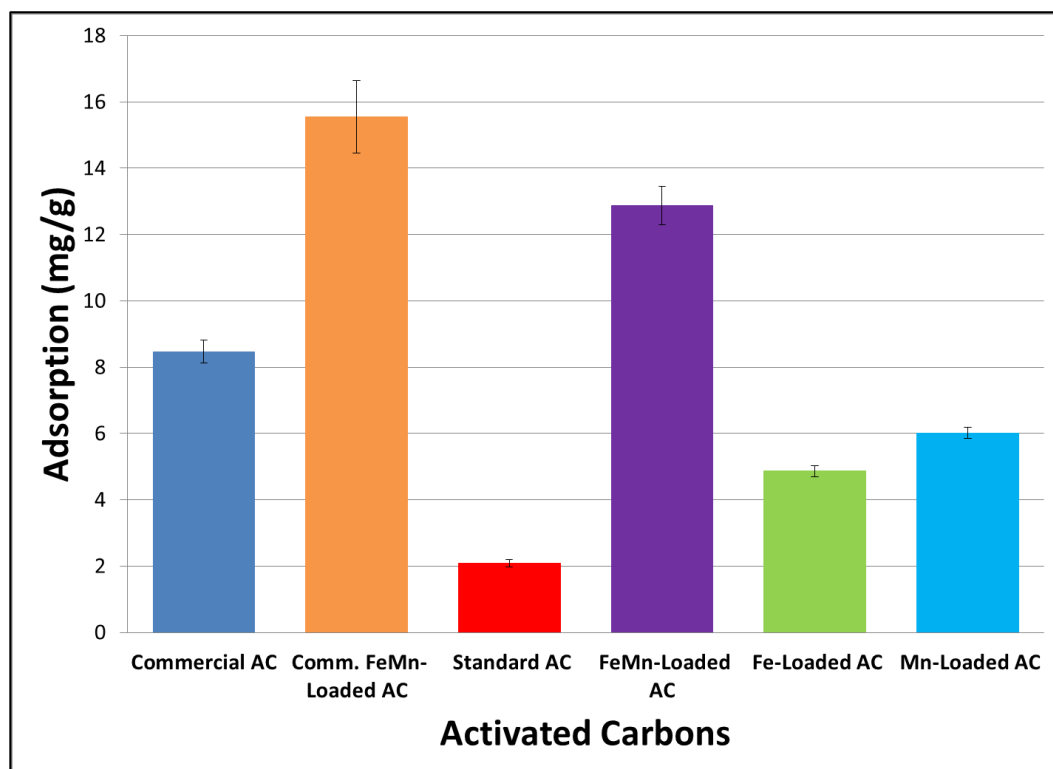


**Figure 12:** Comparison of various activated carbons investigating the adsorption efficiency of arsenic (V) after a 6 hour exposure time.

#### 4.3.3. As (V) Efficacy Comparison: Normalized Surface Area Substrates

The arsenic species adsorption is also impacted by the variation of specific surface area of the activated carbon substrates particularly as the loading of iron and manganese species significantly reduces the specific surface area of the substrate. Similar to the mg/g comparison, the arsenic (V) adsorption efficiencies of each activated carbon were calculated but then normalized to a surface area of 1000 m<sup>2</sup>. Table 11 shows the adsorption of arsenic (V) for the five activated carbon materials each normalized to a surface area of 1000 m<sup>2</sup>. The metal-loaded activated carbons, despite having a lower

surface area, have a comparable, or better, adsorption than the higher surface area of the Commercial AC. This again, demonstrates the greater significance of the surface functionality on the arsenic adsorption over that of the surface area.

**Table 11:** Arsenic (V) adsorption capacity comparisons normalized to surface area.

<b>Activated Carbon Material:</b>	<b>Adsorption of As (V) Normalized to 1000 m<sup>2</sup> (mg/m<sup>2</sup>)</b>
Commercial AC	$6.37 \pm 0.46$
Standard AC	$2.13 \pm 0.10$
Fe-Loaded AC	$6.50 \pm 0.12$
Mn-Loaded AC	$12.36 \pm 0.08$
FeMn-Loaded AC	$32.43 \pm 0.23$

The reduction of the activated carbon surface area due to metal-impregnation of the activated carbon surface is expected. With inclusion of the metal species, the density of the material increases so there will be a decrease in specific surface area due to this effect. A more significant impact on the surface area occurs when metal species are adsorbed into the pores of the activated carbon, clogging the pores at the neck of an opening. This pore filling will make the area deeper within the pores inaccessible, effectively removing the surface area that these pores would provide, significantly lowering the surface area of the material. XPS of the activated carbon samples showed that iron-loading on the iron-loaded sample made up 6.8 atomic percent (25 weight-percent) of the activated carbon and that manganese-loading in the manganese-loaded sample made up 28.4 atomic percent (64.5 weight-percent) of the activated carbon. This corresponds well with the observed decrease in surface area as the higher loading of the manganese filled more of the pores in the manganese-loaded activated carbon, blocking off more surface area than what was observed in the iron-loaded activated carbon. This is

also consistent with the nitrogen adsorption measurements presented in Table 10 that indicate that the Mn-Loaded AC has less pore volume than the other activated carbons and a larger average pore size. This would indicate that the manganese is blocking the majority of the micropores, decreasing the available surface area, pore volume, and increasing the average pore size. XPS of the FeMn-Loaded AC showed that total metal-loading on the activated carbon was 16 atomic percent (46.8 weight percent), consisting of 8.2 atomic percent (24.1 weight percent) iron, and 7.8 atomic percent (22.7 weight percent) manganese. This binary metal system also decreases the surface area of the activate carbons. Interactions between the iron and manganese likely produced larger mixed metal precipitates that blocked pores earlier in the pore channel causing larger amounts of micropore volume to be inaccessible, decreasing surface area further than the single metal system of either iron or manganese. This is consistent with the nitrogen adsorption measurement results in Table 10 that show the much larger average pore size of the FeMn-loaded AC. The total pore volume is larger than those of the single metal-loaded activated carbons, likely due to the very large macropores driving the pore volume up.

#### **4.3.4. As (V) Efficacy Comparison: Normalized Microporosity Substrates**

Similar to the surface area normalization, normalization of the adsorption relative to the microporosity of the various activated carbons was investigated. Adsorption of arsenic (V) was normalized to 1 cm<sup>3</sup> of micropore volume so that adsorption per micropore volume could be analyzed. Trends in this graph would indicate the influence of microporosity on the adsorption and whether microporosity is a driving factor for arsenic

(V) adsorption in these activated carbons. Table 12 summarizes the microporosities of the activated carbons and their respective adsorption capacities normalized to microporosity.

**Table 12:** Arsenic (V) adsorption capacities comparison normalized to microporosity.

<b>Activated Carbon Material:</b>	<b>Adsorption Capacity Normalized to 1 cm<sup>3</sup> Micropores (mgcm<sup>3</sup>)</b>
Commercial AC	9.00 ± 0.64
Standard AC	3.84 ± 0.15
Fe-Loaded AC	9.78 ± 0.25
Mn-Loaded AC	14.21 ± 0.27
FeMn-Loaded AC	11.51 ± 1.86

No observable trends are found with respect to adsorption capacity normalized to microporosity of a material therefore it is concluded that the microporosity of a given material is not a driving factor in the adsorption of arsenic (V) and that surface functionality of the material is much more important. The findings from sections 4.3.2. to 4.3.4. indicate that the adsorption capacity of the activated carbon is not restricted by surface area or by the pore size, but rather, the adsorption capacity is a result of the surface functionality where we are reaching an equilibrium point between the arsenic and the functional groups present on the surface before we are reaching the saturation of the activated carbon surface.

#### 4.3.5. XPS Characterization of Metal Modified Activated Carbons Pre- and Post-Arsenic (V) Adsorption

The deconvolution, species assignments, and percent of total peak area for the Fe2p 3/2, Mn2p 3/2, and As2p 3/2 XPS peak signals for the FeMn AC pre- and post-arsenic exposure, the Fe-Loaded AC post-arsenic exposure and the Mn-Loaded AC post-arsenic exposure are shown in Table 13. Note that the Fe<sub>2</sub>O<sub>3</sub>, Fe<sub>3</sub>O<sub>4</sub><sup>2+</sup>, Fe<sub>3</sub>O<sub>4</sub><sup>3+</sup>, FeOOH, MnO, MnOOH, and MnO<sub>2</sub> species identification is made more complex by the well-known XPS multiplet splitting for these iron and manganese species [90,91,92]. XPS spectra of Fe2p, Mn2p, and As2p deconvolution of the FeMn-loaded AC, post-arsenic adsorption are depicted in Figure 13 as an example of the deconvolution of the relevant peaks for each activated carbon sample. The Fe2p, Mn2p, and As2p XPS spectra for the FeMn-Loaded AC pre-arsenic exposure, Fe-Loaded AC post-arsenic exposure and Mn-Loaded AC post-arsenic exposure can be found in Appendix A, Figure 39 **Figure A1: XPS deconvolution of the Fe2p (left) and Mn2p (right) peaks in the FeMn-Loaded AC pre-arsenic exposure.**, **Figure A2: XPS deconvolution of the Fe2p (left) and As2p (right) peaks in the Fe-Loaded AC post-arsenic exposure.**, and **Figure A3: XPS deconvolution of the Mn2p (left) and As2p (right) peaks in the Mn-Loaded AC post-arsenic exposure.**

One possible explanation of the increased arsenic adsorption observed in the metal-loaded activated carbons is arsenide formation. If arsenide formation was the reason for the increased adsorption, XPS spectra of the arsenic 2p 3/2 peak would show arsenides at a binding energy of 1322.9 eV [93]. Since no peaks are present in this region, arsenide formation does not occur and the enhanced adsorption observed must be through a different mechanism. Based on our characterization of the pre- and post-arsenic exposure

AC samples, with and without iron and manganese loading, we have concluded that an oxidation/reduction reaction is likely occurring.

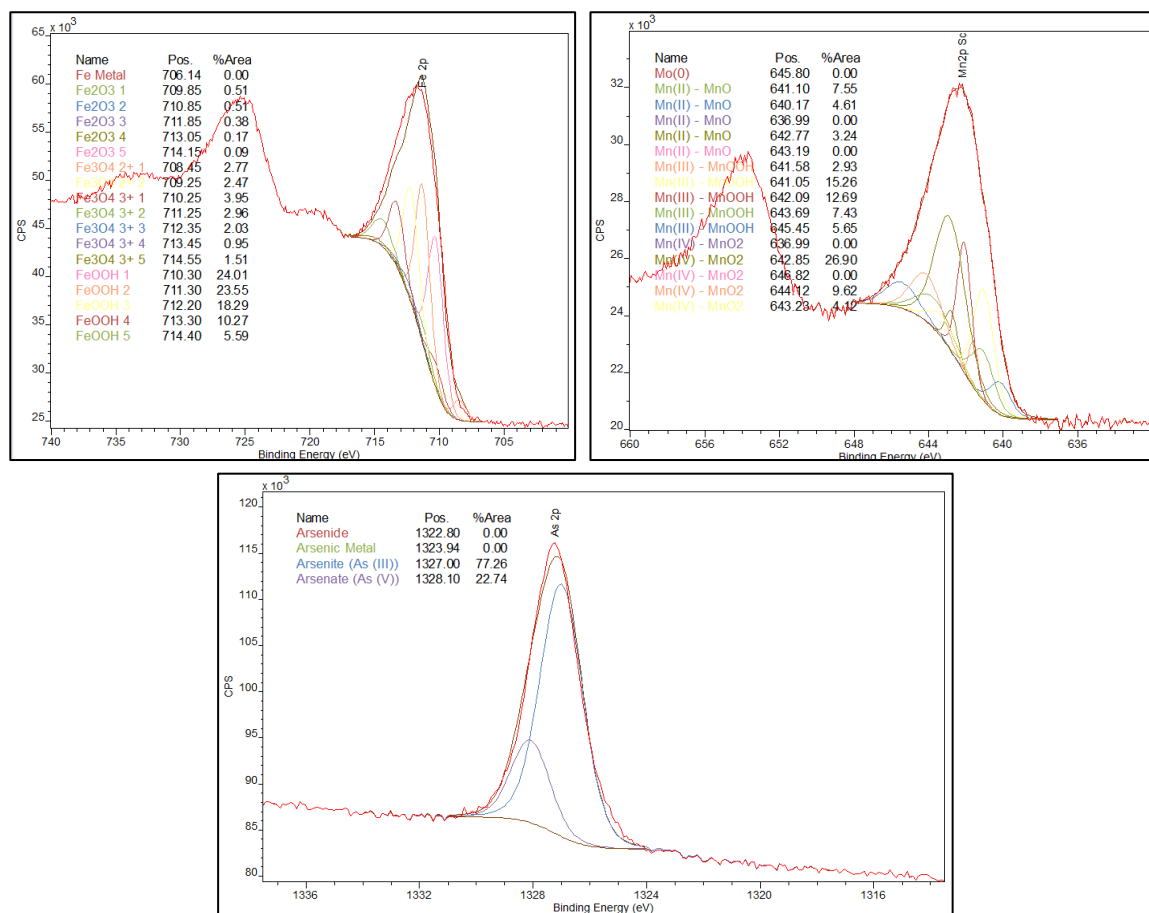


**Figure 13:** Deconvolution of the Fe (top Left), Mn (Top Right), and As (Bottom) XPS peaks in the FeMn-Loaded AC, post-As exposure.

This is consistent with the XPS results, particularly for the arsenic 2p 3/2 peaks which show that the arsenic species present on the surface of the activated carbon materials are reduced to arsenic (III). Table 13 provides the XPS deconvolution results for the metal-loaded activated carbon materials both pre- and post-arsenic adsorption. Table

14 provides the XPS survey scan results with elemental composition of the species listed as atomic percent.

**Table 13:** XPS species summary for metal-loaded activated carbons. [68,90,91,92,93,94,95].

Peak	Species	Binding Energies (eV)	FeMn AC Pre-As (% deconvolution)	FeMn AC Post-As (% deconvolution)	Fe AC Post-As (% deconvolution)	Mn AC Post-As (% deconvolution)
	Fe-Metal	706.14	0.00	0.00	0.00	-
Fe2p 3/2	Fe <sub>2</sub> O <sub>3</sub>	709.75; 710.75; 711.75; 712.95; 714.05	32.18	1.66	16.73	-
	Fe <sub>3</sub> O <sub>4</sub> <sup>2+</sup>	708.45; 709.25 710.25; 711.25;	4.61	5.24	5.43	-
	Fe <sub>3</sub> O <sub>4</sub> <sup>3+</sup>	712.35; 713.45; 714.55	10.04	11.40	11.81	-
	FeOOH	710.30; 711.30; 712.20; 713.30; 714.40	53.16	81.71	65.67	-
	Mn (0)	646.83	0.00	0.00	-	0.00
Mn2p 3/2	Mn (II) – MnO	640.49; 640.53; 641.62; 642.87; 644.05	26.82	15.40	-	8.25
	Mn (III) – MnOOH	641.09; 641.57; 642.17; 643.48; 646.05	39.98	43.96	-	48.24
	Mn (IV) – MnO <sub>2</sub>	642.00, 643.51, 643.66, 644.04, 644.87	33.20	40.64	-	43.51
	Arsenide	1322.90	-	0.00	0.00	0.00
As2p 3/2	Arsenic Metal	1323.90	-	0.00	0.00	0.00
	As (III)	1327.00	-	77.26	85.87	100
	As (V)	1328.10	-	22.74	14.13	0.00

**Table 14:** XPS survey scan breakdown for the various activated carbon materials.

Activated Carbon	C atomic %	O atomic %	Mn atomic %	Fe atomic %	As atomic %	Other (Si, S, K) atomic %
Standard AC:	78.88	17.44	0.10	0.29	0.43	2.86

---

Pre-As Exposure						
Standard AC: Post-As Exposure	60.89	30.45	0.17	0.03	4.06	4.40
FeMn-loaded AC: Pre-As Exposure	42.08	41.88	8.02	6.87	0.20	0.94
FeMn-loaded AC: Post-As Exposure	40.53	38.85	8.20	7.80	3.18	1.43
Fe-loaded AC: Post-As Exposure	28.90	49.36	0.21	6.80	7.51	7.21
Mn-loaded AC: Post-As Exposure	36.53	33.13	28.40	0.33	1.43	0.17

---

#### 4.3.6. Energy-Dispersive X-Ray Spectroscopy (EDS)

EDS was performed on the activated carbon samples to investigate the elemental distribution on the surface of the materials. In the Fe-Loaded AC, EDS shows that the iron on the activated carbon is distributed fairly evenly across the surface. There are small clumps of iron located on the surface in no particular pattern. This would be consistent with the small decrease in surface area observed between the standard activated carbon and the Fe-Loaded AC. Similarly, the Mn-Loaded AC shows fairly even distribution across the surface of the material but does show larger concentrations of manganese present around high concentrations of carbon. Again, this is consistent with the observed decrease in surface area where a much larger decrease is observed due to filling of these pores. In the FeMn-loaded AC, both iron and manganese distribution is heavily concentrated in the pores and spaces between clusters of carbon. This would be consistent with the significant decrease in the surface area as the iron and manganese block the access to these pores.

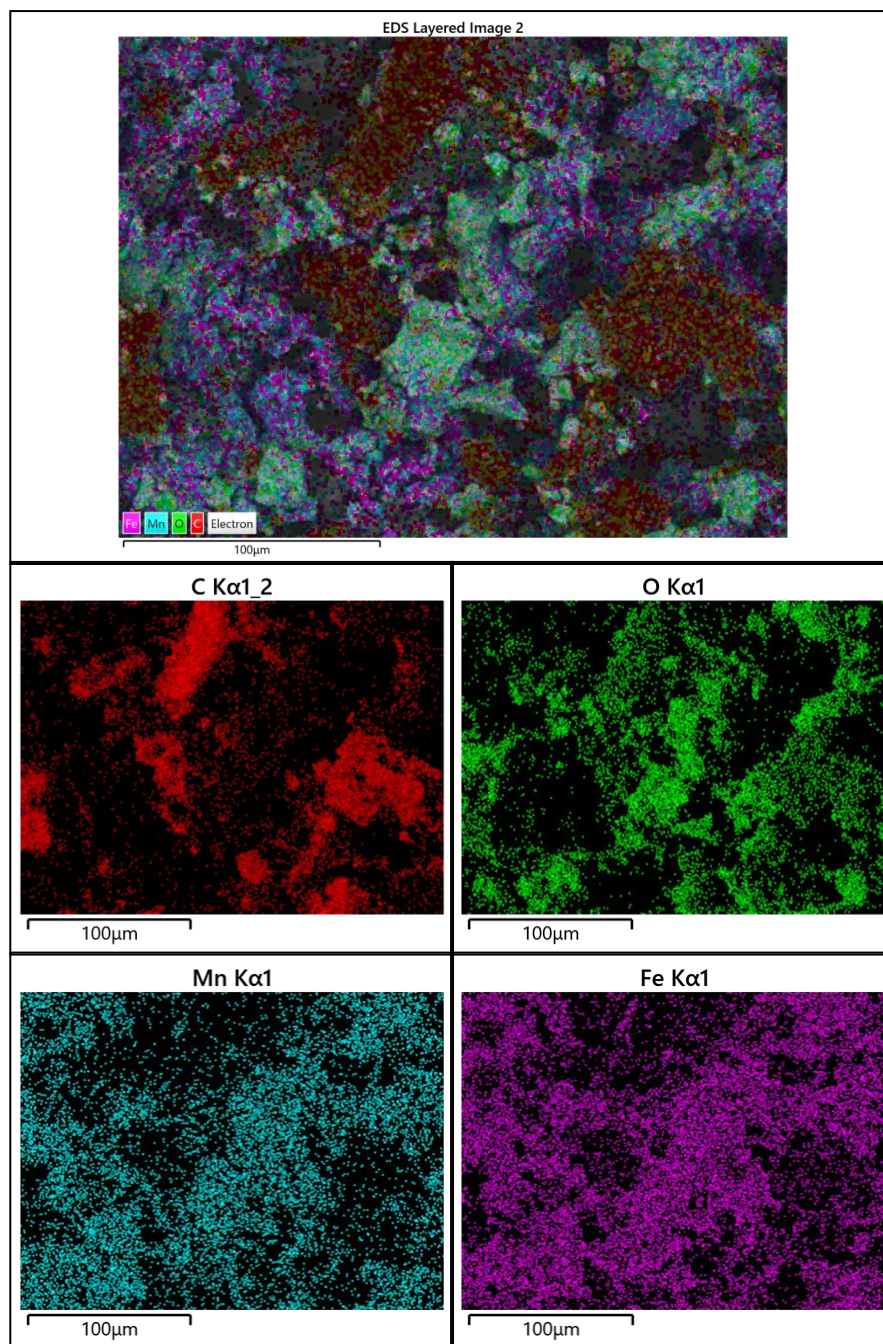


**Figure 14:** Elemental distribution mapping of carbon (Middle Left), oxygen (Middle Right), manganese (Bottom Left), and iron (Bottom Right) present within the FeMn-Loaded Activated Carbon. A layered distribution map of the surface's elemental composition is shown in the top figure.

Oxygen distribution in the iron-only sample seems to be mostly concentrated to the carbon clusters with small clusters of iron-oxides present in the sample. This is consistent with the XPS of the iron-only sample which shows the oxygen deconvolution is made primarily of carbon-oxygen species with metal oxides making up only 17.5% of the oxygen species present on the surface. Oxygen distribution in the manganese-only sample seems to be mostly concentrated to the carbon clusters with larger clusters of manganese-oxides present compared to the iron-only sample. This is again consistent with the XPS of the manganese-only samples where the majority of the oxygen deconvolution is carbon-oxygen species and the metal oxides make up 40.1% of the oxygen within the sample indicating slightly larger clusters of metal oxides compared to the iron-only sample. The FeMn-Loaded AC shows high concentrations of oxygen present where the carbon clusters are located but also significant concentrations of metal-oxide clusters. This is consistent with the XPS of the FeMn-Loaded AC where the majority of the oxygen deconvolution is the carbon-oxygen species with metal oxides making up 42.3% of the oxygen species as a mixture of clusters of iron-oxides and manganese-oxides. Figure 14 show the EDS images for the FeMn-Loaded AC at a magnification of 500. Appendix B, Figure 42

**Figure B1: Elemental distribution mapping of the carbon (bottom left), and oxygen (bottom right) present within the Standard AC at 500x magnification. A layered distribution map of the surface's elemental composition is shown at the top.,**

Figure B2: Elemental distribution mapping of carbon (middle left), oxygen (middle right), and iron (bottom) present within the Fe-Loaded activated carbon at 500x magnification. A layered distribution map of the surface's elemental composition is shown at the top., and Figure

**Figure B3: Elemental distribution mapping of carbon (middle left), oxygen (middle right), and manganese (bottom) present within the Mn-loaded activated carbon at 500x magnification. A layered**

distribution map of the surface's elemental composition is shown at the top. shows the EDS images for the Standard, Fe-Loaded and Mn-Loaded activated carbons. XPS deconvolution of the oxygen species is presented in Table 15, below. XPS images of the oxygen deconvolution of the Fe-, Mn-, and FeMn-Loaded ACs are presented in Appendix C, Figure 45 Figure C1: XPS deconvolution of the O1s peak for the Fe-Loaded AC., Figure Figure C2: XPS deconvolution of the O1s peak for the Mn-Loaded AC., and Figure Figure C3: XPS deconvolution of the O1s peak for the FeMn-Loaded AC.

**Table 15:** O1s deconvolution of the metal-loaded activated carbons [67,68]

Species	Binding Energy	Fe-loaded AC (% deconvolution)	Mn-Loaded AC (% deconvolution)	FeMn-loaded AC (% deconvolution)
C=O (aliphatic), -O-(C=O)	532.50	0.00	1.25	0.00
C=O (aromatic)	531.40	72.33	49.26	47.65
O <sub>2</sub> /C	537.70	0.56	0.00	0.36
-O-(C=O)-O- (C=O)-O- (C=O)-	535.60	1.86	0.04	3.35
C-OH (aliphatic)	532.92	1.89	4.03	0.12
C-OH (aromatic)	533.65	3.78	3.62	4.76
O-(C=O)-C (aliphatic)	534.70	0.26	0.02	1.07
SiO <sub>2</sub>	532.67	1.82	1.72	0.40
Metal Oxides	529.78	17.50	40.06	42.29

#### 4.3.7. Scanning Electron Microscope (SEM) Images

SEM images of the activated carbon materials were obtained at magnifications of between 150, and 15000 times. The SEM images of the standard activated carbon show the extremely porous surface of the material. All pores that are observed in the SEM

images are macropores as the smallest visible pore (in the standard AC 15000 magnification) is approximately 250 nm in diameter, shown in Figure 15.

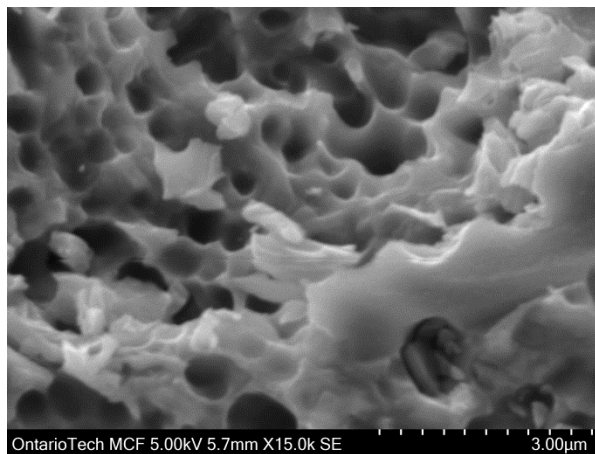


**Figure 15:** SEM imaging (Magnification x15000) of the Standard Activated Carbon to show the smallest pore size visible with the SEM images obtained.

The SEM images of the Fe-Loaded (Figure 16) AC show a much less porous surface. Pores and cracks in the surface are visible; however the iron loaded onto the surface blocks the majority of the pore structure. This is consistent with the decreased pore volume observed in the Fe-Loaded sample. The SEM images of the Mn-Loaded AC show almost no visible pores as the manganese blocks almost all of the pore structure; again this is consistent with the observed decrease in the pore volume from the nitrogen adsorption measurements. The SEM images of the FeMn-Loaded AC shows a significant amount of macropores within the material with the material itself being made of much smaller particles than the other activated carbons which consisted of larger chunks.

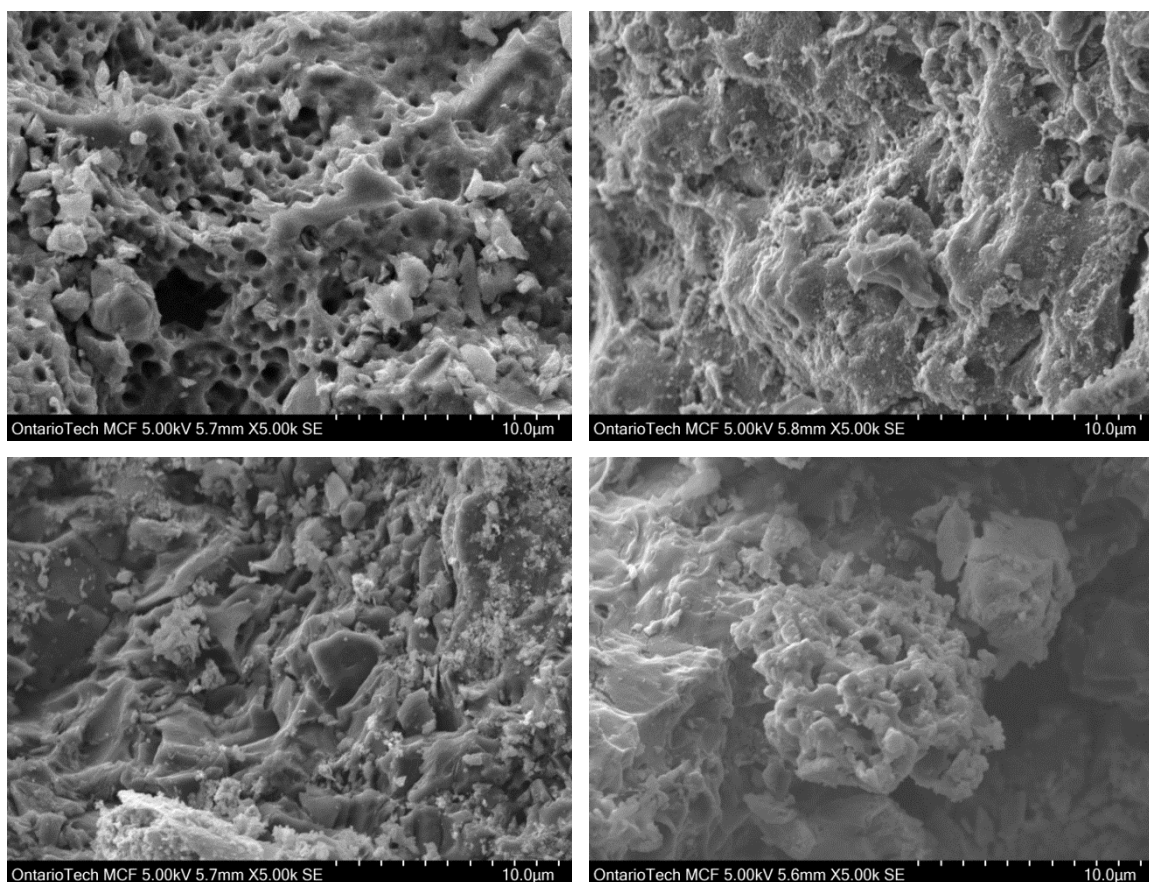


**Figure 16:** SEM imaging (Magnification x5000) of the Standard (top left), Fe-Loaded (top right), Mn-loaded (bottom left), and FeMn-loaded Activated Carbons used in this study.

#### 4.3.8. Proposed Mechanisms: Iron-Based Arsenic Adsorption

Investigating the XPS results presented in Table 13, it can be observed that the iron species on the surface of the pre-arsenic-exposed FeMn-Loaded AC are mainly  $\text{Fe}_2\text{O}_3$  and  $\text{FeOOH}$  species, comprising 32% and 53% of the iron species, respectively. After arsenic exposure, these percentages significantly change to 1.7%  $\text{Fe}_2\text{O}_3$  and 82%  $\text{FeOOH}$ . Speciation of the arsenic (V) in a pH 3.0 solution is known to be  $\text{H}_2\text{AsO}_4^-$ , and XPS of the  $\text{As}2p\ 3/2$  peak post-adsorption shows that arsenic (V) is significantly reduced to arsenic (III) during the adsorption process.

During the functionalization process iron is loaded onto the surface of the activated carbon and is physisorbed to the surface through dipole-dipole intermolecular forces, as shown in Figure 17A where R represents the activated carbon. While some of the arsenic (V) is shown in the XPS to physisorb to the surface without being reduced, arsenic (V) is more likely to be reduced to arsenic (III) prior to adsorption due to the highly oxophilic character of the iron. The highly oxophilic character of iron would be an ideal surface for the negatively charged oxygen of the arsenic to form an iron-oxide bond, breaking the  $\text{Fe}_2\text{O}_3$  species into an  $\text{FeOO}^-$  that can be hydrolyzed to  $\text{FeOOH}$  and an intermediate species where arsenic and iron are bound through a shared oxygen as shown in Figure 17B. This intermediate would be quickly broken by electrons in the activated carbon using the iron as a conductor through which the electrons can freely flow to the arsenic and reduce the arsenic species from arsenic (V) to arsenic (III). The iron in this case acts only as a pathway for the electrons to flow with the activated carbon itself acting as the reducing agent. This is known based on the XPS speciation of iron where Fe (III) remains as Fe (III), indicating that it is not acting as the reducing agent but rather as a shuttle for the electrons to reach the arsenic. In this reduction process, the chemical bond of the arsenic would be broken from the shared oxygen on the iron species and the reduced arsenic (III) species would be physisorbed through hydrogen bonding to the iron-loaded surface of the activated carbon as observed in Figure 17C.

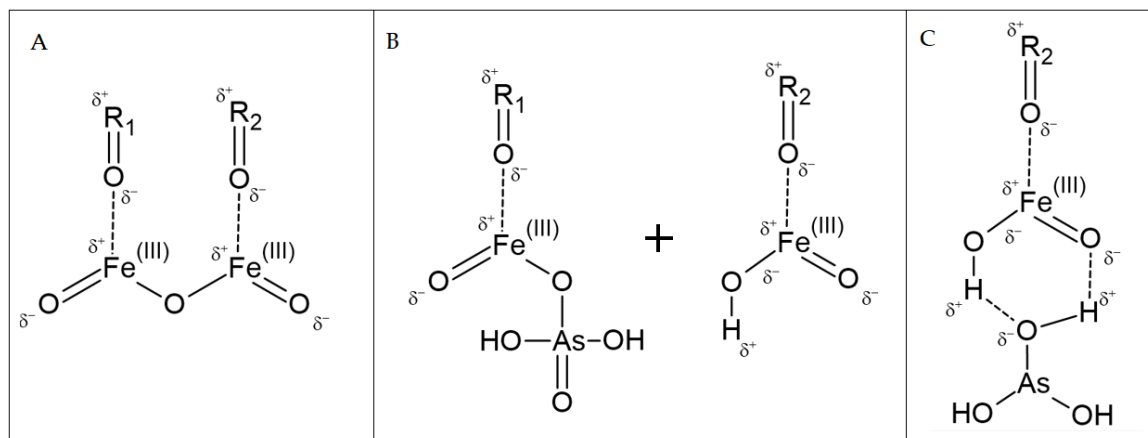


**Figure 17:** **A)** Shows the iron physisorbed to the surface of the activated carbon. **B)** Shows the two iron products, FeOOH, and the Intermediate FeO-O-AsH<sub>2</sub>O<sub>3</sub>, formed as a result of the exposure to arsenic. **C)** Shows the reduced As (III), as a result of the electron flow from the activated carbon through the iron, physisorbed to the iron-loaded surface through Hydrogen Bonding.

This series of events would be consistent with the decrease in the Fe<sub>2</sub>O<sub>3</sub> species and the increase in the FeOOH species observed due to the adsorption of arsenic. It would also be consistent with the observed reduction of the arsenic (V) species to arsenic (III) observed in the XPS. Finally, it would explain how the arsenic (V) species is being reduced to arsenic (III) without observing a change in the iron speciation; the iron is simply being used as a conduit for electrons to flow from the activated carbon, to the arsenic. The higher adsorption capacity observed in this study due to the iron-loading on the activated carbon surface is consistent with previous literature on the adsorption of arsenic using iron nanoparticles where iron oxide nanoparticles are shown to be highly efficient adsorbents for both arsenic (III) and arsenic (V) [96,97].

#### 4.3.9. Proposed Mechanisms: Manganese-Based Arsenic Adsorption

Investigating the XPS results in Table 13, it can be observed that a significant decrease in the MnO species is observed, from 27% pre-exposure to 15% post-exposure. This decrease in the MnO species leads to an increase in both the MnOOH and MnO<sub>2</sub>

species present on the activated carbon. In a fashion similar to the iron-based arsenic adsorption, during functionalization of the activated carbon, MnO is physisorbed to the activated carbon surface through dipole-dipole interactions. Unlike iron, in the case of manganese, two different processes can be observed. The first process is the oxidation of manganese (II) to manganese (III). In this process, the arsenic takes one electron from two different manganese molecules as observed in the redox reaction equation shown in Figure 18A. This reaction would use the manganese as a reducing agent to reduce arsenic (V) to arsenic (III) that would be physisorbed through hydrogen bonding to the MnOOH species that would be formed from this process as observed in Figure 19A.

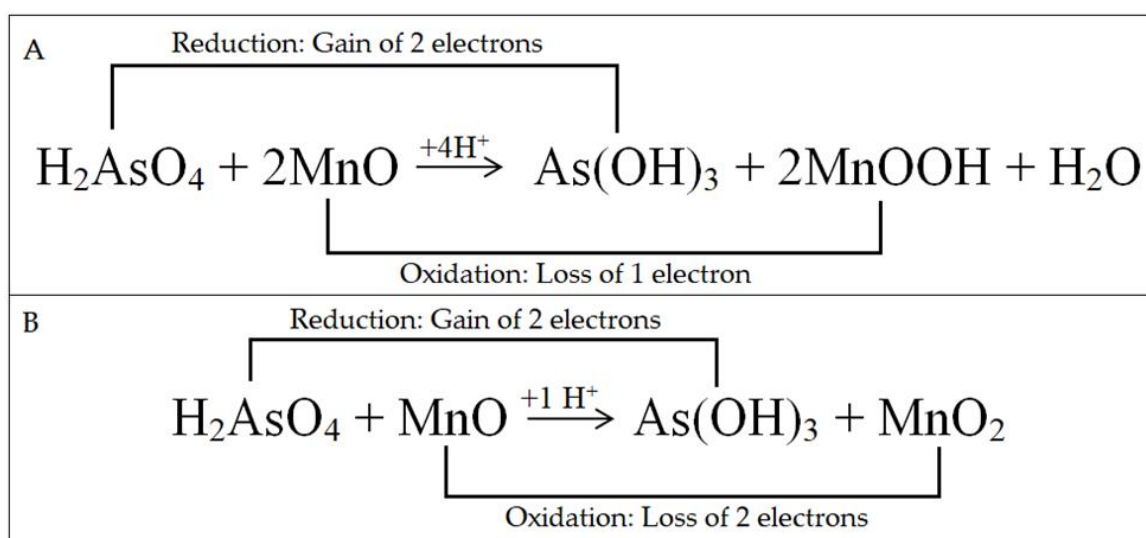


**Figure 18:** **A)** Shows the redox reaction between As (V) and Mn (II) where As (V) is reduced to As (III) and Mn (II) is oxidized to Mn (III). **B)** Shows the redox reaction between As (V) and Mn (II) where As (V) is reduced to As (III) and Mn (II) is oxidized to Mn (IV).

The second process is the oxidation of manganese (II) to manganese (IV). In this process, the arsenic would take both electrons from a manganese molecule as observed in the redox reaction equation shown in Figure 18B. This process would use the manganese as a reducing agent to reduce arsenic (V) to arsenic (III) that would be physisorbed

through hydrogen bonding to the  $\text{MnO}_2$  species that would be formed from this process as observed in Figure 19B. This series of events would be consistent with the decrease observed in the  $\text{MnO}$  species and the increases observed in the  $\text{MnOOH}$  and the  $\text{MnO}_2$  species. It would also be consistent with the observed reduction of arsenic (V) to arsenic (III). Unlike the iron-based adsorption proposed above, the activated carbon is not involved in the redox process of adsorption as is observed in the iron-based adsorption. The activated carbon, in this case, is providing an important surface on which the chemistry can occur so that the arsenic can be adsorbed and removed from solution.

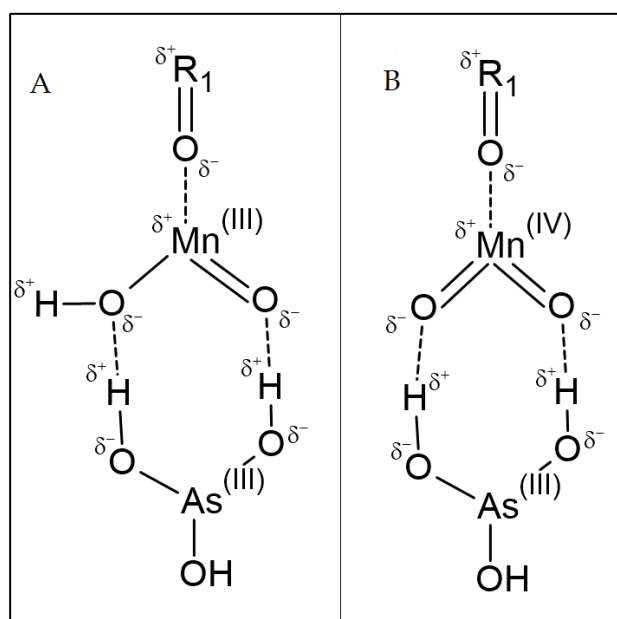


**Figure 19:** A) Shows the product of reaction (1) where  $\text{MnO}$  is oxidized to  $\text{MnOOH}$ . B) Shows the product of reaction (2) where  $\text{MnO}$  is oxidized to  $\text{MnO}_2$ . As (III) is physisorbed to the Mn-Loaded AC surface through Hydrogen Bonding.

#### 4.3.10. Arsenic Kinetics: As (V) Kinetics Curves

Adsorption kinetics of arsenic (V) using the metal-loaded activated carbons, standard activated carbon, and commercial activated carbon were evaluated and the

results are shown in Figure 20. For each of the carbon materials, adsorption of the arsenic (V) reaches equilibrium after six hours. The Standard Activated Carbon shows the lowest adsorption capacity, reaching  $8.1 \pm 0.2\%$  of the total possible adsorption after six hours. The Fe-Loaded AC and Mn-Loaded AC both show higher adsorption capacities than the Standard AC, showing that metal-loading of the surface does improve the adsorption capacity of the activated carbon. The Fe-Loaded and Mn-Loaded activated carbons show significant improvements over the standard activated carbon with regards to adsorption of arsenic both at short and long stirring times, reaching  $19.9 \pm 0.7\%$  and  $23.2 \pm 0.2\%$ , respectively after 6 hours. The combined iron-manganese loaded activated carbon shows the highest adsorption capacity with adsorption after six hours reaching  $50.9 \pm 1.2\%$ . This shows a significant improvement over both the Standard Activated Carbon and the single-metal loaded activated carbons. The binary system of the iron-manganese loaded activated carbon works together, using all of the adsorption mechanisms presented above in the adsorption process, allowing the adsorption capacity to increase more than that of the single-metal loaded activated carbon materials.

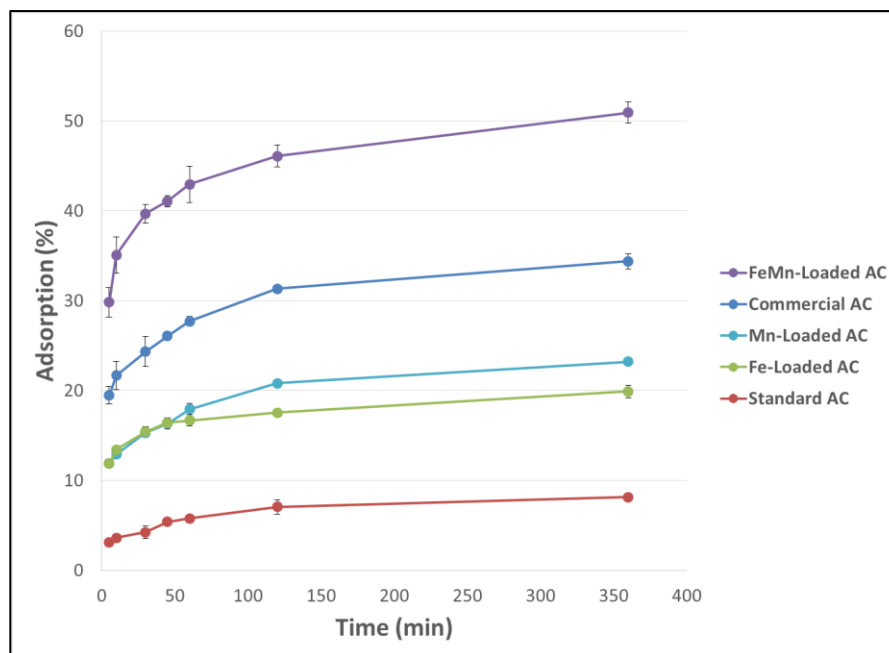


**Figure 20:** Kinetics curves of As (V) adsorption for the various activated carbons investigated. Arsenic adsorption is given in percent adsorption with a maximum adsorption (i.e. 100%) of 25 mg/g.

#### 4.3.11. Arsenic Kinetics: Arsenic (V) Kinetic Modelling

Pseudo first-order and pseudo second-order kinetic modelling was performed on each of the activated carbons following adsorption kinetic modelling. Modelling was performed using the data provided in Figure 20. A review article by Tran et al. [70] provides information regarding modelling of kinetic data. Tran et al. mentions the original work by Lagergren in 1898 who first presented the first-order rate equation, where the pseudo first-order kinetic modelling should be linear with respect to Equation 1 [98]:

$$\ln[q_e - q(t)] = -k_1 t + \ln(q_e) \quad (1)$$

where  $q(t)$  and  $q_e$  are the amount (in mg/g) of adsorbate adsorbed at any given time,  $t$ , and at equilibrium, respectively, and where  $k_1$  is the rate constant for the pseudo first-order kinetic model. Tran et al. also mentions Blanchard et al. who initially proposed

the second-order rate equation in 1984 for the removal of heavy metals in water and that the pseudo second-order kinetic model should be linear with respect to Equation 2 [99]:

$$\frac{t}{q(t)} = \left(\frac{1}{q_e}\right)t + \frac{1}{k_2 q_e^2} \quad (2)$$

where  $q(t)$  and  $q_e$  are the amount (in mg/g) of adsorbate adsorbed at any given time,  $t$ , and at equilibrium, respectively, and where  $k_2$  is the rate constant for the pseudo second-order kinetic model. Table 16 provides a summary of the kinetic modelling for each of the activated carbons used in this study.

**Table 16:** A summary of the Pseudo First- and Pseudo Second-Order kinetic modelling for the activated carbons used for arsenic (V) adsorption.

Activated Carbon:	PFO or PSO Model	Model Equation	Linearity ( $R^2$ ) of the Model	$k$ Value	$q_e$ Value (mg/g)	
					1 <sup>st</sup> order units (1/s)	2 <sup>nd</sup> order units 1/(M*s)
Commercial AC	First	$y = -7.9 \times 10^{-3}x + 1.0677$	0.8550	$7.9 \times 10^{-3}$	2.91	8.46 ± 0.34
	Second	$y = 0.1161x + 1.2845$	0.9968	0.0105	8.61	
Standard AC	First	$y = -0.0135x + 0.2616$	0.9955	0.0135	1.30	2.08 ± 0.11
	Second	$y = 0.4605x + 9.0164$	0.9967	0.0235	2.17	
Fe-Loaded AC	First	$y = -9.9 \times 10^{-3}x + 0.5587$	0.9330	$9.9 \times 10^{-3}$	1.75	4.86 ± 0.17
	Second	$y = 0.2019x + 2.1041$	0.9980	0.0190	4.95	
Mn-Loaded AC	First	$y = -0.0105x + 1.1712$	0.9953	0.0105	3.23	6.02 ± 0.16
	Second	$y = 0.1599x + 3.0148$	0.9948	$8.5 \times 10^{-3}$	6.25	
FeMn-Loaded AC	First	$y = -6.7 \times 10^{-3}x + 1.532$	0.8416	$6.7 \times 10^{-3}$	4.63	12.88 ± 0.58
	Second	$y = 0.0762x +$	0.9951	$5.9 \times 10^{-3}$	13.12	

0.9768

---

Modelling of kinetic data provides information regarding the adsorption process of the reaction. The pseudo first-order kinetic modelling assumes that one of the reactants or analytes is present in excess while the pseudo second-order kinetics assumes that the rate-limiting step in the reaction or adsorption is the chemical adsorption itself [55,70]. This would indicate that the adsorption rate is dependent on the adsorption capacity of the adsorbent rather than the concentration of the adsorbate.

The Commercial AC, Fe-Loaded AC, and FeMn-Loaded ACs all fit pseudo second-order kinetic modelling better than the pseudo first-order modelling. This is clear by the linear correlation observed in the models, for example, 0.9968 in the pseudo second-order model of the Commercial AC versus 0.8550 in the pseudo first-order model. This is also consistent with the model  $q_e$  value obtained compared to the experimental  $q_e$  value for the activated carbon materials. For example, the FeMn-Loaded AC has an experimental  $q_e$  of  $12.9 \pm 0.6$  mg/g after 6 hours while the pseudo first-order model  $q_e$  is 4.6 mg/g and the pseudo second-order model  $q_e$  is 13.1 mg/g. This indicates that these materials follow pseudo second-order modelling as the experimental  $q_e$  value is significantly different than the first-order model and is comparable to the second-order model.

The Standard AC and the Mn-Loaded AC fits both the pseudo-first and pseudo second-order kinetic models based on linear correlation of the models. For example, linearity observed for the Standard AC in the first-order model is 0.9955 and in the second-order model is 0.9967, indicating a high degree of linearity for both models. The

biggest difference between the two models is the calculated  $q_e$  value. In the pseudo first-order model of the Standard AC,  $q_e$  is calculated to be 1.3 mg/g, while in the pseudo second-order model,  $q_e$  is calculated to be 2.2 mg/g. The calculated  $q_e$  value from the pseudo second-order kinetic model is closer to the experimental  $q_e$  obtained after 6 hours of  $2.1 \pm 0.1$  mg/g indicating that the standard activated carbon has a better fit to the pseudo second-order modelling. This is also observed for the Mn-Loaded AC where  $q_e$  for the pseudo first-order model is 3.2 mg/g and 6.3 mg/g for the pseudo second-order model. The pseudo first-order model  $q_e$  is significantly different than the experimental  $q_e$  of  $6.0 \pm 0.2$  mg/g while the experimental  $q_e$  is consistent with the second-order model.

Based on the kinetic modelling, all of the materials investigated in this study follow pseudo second-order kinetics more consistently than pseudo first-order modelling, indicating that the rate of adsorption is dependent the adsorption capacity of the material for adsorption of arsenic, not on the concentration of the arsenic. Figure 21, below, provides an example of the pseudo first- and pseudo second-order kinetic modelling of the FeMn-Loaded AC. Appendix D, Figure 48 **Figure D1: Pseudo First- (left) and Pseudo Second- (right) Order kinetic models for the adsorption of As (V) using the Standard AC.**, Figure

**Figure D2: Pseudo First- (left) and Pseudo Second- (right) Order kinetic models for the adsorption of As (V) using the Commercial AC.**, Figure **Figure D3: Pseudo First- (left) and Pseudo Second- (right) Order kinetic models for the adsorption of As (V) using the Fe-Loaded AC.**, and Figure **Figure D4: Pseudo First- (left) and Pseudo Second- (right) Order kinetic models for the adsorption of As (V) using the Mn-Loaded AC.** show the pseudo first- and pseudo second-order kinetic models of the other activated carbon materials.

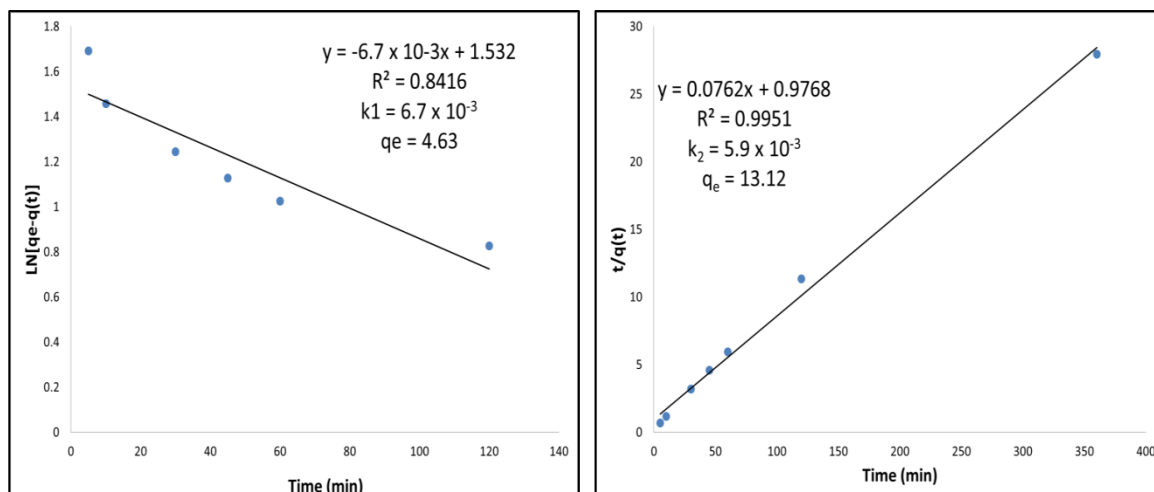


**Figure 21:** Pseudo First- (Left) and Pseudo Second- (Right) Order kinetic modelling of the As (V) adsorption using the FeMn-Loaded AC.

#### 4.3.12. Arsenic Kinetics: As (III) Kinetics Curves

To demonstrate that the FeMn-Loaded AC was effective for arsenic (III) adsorption without the need for oxidation, adsorption kinetics of arsenic (III) were obtained for the FeMn-Loaded AC and compared to the arsenic (III) kinetics of the Standard AC, and Commercial AC. As expected, the maximum arsenic (III) adsorption was lower than the maximum arsenic (V) adsorption, despite having a longer adsorption period. This is consistent with previous research in the literature stating arsenic (III) must generally be oxidized to arsenic (V) before removal as adsorption is very efficient for the pentavalent arsenic species but not the trivalent arsenic species on most adsorbent materials [100]. The adsorption of arsenic (III) being slower than the adsorption of arsenic (V) makes sense as we know that the rate of adsorption is dependent on the adsorption capacity of the material for the adsorption of arsenic. Since the adsorption capacity of the material for arsenic (III) adsorption is lower than that of arsenic (V) and the rate of adsorption is dependent on the adsorption capacity, it stands that the arsenic (III) adsorption would be slower than the arsenic (V) adsorption. Once again, the metal-

loaded activated carbon presented in this work out-performs the adsorption capacity of the standard activated carbon and the commercial benchmark, reaching  $37.2 \pm 2.0\%$  total arsenic (III) adsorption ( $9.3 \pm 0.6$  mg/g) compared to the  $15.1 \pm 0.1\%$  ( $3.6 \pm 0.1$  mg/g) and  $12.8 \pm 0.8\%$  ( $2.9 \pm 0.1$  mg/g) observed in the Standard and Commercial Activated Carbons, respectively. Kinetics curves for arsenic (III) adsorption are given in Figure 22.

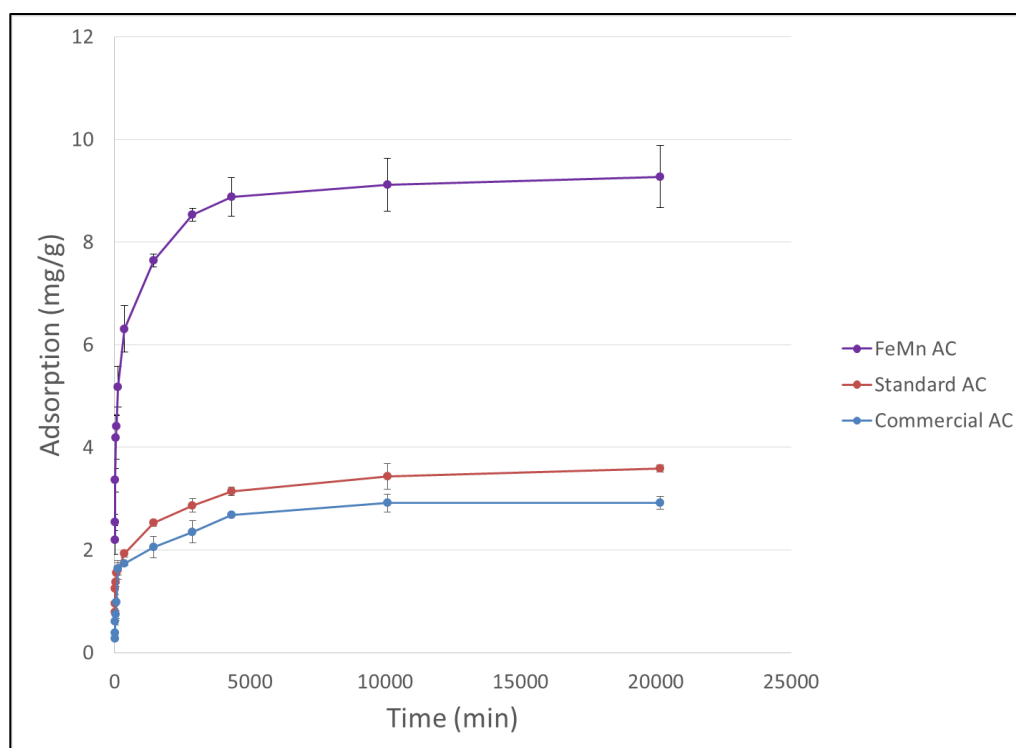


**Figure 22:** Kinetics curves of the As (III) adsorption using the FeMn-Loaded, Standard, and Commercial Activated Carbons.

#### 4.3.13. Arsenic Kinetics: As (III) Kinetic Modelling

Kinetic modelling of the arsenic (III) kinetics curves was also done using the kinetic modelling described in 4.3.11. Table 17 provides a summary of the kinetic modelling for the adsorption of arsenic (III).

**Table 17:** A summary of the Pseudo First- and Pseudo Second-Order kinetic modelling for the activated carbons used for the arsenic (III) adsorption.

Activated Carbon:	PFO or PSO Model	Model Equation	Linearity ( $R^2$ ) of the Model	$k$ Value	$q_e$ Value (mg/g)	$q_e$ Experimental (mg/g)
Commercial AC	First	$y = -8.23 \times 10^{-4}x + 0.9304$	0.9515	$8.23 \times 10^{-4}$	2.54	$2.92 \pm 0.12$
	Second	$y = 0.3399x + 80.979$	0.9986	0.0123	2.94	
Standard AC	First	$y = -2.87 \times 10^{-4}x + 0.7332$	0.9450	$2.78 \times 10^{-4}$	2.08	$3.59 \pm 0.43$
	Second	$y = 0.2789x + 71.431$	0.9981	0.0140	3.59	
FeMn-Loaded AC	First	$y = -3.85 \times 10^{-4}x + 1.4759$	0.8701	$3.85 \times 10^{-4}$	4.37	$9.28 \pm 0.61$
	Second	$y = 0.1076x + 13.34$	0.9997	0.0750	9.29	

All three activated carbons investigated for arsenic (III) adsorption very clearly follow pseudo second-order kinetic modelling. This is evident due to their strong linear correlation to the second-order modelling. This is also evident when comparing the calculated  $q_e$  values to the experimental  $q_e$  values for each activated carbon. For the Commercial Activated Carbon, experimental  $q_e$  was  $2.9 \pm 0.1$  mg/g, for the Standard AC,  $3.6 \pm 0.4$  mg/g, and for the FeMn-Loaded AC,  $9.3 \pm 0.6$  mg/g. When comparing these to the modelling  $q_e$  values, there is a significant difference observed between the pseudo first-order  $q_e$  values and the experimental values while no significant difference is observed between the experimental  $q_e$  and the pseudo second-order model  $q_e$  values. This implies that the rate-limiting factor is the adsorption capacity of the arsenic (III) onto the activated carbon itself, rather than the adsorbate or adsorbent being present in excess. Kinetic modelling of the activated carbons for arsenic (III) adsorption kinetics are provided in Appendix E, Figure 52 Figure E1: **Pseudo First- (left) and Pseudo Second- (right)**

**Order kinetic models for the adsorption of As (III) using the Standard AC., Figure E2: Pseudo First- (left) and Pseudo Second- (right) Order kinetic models for the adsorption of As (III) using the Commercial AC., and Figure E3: Pseudo First- (left) and Pseudo Second- (right) Order kinetic models for the adsorption of As (III) using the FeMn-Loaded AC..**

#### **4.3.14. Literature Comparison**

As indicated in Table 18, many studies have been done to investigate the adsorption of arsenic using various adsorbent materials. While the activated carbon materials presented in this study outperform some adsorbents outlined in the literature, it is outperformed by others. Despite being outperformed by some adsorbent materials presented in the literature, this activated carbon is a cost-effective and efficient means of removing arsenic from acidic waters. The abundance of the feedstock and the high carbon content in the raw feedstock allows for the adsorbent to be produced with lower costs associated and resources allocated to the preparation of the material. In addition, intentionally low amounts of KOH are used to activate the material with parallel studies investigating the potential for KOH recycling to further increase the cost-effectiveness of the material.

**Table 18:** Comparison of petroleum coke derived activated carbons for As (V) and As (III) adsorption with other studies in the literature.

<b>Material</b>	<b>As (V) Adsorption Capacity (mg/g)</b>	<b>As (III) Adsorption Capacity (mg/g)</b>	<b>pH</b>	<b>Surface Area (m<sup>2</sup>/g)</b>	<b>References</b>
Standard AC	2.08 ± 0.11	3.59 ± 0.43	3.0, 3.0	975 ± 19	This study
Fe-loaded AC	4.86 ± 0.17	-	3.0, 3.0	748 ± 13	This study
Mn-loaded AC	6.02 ± 0.16	-	3.0, 3.0	487 ± 15	This study
FeMn-loaded AC	12.88 ± 0.58	9.28 ± 0.61	3.0, 3.0	397 ± 11	This study
Commercial AC	8.46 ± 0.34	2.92 ± 0.12	3.0, 3.0	1329 ± 38	This study
Granular Ferric Hydroxide	29.07	-	6.0	306	81
MIRESORB™	50.38	-	6.0	233	
UiO-66- NDC/GO	147.06	-	3.0	279.77	82
Saxaul Ash	4.203	-	7.0	Not reported	83
Diatom Silica Shells	-	10.99	4.0	7.30 ± 0.03	85
Iron Oxide/ 12x40 Granular Coconut AC Composite	0.4123 1.0389 2.0716	- - -	2.0 5.0 10.0	678.3	86
Biosorbent Egg Shell	8.43 ± 2.1	11.69 ± 2.5	4.1, 7.0	7.91 ± 0.49	
Biosorbent Java Plum Seed	4.62 ± 0.43	4.63 ± 0.65	5.3, 7.0	6.99 ± 0.61	
Biosorbent Water Chestnut Shell	7.73 ± 0.9	9.61 ± 1.21	4.1, 7.0	6.91 ± 0.42	
Biosorbent Corn Cob	5.71 ± 0.32	4.33 ± 0.76	6.0, 7.0	4.16 ± 0.57	101
Biosorbent Tea Waste	4.92 ± 1.21	7.36 ± 1.28	4.1, 7.0	4.03 ± 0.61	
Biosorbent Pomegranate Peel	4.50 ± 0.42	5.57 ± 1.28	4.1, 9.0	3.96 ± 0.72	

#### ***4.4. Conclusion***

An efficient activated carbon produced using minimal KOH activating agent and a readily available petcoke feedstock was used for arsenic (V) and arsenic (III) adsorption using metal-doped activated carbons. Metal loading of the activated carbons resulted in a significant increase in the adsorption capacity for arsenic, surpassing that of the benchmark commercial activated carbon. Adsorption capacity comparisons normalized to surface area and microporosity indicate that functionality of the activated carbon's surface is a more crucial factor in adsorption than high surface area or extensive microporosity. Adsorption of arsenic in the binary FeMn-Loaded AC far exceeded those of the other activated carbons investigated. XPS of the activated carbons showed significant changes in the speciation of the iron and manganese present on the activated carbon post-arsenic exposure, leading to the conclusion that arsenic is being physisorbed to the metal-loaded surface through redox reactions. The petroleum coke activated carbon produced using this method is effective in the adsorption of arsenic species in solution and is a cost-effective method for the removal of arsenic contamination in waters using excess petroleum coke.

**Chapter 5: Binary Mixture As:Cr Study  
Published as: The Investigation of the Co-  
Adsorptive Relationship between Arsenic (V)  
and Chromium (VI) Using a Petroleum Coke  
Sourced Activated Carbon**

Type: Original Research Article

Submitted to: Not Yet Submitted

Status: Pending

Authors: Kyle S. Fisher<sup>1</sup> and Andrew J. Vreugdenhil<sup>1,2</sup>

<sup>1</sup> Materials Science Graduate Program, Trent University, Peterborough, Ontario, Canada, 1600 W Bank Drive, K9L 0G2.

<sup>2</sup> Department of Chemistry, Trent University, Peterborough, Ontario, Canada, 1600 W Bank Drive, K9L 0G2.

## ***Abstract***

This study aims to investigate the co-adsorptive relationship between chromium and arsenic in solution. In this study, petroleum coke activated carbon is used for the adsorption of arsenic (V) and chromium (VI) in mixed solutions to determine the extent of the competition/co-adsorption onto the surface binding site. It has been shown that chromium (VI) is adsorbed onto the surface through a reduction process involving conversion of the hydroxyl functional groups on the AC surface to carbonyl functional groups with reduction of the chromium (VI) species to chromium (III). It is also known that arsenic is adsorbed to the AC surface through a redox reaction between the hydroxyl functional groups on the surface. This reduces arsenic (V) to arsenic (III) and oxidizing the hydroxyl groups to carbonyl groups. As such, competition between the chromium and arsenic should be observed as they are competing for the same binding site; however, rather than competition between the species, a co-adsorptive relationship was observed. At low concentrations of chromium, the arsenic in solution is able to act as a ligand to form a hybrid transition-metal, main-group complex with the chromium. This allows for the arsenic to be pulled from solution as the chromium is adsorbed onto the surface. In acidic solutions, this co-adsorption phenomenon is reduced as the concentration of chromium increases in solution and competition emerges between excess chromium and the chromium-arsenic complex. This is due to the fact that these solutions follow the Langmuir isotherm model, indicating that once an adsorbate molecule has been adsorbed to a binding site, that binding site is no longer available for the adsorption of other adsorbate molecules. Unlike acidic solutions, in neutral solutions, this co-adsorption phenomenon is not reduced as the concentration of chromium is increased because the

neutral solutions follow Freundlich isotherm modelling, indicating that multilayer adsorption occurs at neutral pHs. Therefore, the adsorbate molecules in solution are able to undergo multilayer adsorption, allowing both the chromium-arsenic complexes and the excess chromium molecules onto the AC surface, eliminating competition between the species.

***Keywords***

Adsorption; Co-adsorption; Arsenic (V); Chromium (VI); Activated Carbon; Petroleum  
Coke; Isotherm Modelling; Kinetic Modelling

## ***5.1. Introduction***

Household plumbing, mining operations, natural mineral deposits, cement plants, and electronic waste are all potential sources of heavy metal contamination in groundwater and other water supplies [4]. The global mining market represents one of the largest markets in the world and in 2022 was estimated to be worth 2.0 trillion USD and is forecasted to grow to 2.8 trillion USD by 2027 [102]. Wastewater from the hard rock mining and oil and gas mining industries around the world contribute significantly to the potential contamination of groundwater supplies.

Mine tailings produced from the refining processes contain significantly high concentrations of heavy metals including arsenic (As) and chromium (Cr) [103]. The World Health Organization (WHO) has reported that over 140 million people across 50 countries have drinking water that contains arsenic concentrations above 10 ug/L, which is above the WHO's accepted concentration level of arsenic in drinking water [79,80]. The Government of Canada has an accepted concentration level of total chromium in drinking water of 100 ug/L [58]. These accepted concentration levels are significantly surpassed in mine tailings around the world leading to the contamination of nearby groundwater and drinking water supplies. Chromium and arsenic often appear together in the tailings of gold mines. Chromium generally appears as chromate ( $\text{Cr}_2\text{O}_4^{2-}$ ) or dichromate ( $\text{Cr}_2\text{O}_7^{2-}$ ) species in minerals such as chromite ( $\text{FeCr}_2\text{O}_4$ ,  $\text{MgCr}_2\text{O}_4$ , and/or  $\text{AlCr}_2\text{O}_4$ ) [22]. Arsenic generally appears in the mineral arsenopyrite ( $\text{FeSAs}$ ) where arsenic is in the  $\text{As}^{1-}$  oxidation state; however, in the presence of water and oxygen, the arsenic in arsenopyrite rapidly oxidizes to  $\text{As}^{3+}$  and/or  $\text{As}^{5+}$  species to form scorodite

( $\text{FeAsO}_4 \cdot 2\text{H}_2\text{O}$ ) or iron (III) arsenate [22,104]. Beaver Mine in Cobalt, Ontario, Canada, is a silver and cobalt mine that contains arsenic. Mine tailings have arsenic concentrations as high as 4330 mg/kg [105]. Gold mining in Oman has also shown contamination in their tailings with concentrations of chromium as high as 486 mg/kg [22].

Exposure to heavy metal contaminated drinking water is a major concern due to the toxicity of these heavy metals. Arsenic has a litany of well documented symptoms for both acute and long-term poisoning; ranging from lesser symptoms of vomiting, diarrhea, and abdominal pain to more permanent and deadly symptoms such as skin, lung, and bladder cancer, pulmonary diseases, and cardiovascular diseases. Arsenic exposure has also been shown to increase infant mortality rates and have negative impacts on cognitive development, intelligence, and memory [79,106]. Hence, arsenic exposure is a significant concern for locations that access drinking water from sources in close proximity to mine tailings [79,80].

Also of concern is chromium, especially in its more toxic form, the 6+ oxidation state. Both chromium (III) and chromium (VI) are known for being quite toxic to plant and animal life, but it is chromium (VI) that is widely recognized as a carcinogen [59]. The Government of Canada reports that average concentrations of *total* chromium in uncontaminated surface waters should be generally below 1  $\mu\text{g/L}$ , but the Alberta Oil Sands report that chromium (VI) concentrations in tailings ponds waters reach up to 2000  $\mu\text{g/L}$  [57,58]; meaning that seepage of the chromium species into nearby groundwater supplies is a major concern. Chromium (VI), or hexavalent chromium, can be 10 to 100 times more toxic than the chromium (III) when consumed orally [107]. Developmental issues, damage to the skin, respiratory, reproductive, and digestive system, and cancer are

major health risks from exposure to chromium (VI). Chromium (VI) excretion from the human body is very slow due to its ability to accumulate in tissues, therefore, elevated chromium concentrations in individuals are observed even decades after exposure to the contamination has stopped [60,106,108].

Due to the many health risks of these heavy metals, many studies have been done on the remediation of these contaminants from water supplies. A study by Ding et al. investigated the redox behaviour of As (III) and Cr (VI) in pH 3.0 to 11.0 solutions on Al-containing ferrihydrite. This study found that redox transformations occurred between the As (III) and Cr (VI) species to oxidize As (III) to As (V) and to reduce Cr (VI) to Cr (III) [109]. This study does not, however, compare the adsorption capacities of individual solutions to the mixture and therefore does not determine whether the co-adsorbing species undergo competitive or cooperative adsorption. A study by Azzam et al. investigated the use of  $\alpha$ -Fe core, organic ethylenediaminetetraacetic acid shell, nanospherical necklace for the adsorption of arsenic (V) and Cr (VI). They obtained high adsorption capacities of 306.7 and 406.5 mg/g at pH values of 5.0 and 7.0 and focused on the effect on chromium adsorption as a result of changing the pH of the solution. The authors assume competitive interactions between the co-adsorbing species exists [110]. The work of Mahato and Krithiga does investigate both binary mixtures and individual solutions of As (V) and Cr (VI) using synthesized  $\text{Fe}_2\text{O}_3/\text{AISBA-15}$  adsorbent. The adsorption capacity of the material used in their study showed values of 1.3 and 2.25 mg/g for Cr (VI) and As (V), respectively, in the binary model and adsorption capacities of 1.53 and 2.02 mg/g for Cr (VI) and As (V), respectively, in the independent models indicating a competitive environment for Cr (VI) adsorption and an enhancing

environment for As (V) [111]. This study focuses on only one starting concentration of 10 ppm for both contaminants and does not investigate the effect that changing this starting concentration on the adsorption of the contaminants.

The studies mentioned above are significantly different than the study presented in this work for multiple reasons. The studies above focus on pH change alone, assume competition between species, and/or focus on a single concentration ratio rather than a range of concentrations. They also use heavily modified adsorbent materials that would be costly and difficult for upscaling in order to treat significant volumes of contaminated mine tailings. Mine tailings and tailings ponds are a complex mixture of many contaminants that can vary significantly in concentration therefore there will be some kind of interaction, either competition for adsorption sites or enhancement of adsorption capacities, between the contaminants. The work presented herein focuses on the difference between the model behaviour of the independent contaminants under different pH conditions and the effects on the adsorption when the contaminants are present in a binary system. While the binary mixture is not as complex a matrix as true mine tailings, this study offers an insight into the effect that the contaminants have on one another during the adsorption process at a range of concentration ratios. This study also aims to investigate the mechanism by which the adsorption occurs and how the contaminants act either competitively or cooperatively for adsorption on an adsorbent material; a material that is easy to produce and has the potential for upscaling to treat large volumes of contaminated waters.

## ***5.2. Experimental Procedure and Methods***

Please refer to Chapter 2 for all experimental procedures and methods performed.

### ***5.3. Results and Discussion***

#### **5.3.1. Nitrogen Adsorption Measurements**

Despite following the same procedure as previous studies by Fisher et al. [1,2], a new oven and crucibles were obtained before the start of this study and resulted in the activated carbon being prepared having a higher surface area than previously obtained. Brunauer-Emmett-Teller (BET) surface analysis of the activated carbon used in this study provided a surface area of  $1127 \pm 63 \text{ m}^2/\text{g}$ . Nitrogen adsorption measurements of the activated carbon shows that the standard used in this study follows both a type I and type II nitrogen adsorption isotherm with a large increase of adsorption in the lower pressure region, indicating that the activated carbon is highly microporous. The small increase observed in the higher pressure region indicates a small degree of mesoporosity in the activated carbon sample. This is confirmed by the pore size distribution which shows that micropores make up 76% of the total porosity of the activated carbon. Desorption of the nitrogen follows type H4 hysteresis, a common hysteresis loop given by many activated carbons and other nanoporous adsorbents [112]. Figure 23 provides the nitrogen adsorption and hysteresis plot of the standard activated carbon used in this study.

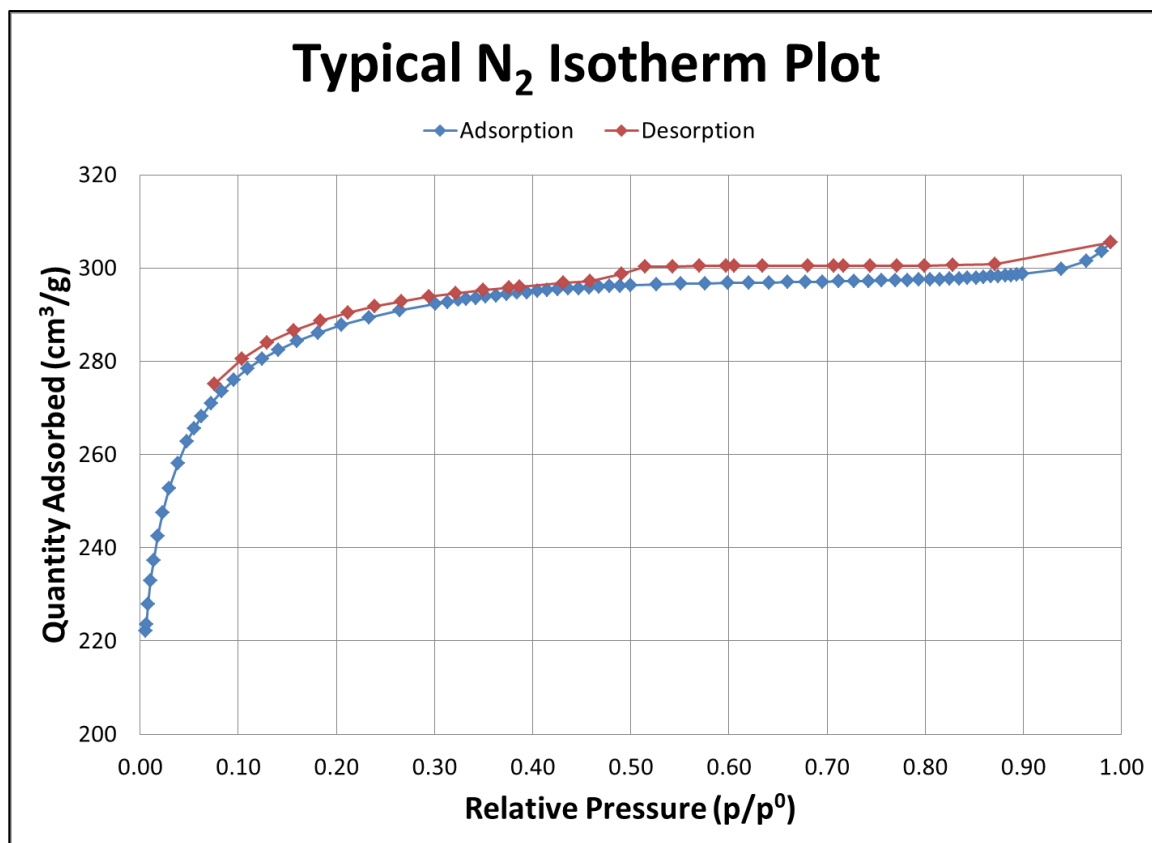


**Figure 23:** Typical nitrogen adsorption isotherm and hysteresis plots of the activated carbon used in this study.

### 5.3.2. Arsenic (V) Adsorption Enhancement and/or Competition

#### Evaluation: Binary Mixture at pH 3

Arsenic adsorption in the binary mixture at pH 3 shows enhancement when chromium is present. The adsorption of arsenic alone (50 ppm:0 ppm As:Cr) was  $7.9 \pm 0.2$  mg/g while the addition of even a nominal amount of chromium in solution (50 ppm:1 ppm As:Cr) increases the arsenic adsorption to  $10.7 \pm 0.1$  mg/g. As the concentration of chromium in solution is increased to a 1:1 ratio (50 ppm:50 ppm As:Cr) of arsenic to chromium, a continual increase in the arsenic adsorption is observed to a maximum of  $62 \pm 2$  mg/g at that concentration. The arsenic adsorption enhancement effect is shown to slow in solutions with concentrations greater than a 1:1

ratio of As:Cr, for example, in a 50 ppm:100 ppm As:Cr ratio, the maximum arsenic adsorbed was only  $45.2 \pm 1.5$  mg/g compared to the maximum of  $62 \pm 2$  mg/g. Similarly, as the concentration of chromium is increased to 250 ppm (50 ppm:250 ppm As:Cr), the adsorption of arsenic is only  $26.4 \pm 0.7$  mg/g. The enhancement of arsenic adsorption caused by the introduction of chromium to the system can be seen in Figure 24.

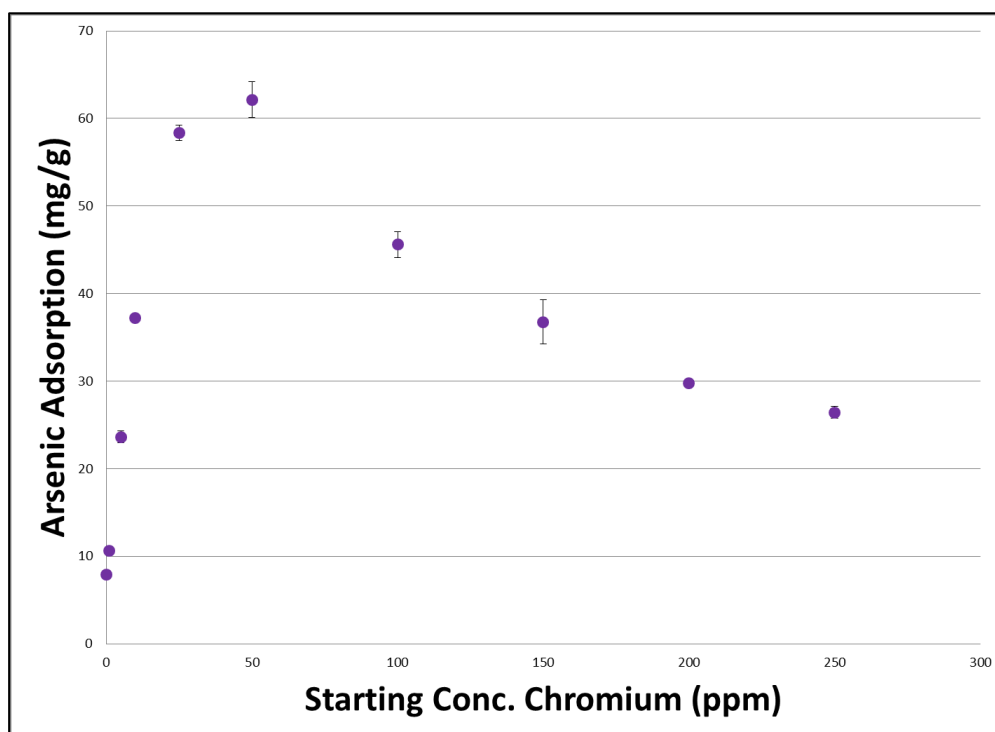


**Figure 24:** Arsenic adsorption enhancement effect as observed by changing the initial concentration of chromium in solution at pH 3 with 50 ppm arsenic.

### 5.3.3. Arsenic (V) Adsorption Enhancement and/or Competition

#### Evaluation: Binary Mixture at pH 8

At pH 8, a very similar effect in the enhancement of arsenic adsorption is observed. When there is only arsenic in solution (50 ppm:0 ppm As:Cr) the adsorption of arsenic is only  $1.1 \pm 0.1$  mg/g. With the introduction of chromium to solution, in concentrations up to a maximum ratio of 1:1 As:Cr (50 ppm:50 ppm), the arsenic

adsorption increases to  $5.4 \pm 0.1$  mg/g. As with pH 3, the enhanced arsenic adsorption effect decreases past this point. For example, at a chromium concentration of 250 ppm, arsenic adsorption is  $4.7 \pm 0.1$  mg/g (Figure 25).

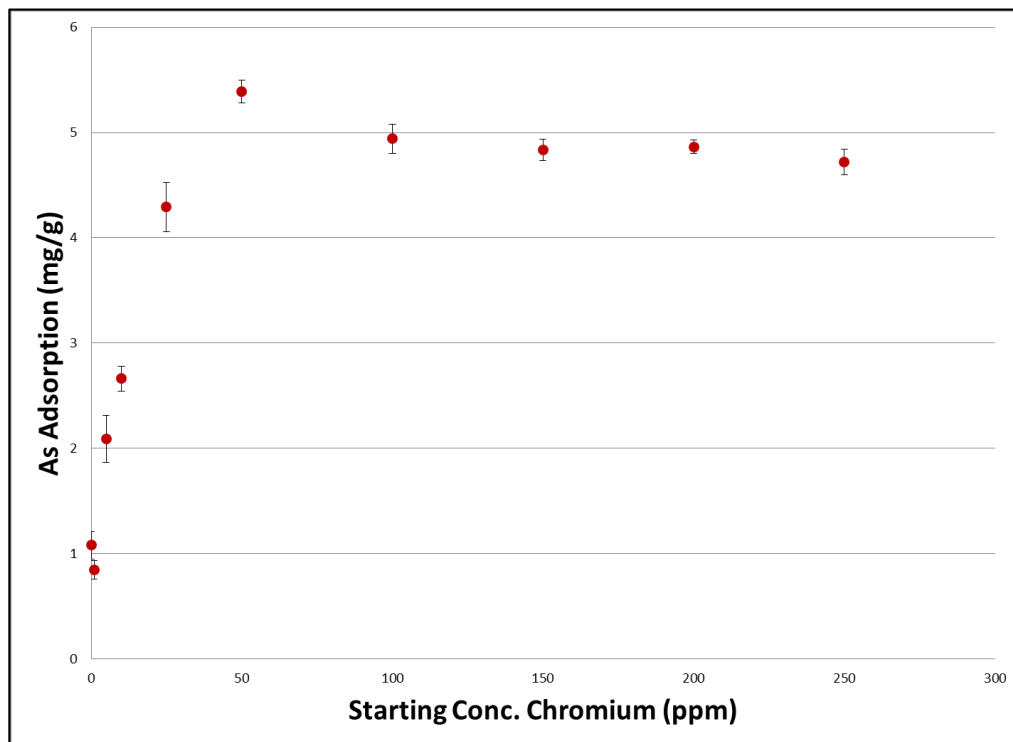


**Figure 25:** Arsenic adsorption enhancement effect as observed by changing the initial concentration of chromium in solution at pH 8 with 50 ppm arsenic.

The data presented above shows the adsorption of arsenic in the pH 3 and pH 8 systems as a function of the starting concentration of chromium. Both pH 3 and pH 8 systems show a maximum arsenic adsorption at a 1:1 ratio of arsenic to chromium (50:50 As:Cr) with increasing adsorption of arsenic until this point. Both systems also show a slowing in this enhancement effect when chromium concentration is increased past this 1:1 ratio. Unlike Figure 24 and Figure 25, Figure 26 shows the concentration of chromium at equilibrium (i.e. the residual concentration) ( $C_e$ ) in the system for both the pH 3 and pH 8 systems.

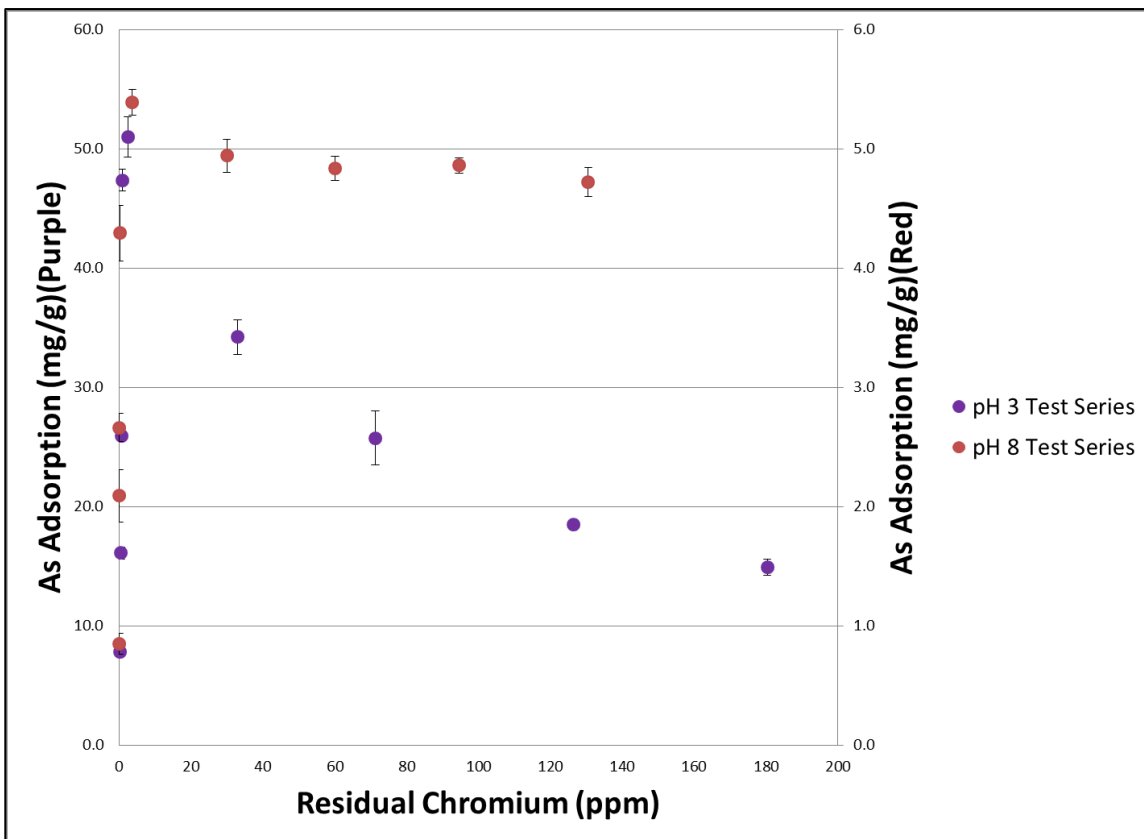


**Figure 26:** This shows the enhancement of arsenic adsorption as a function of the changing chromium concentration in the system. The x-axis is presented as the amount of leftover chromium in solution ( $C_e$ ) rather than the initial starting concentration of chromium in the solution.

When the amount of arsenic adsorbed is plotted against the residual chromium concentration at equilibrium, the arsenic adsorption increases to a maximum when the residual chromium is near zero. The adsorption of arsenic reaches a maximum in both the pH 3 and pH 8 systems when almost all of the chromium in solution is adsorbed onto the activated carbon surface. The decrease in the enhancement of arsenic adsorption occurs once there is leftover chromium in solution.

This is consistent with the kinetics data obtained from the pH 3 mixed metal solutions. When looking at the arsenic adsorption after various times, the maximum adsorption of arsenic occurs at lower and lower concentrations of chromium as time

decreases. This is because less chromium is adsorbed with shorter times. For example at 5 minutes, the maximum arsenic adsorption occurs at a starting chromium concentration of 10 ppm; whereas at 6 hours, the maximum arsenic adsorption occurs at a starting chromium concentration of 25 ppm; and at 1 week, the maximum arsenic adsorption occurs at a starting chromium concentration of 50 ppm (Figure 27).

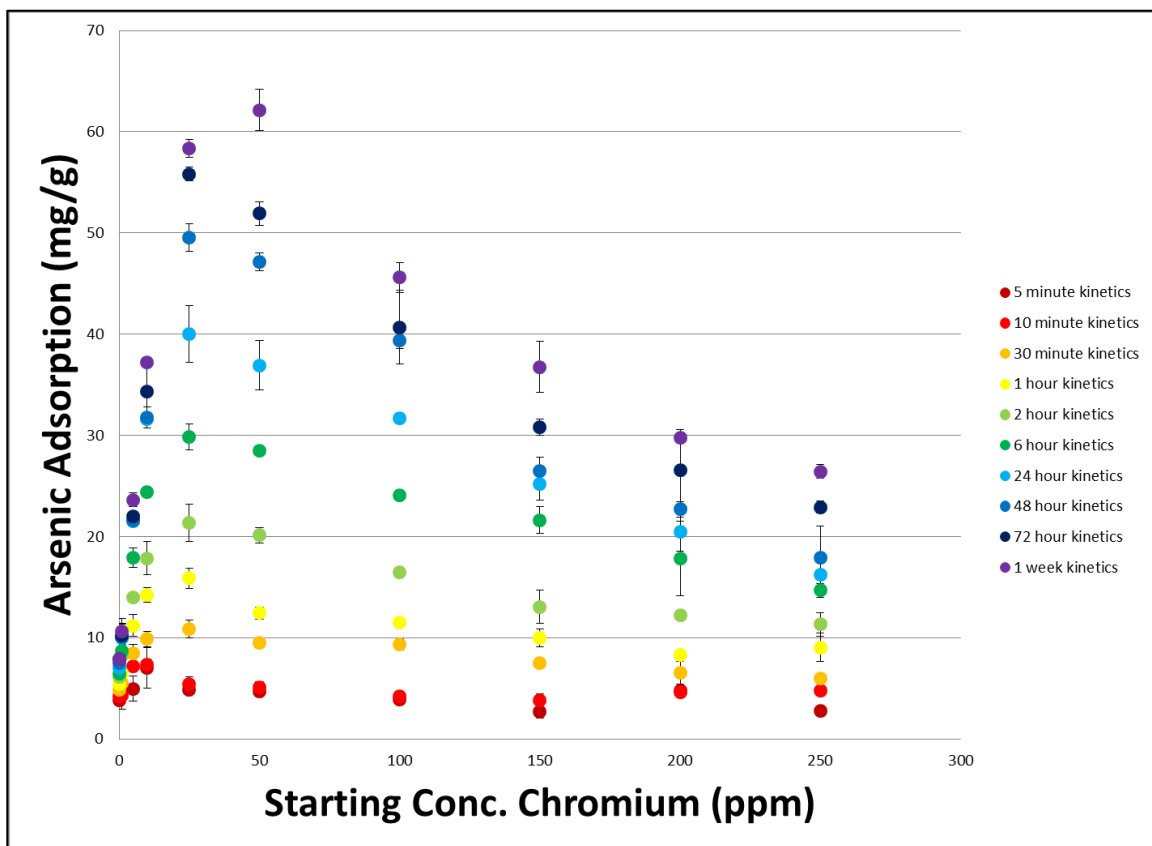


**Figure 27:** This graph shows the arsenic adsorption enhancement phenomenon at the various starting concentrations of chromium over multiple stir times. The maximum arsenic adsorption occurs at lower starting concentrations of chromium as the stir times decrease.

One possible explanation for the observed enhancement of the arsenic adsorption in the binary mixture is a stepwise adsorption process where chromium (VI) is first reduced to chromium (III) and adsorbed to the activated carbon surface as per the mechanism proposed by Fisher et al [1]. This would essentially create a metal-loaded

surface for the arsenic to adsorb to [2], where arsenic would undergo a redox reaction with the chromium on the surface of the activated carbon to oxidize the chromium (III) to chromium (VI) and in turn be reduced to arsenic (III) for adsorption. If the enhancement of the arsenic adsorption is occurring due to this stepwise mechanism, loading the surface of the activated carbon with chromium-only first and then exposing the chromium-loaded activated carbon to arsenic should lead to similar arsenic adsorption capacities as observed in the binary mixtures.

#### **5.3.4. Arsenic (V) Adsorption Enhancement and/or Competition**

##### **Evaluation: Stepwise Adsorption at pH 3**

Similar to the binary mixtures, the stepwise adsorption experiment performed at pH 3 shows that arsenic adsorption is enhanced when low concentrations of chromium are loaded onto the activated carbon surface prior to exposure. However, when higher concentrations of chromium are loaded onto the surface of the activated carbon surface prior to arsenic exposure, the arsenic adsorption is significantly reduced. This is likely due to the fact that there are fewer available binding sites where the arsenic can adsorb. The comparison between the stepwise adsorption and binary mixtures can be seen in Figure 28.

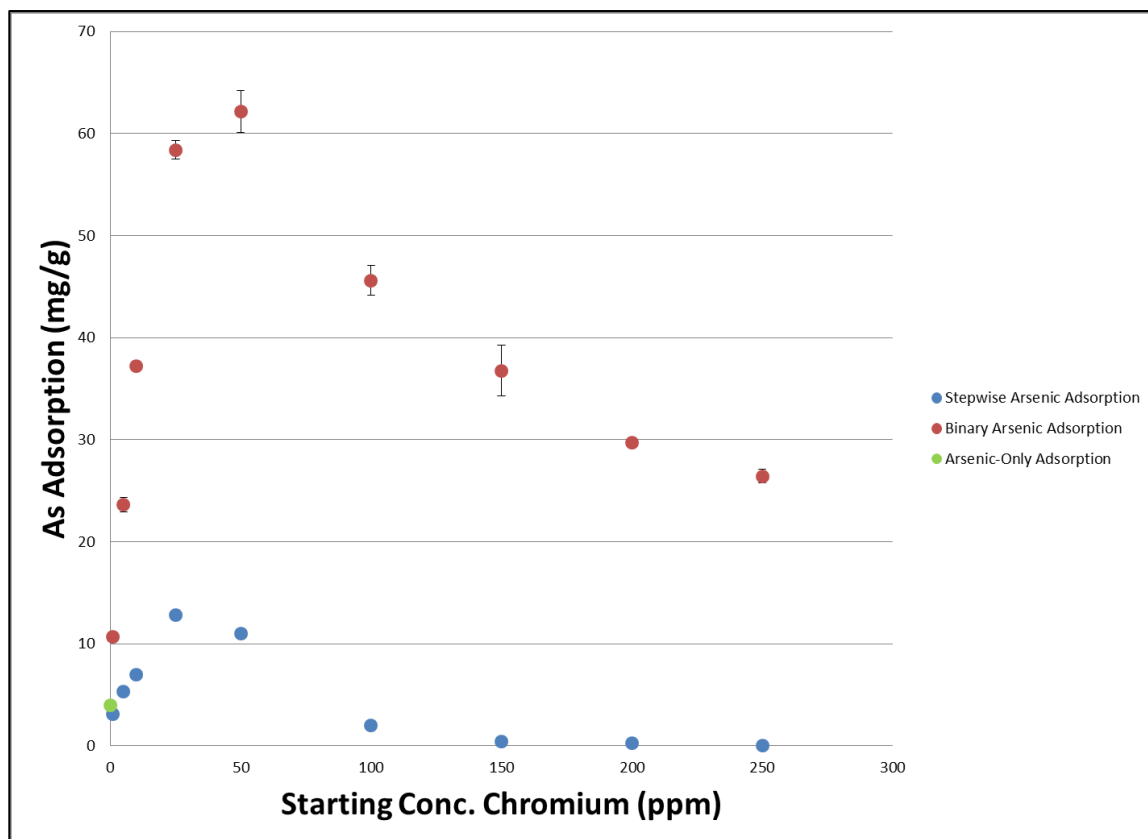


**Figure 28:** Arsenic adsorption comparison for the arsenic only adsorption, the step-wise adsorption, and the binary mixture at pH 3.

### 5.3.5. Arsenic (V) Adsorption Enhancement and/or Competition

#### Evaluation: Binary Mixture at pH 8

Unlike the stepwise adsorption experiment performed at pH 3, the pH 8 stepwise adsorption shows that the arsenic adsorption is not enhanced due to the loading of chromium on the surface first. In fact, arsenic adsorption onto the chromium-loaded activated carbon material showed a lower adsorption capacity than the initial arsenic adsorption (Figure 29).

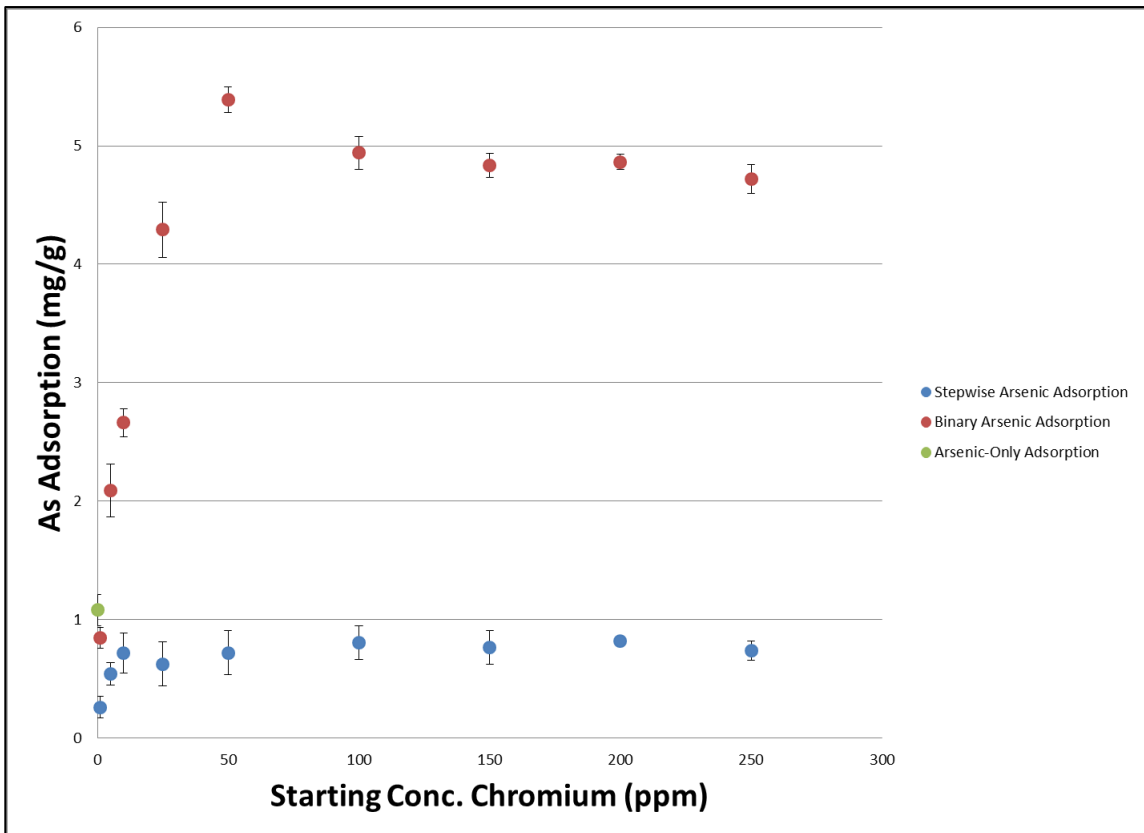


**Figure 29:** Arsenic adsorption comparison for the arsenic only, the step-wise adsorption, and the binary mixture adsorption at pH 8. Note that the concentration of chromium is presented in parts per million as it is the concentration of chromium in solution while the arsenic adsorption is presented in mg/g as this is expressing the mg of arsenic adsorbed per gram of activated carbon added to the solution.

The competition that is observed in the stepwise adsorption study at both pH 3 and pH 8 indicates that there are fewer binding sites for the arsenic to adsorb to after chromium has been loaded to the AC surface and implies that the enhancement of the arsenic is occurring as a result of interactions between the arsenic and chromium species in solution, before adsorption onto the activated carbon surface. It is important to note, and will be discussed further in section 5.3.14., that the decrease in the enhancement of arsenic adsorption observed at the higher concentrations of chromium is significantly larger in the pH 3 solutions than the pH 8 solutions.

### 5.3.6. Chromium (VI) Adsorption Enhancement and/or Competition Evaluation

Isotherm data was collected for chromium (VI) adsorption at both pH 3 and pH 8 for samples containing arsenic and samples not containing arsenic. A comparison of the isotherms and their best fitting models will provide information on how the interaction of arsenic and chromium in the mixture lead to competition or co-adsorption of the species.

Langmuir isotherm modelling makes several assumptions about the system being modelled. A review article by Tran et al. [70] discusses the assumptions and common issues arising when performing Langmuir isotherm modelling. Langmuir modelling assumes: 1) that there are a fixed number of accessible sites available on the adsorbent surface and all sites have the same energy, 2) that adsorption is reversible, 3) that once an adsorbate molecule occupies a site, that site is no longer accessible to any other adsorbate molecules, and 4) that there is no interaction between adsorbate molecules. The non-linear Langmuir model follows Equation 3:

$$q_e = \frac{Q_{max}^0 K_L C_e}{1 + K_L C_e} \quad (3)$$

**Equation 3:** Non-linear isotherm modelling equation for the Langmuir isotherm model.

where  $Q_{max}^0$  is the maximum monolayer adsorption capacity of an adsorbent in mg/g,  $C_e$  is the adsorbate concentration at equilibrium in mg/L,  $q_e$  is the amount of adsorbate uptake at equilibrium in mg/g, and  $K_L$  is a constant indicating the affinity between adsorbate and adsorbent. The chromium isotherm data obtained in this study was modelled using Langmuir isotherm modelling to determine if a monolayer adsorption mechanism is likely.

Another common isotherm model is the Freundlich isotherm model. Kalam et al. [113] describes the differences between the Langmuir and the Freundlich models. Unlike the Langmuir model, the Freundlich model is used to assess multilayer adsorption and assumes that adsorbate molecules may interact with one another. Tran et al. [70] describes the Freundlich isotherm modelling being non-linear with respect to Equation 4:

$$q_e = K_F C_e^{1/n} \quad (4)$$

**Equation 4:** Non-linear isotherm modelling equation for the Freundlich isotherm model.

where  $q_e$  is the amount of adsorbate uptake at equilibrium in mg/g,  $C_e$  is the adsorbate concentration at equilibrium in mg/L,  $K_F$  is the Freundlich constant which indicates the adsorption capacity and is given in  $(\text{mg/g})/(\text{mg/L})^n$ , and  $n$  is the Freundlich intensity parameter, a dimensionless variable that indicates the magnitude of the adsorption driving force or the surface heterogeneity. The chromium isotherm data obtained in this study was modelled using Freundlich isotherm modelling to determine if multilayer adsorption is the likely adsorption mechanism that occurs in these solutions.

### 5.3.7. pH 3 Isotherm Data and Modelling

The chromium adsorption observed at pH 3 showed that, when mixed with arsenic, chromium had a competitive relationship at the higher chromium concentrations. At low starting concentrations of chromium (between 1 and 50 ppm), there was no significant difference in the chromium adsorption of the mixed solution versus the individual solution. However, at starting chromium concentrations of over 50 ppm, there is a significant difference in the chromium adsorption between the mixed and individual solutions. While the arsenic adsorption is enhanced by the presence of the chromium, the chromium adsorption is actually hindered by the presence of the arsenic. Figure 30 shows

the isotherm data for the pH 3 solutions, that is, the adsorption of chromium in the individual and mixed solutions as a function of the equilibrium concentration ( $C_e$ ) in ppm.

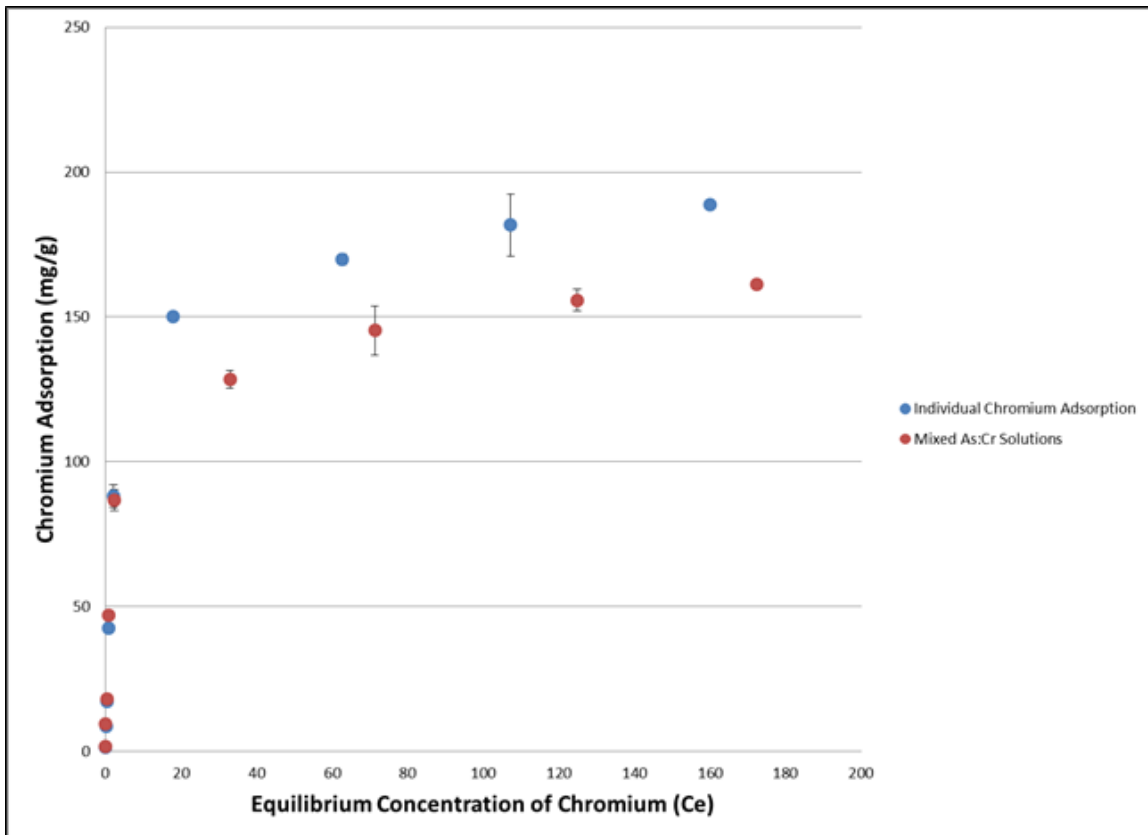


**Figure 30:** Isotherm data of chromium adsorption in the individual and mixed solutions at pH 3.

A good fit for the modelling occurs when the sum of the squares for the residual (SSR) is close to zero and when the  $R^2$  of the model is close to 1. The Langmuir modelling of the As:Cr mixture provides an SSR of 921 and an  $R^2$  of 0.9795, while the Freundlich model provides an SSR of 4281 and an  $R^2$  of 0.9048. Similarly, the Langmuir modelling of the chromium only solutions provided an SSR of 405 and an  $R^2$  of 0.9944 while the Freundlich model had an SSR are 4345 and an  $R_2$  of 0.9396. In both cases, isotherm modelling of the pH 3 chromium adsorption data shows that the adsorption follows the Langmuir model more closely than the Freundlich model. This implies that

the monolayer adsorption occurs on the activated carbon surface, in other words, one binding site for one adsorbate molecule. It is important to note that while the SSR of the Langmuir modelling is closer to zero than the Freundlich modelling, the SSR values are still quite high, indicating a significant difference between the predicted curve and the experimental data. This is likely due to the fact that the isotherm models assume a one-component system and the experimental data is being shifted from the predicted curve due to the presence of a second component in the system. This proves that the arsenic in the system is affecting the adsorption of the chromium. The Langmuir isotherm models at pH 3 can be found in

Figure 31. The Freundlich isotherm models for the pH 3 data are shown in Appendix F, Figure 55 **Figure F1:** Freundlich isotherm modelling of the chromium adsorption for the pH 3 isotherm data..

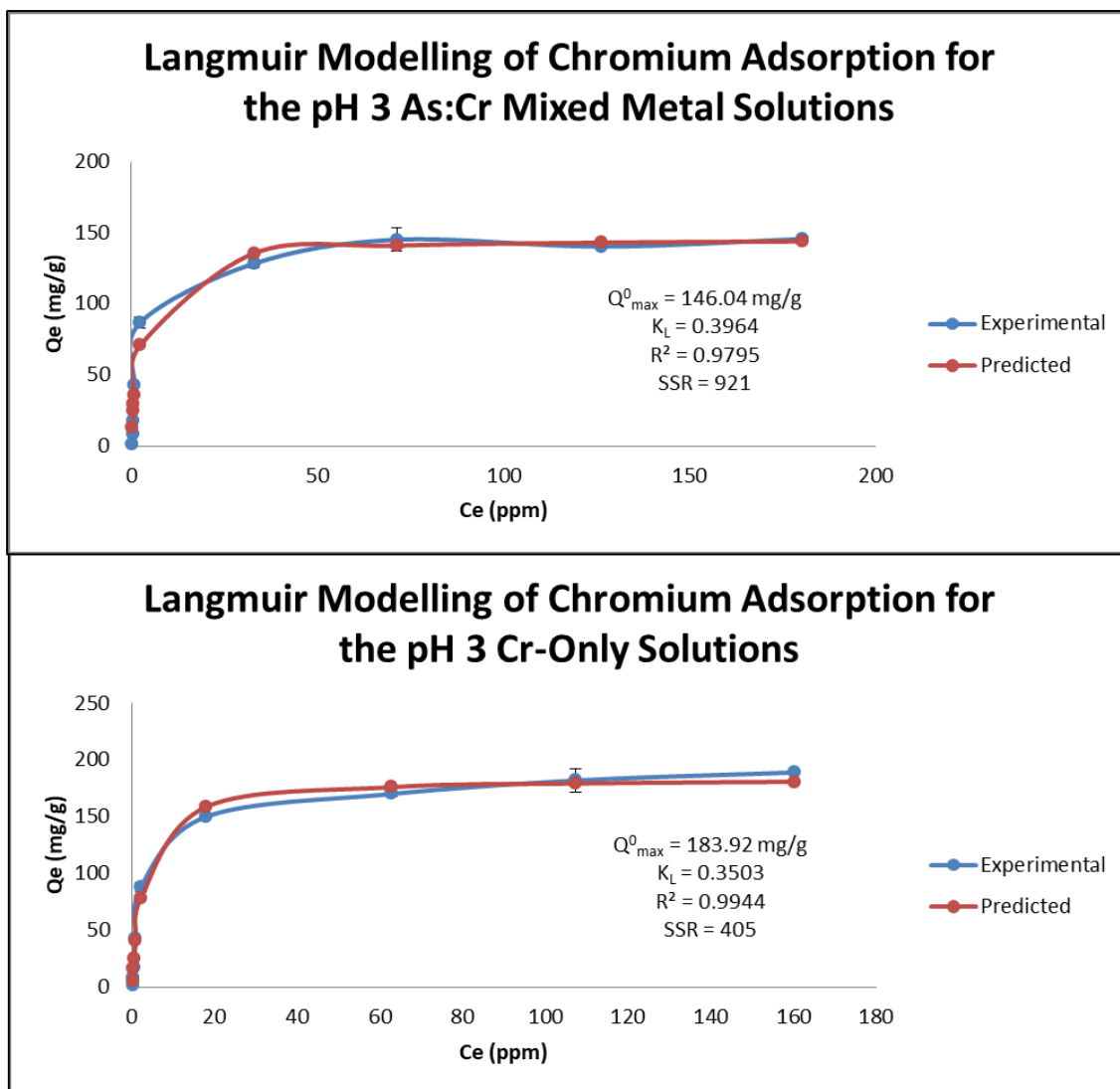
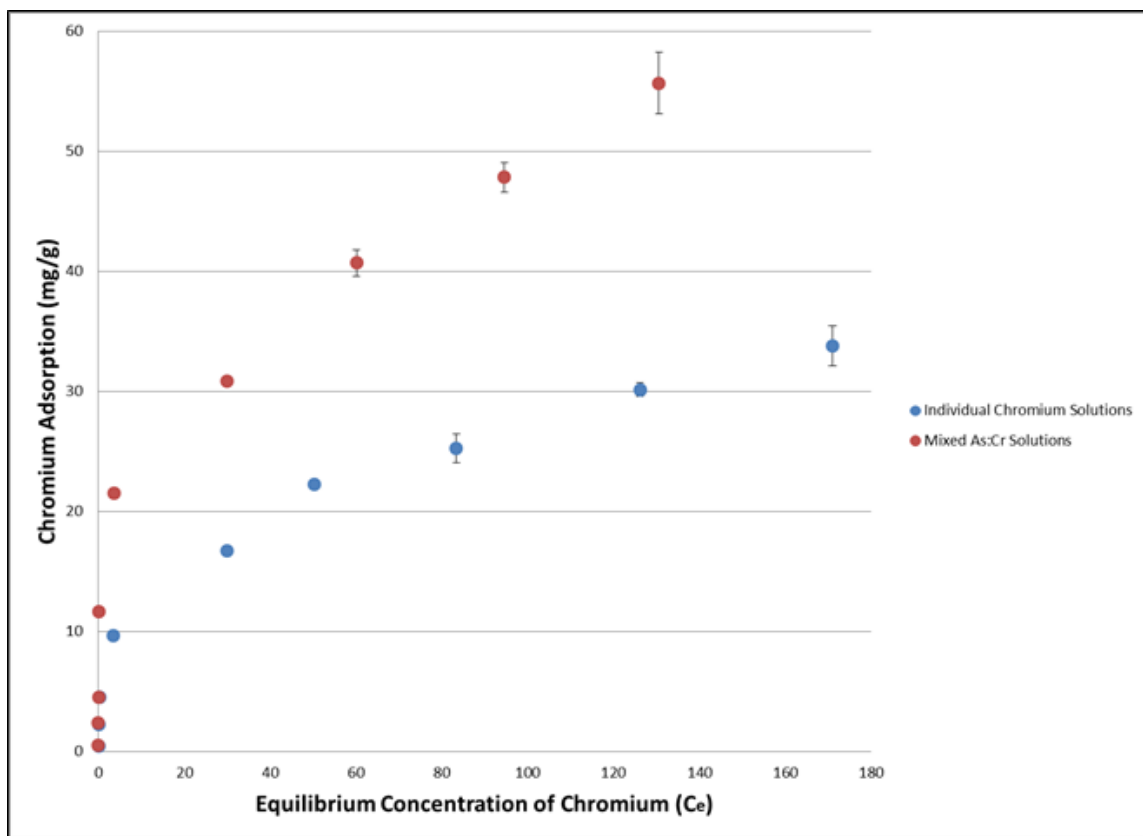


Figure 31: Langmuir isotherm modelling for the adsorption of chromium at pH 3.

### 5.3.8. pH 8 Isotherm Data and Modelling

The chromium adsorption observed at pH 8 showed that, when mixed with arsenic, chromium had enhanced adsorption at the higher chromium concentration levels. The isotherms showed that at chromium starting concentrations of 1, 5 and 10 ppm, there was no significant difference in the chromium adsorption of the mixed solution versus the individual solution. However, at starting chromium concentrations above 25 ppm, there is

a significant difference in the chromium adsorption between the mixed and individual solution. This shows that the adsorption of arsenic in solution is not only enhanced by the presence of the chromium but that the adsorption of chromium in solution is also enhanced by the presence of the arsenic in solution. Figure 32 shows the isotherm data for the pH 8 solutions, that is, the adsorption of chromium in the individual and mixed solutions as a function of the equilibrium concentration ( $C_e$ ) in ppm.



**Figure 32:** Isotherm data of chromium adsorption in the individual and mixed solutions at pH 8.

Unlike the pH 3 data, the isotherm modelling of the pH 8 chromium adsorption data shows that the adsorption follows the Freundlich model more closely than the Langmuir model. This indicates that, at pH 8, multilayer adsorption occurs on the

activated carbon surface. This is true for both the chromium-only adsorption isotherm and the chromium isotherm of the mixed metal data.

Langmuir modelling of the mixed solution shows an SSR value of 331 and an  $R^2$  of 0.9308 while the Freundlich model shows an SSR of 58.7 and an  $R^2$  of 0.9877. Similarly, the Langmuir model of the individual chromium data shows an SSR value of 67.9 and an  $R^2$  of 0.9596 while the Freundlich model gives an SSR of 10.4 and an  $R^2$  of 0.9938. The Langmuir isotherm models at pH 8 are provided in Appendix G, Figure 56 **Figure G1:** Langmuir isotherm modelling of the chromium adsorption for the pH 8 isotherm data.. The Freundlich isotherm models for the pH 8 data are provided in Figure 33.

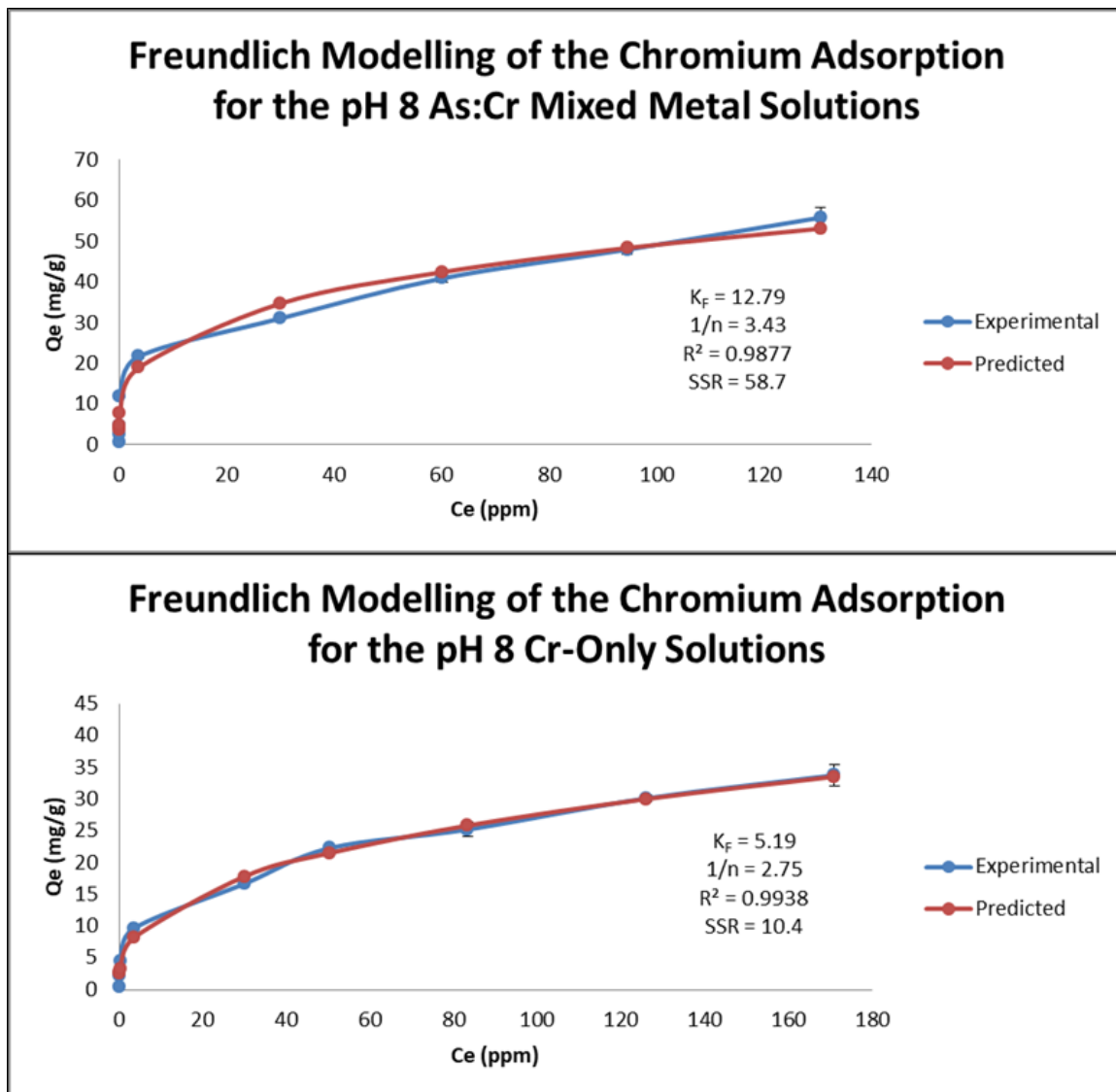


**Figure 33:** Freundlich isotherm modelling for the adsorption of chromium at pH 8.

Interestingly, when comparing the isotherm modelling of the chromium adsorption, the experimental data in the individual chromium solutions in both the Langmuir and Freundlich models are closer to the predicted model than the mixed solutions. This is consistent in both the pH 3 and the pH 8 data and is likely due to these isotherm models assuming a one-component system. This proves that the arsenic in solution, which is a second component in the system; a component that the model does not account for, is in fact affecting the adsorption of the chromium. This is demonstrated

by the experimental data being shifted from the predicted curve, as explained in section 5.3.7..

### **5.3.9. XPS Characterization: Standard AC Prior to Adsorption of Heavy Metals**

Investigation of the surface functionality of the activated carbon materials before and after adsorption of arsenic and/or chromium provides information on how the adsorption of the species may be occurring on the material's surface.

The XPS survey scan of the Standard Activated Carbon used in this study shows that carbon makes up 81% of the activated carbon surface and oxygen makes up 14.9% of the surface. The remainder of the surface is made up of impurities such as nitrogen, silicon, iron, sulfur, aluminium, and potassium; however, the arsenic and chromium adsorption occurs due to oxygen speciation on the surface [1,2] therefore the focus of this study will be on the change in the oxygen speciation. Previous studies with chromium and arsenic have shown that the predominant species of oxygen that affect adsorption of these metals are the carbonyl and hydroxyl functional groups.

Deconvolution of the O1s peak shows that prior to exposure to arsenic or chromium, the carbonyl functional groups present on the surface make up 27.5% of the oxygen functionality while hydroxyl functional groups make up 30.1% of the oxygen functionality (Figure 34).

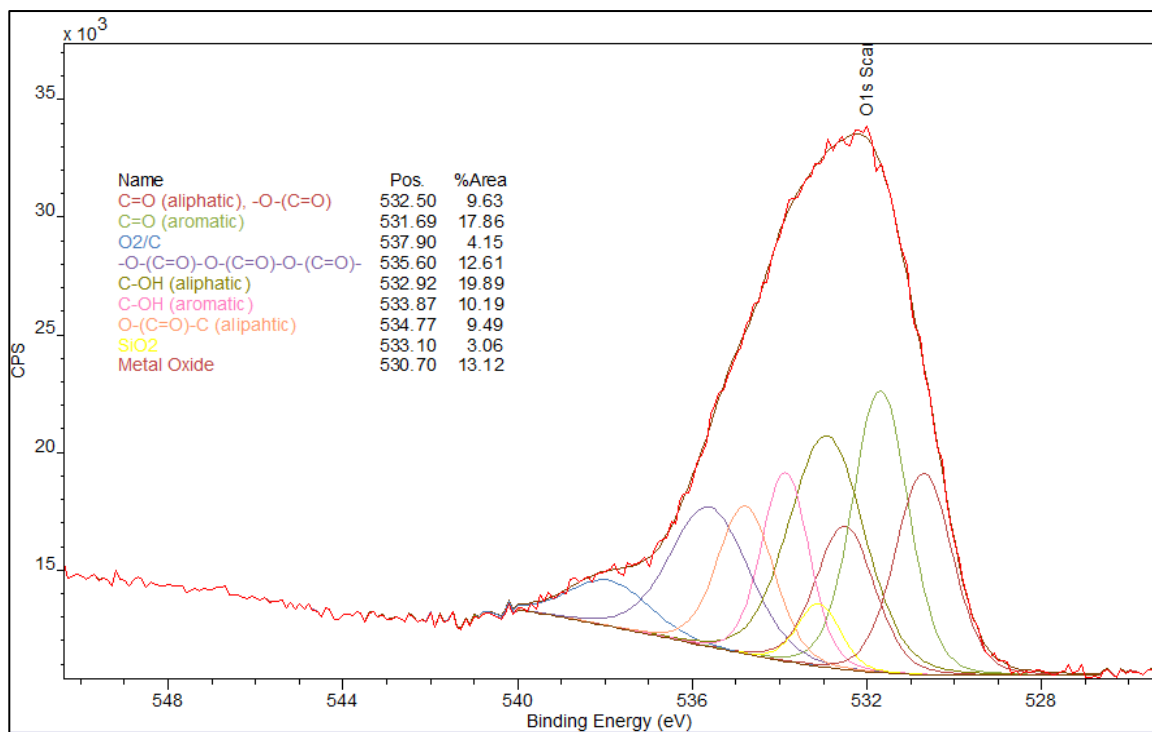


**Figure 34:** XPS deconvolution of the O1s peak for the Standard AC before adsorption of chromium or arsenic [67].

### 5.3.10. XPS Characterization: Post-Adsorption of Arsenic-Only

#### Samples

The XPS deconvolution of the O1s peak post-arsenic exposure shows that the carbonyl functional groups are increased from 27.5% to 35.1% while the hydroxyl groups decrease from 30.1% to 11.9%. The metal oxide functionality is increased from 13.1% to 38.8% of the oxygen species indicating that arsenic had been adsorbed onto the surface of the activated carbon (Figure 35).

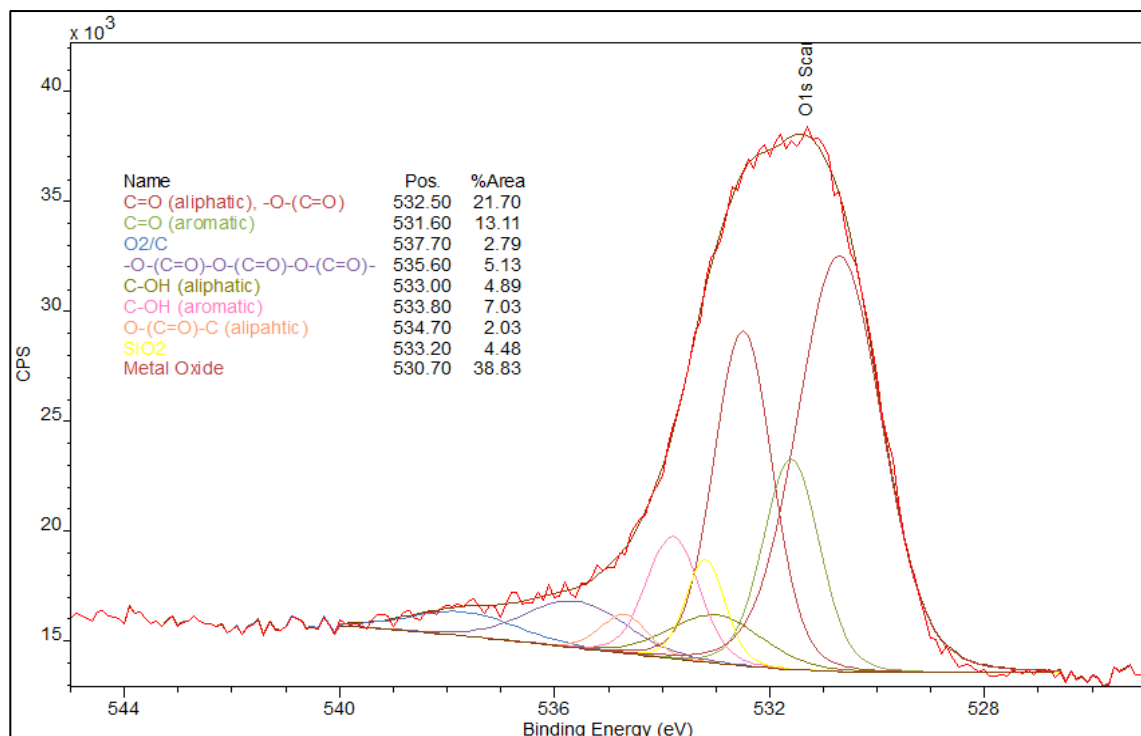


**Figure 35:** XPS deconvolution of the O1s peak for the activated carbon after arsenic-only adsorption [67].

The XPS deconvolution of the As2p peak shows that the predominant species of arsenic adsorbed onto the surface of the activated carbon is arsenite (As (III)). Arsenite makes up 68.2% of the arsenic on the surface while arsenate (As (V)) makes up 31.8% of the arsenic on the surface. This indicates that the majority of the arsenic being adsorbed onto the surface of the activated carbon is being reduced from arsenic (V) to arsenic (III) during the adsorption process. This is discussed further in section 5.3.13..

### 5.3.11. XPS Characterization: Post-Adsorption of Chromium-Only Samples

The XPS deconvolution of the O1s peak post-chromium exposure shows that the carbonyl functional groups are increased from 27.5% to 60.4% while the hydroxyl groups decrease from 30.1% to 6.5%. The metal oxide functionality is increased from 13.1% to

28.1% of the oxygen species indicating that chromium had been adsorbed onto the surface of the activated carbon (Figure 36).

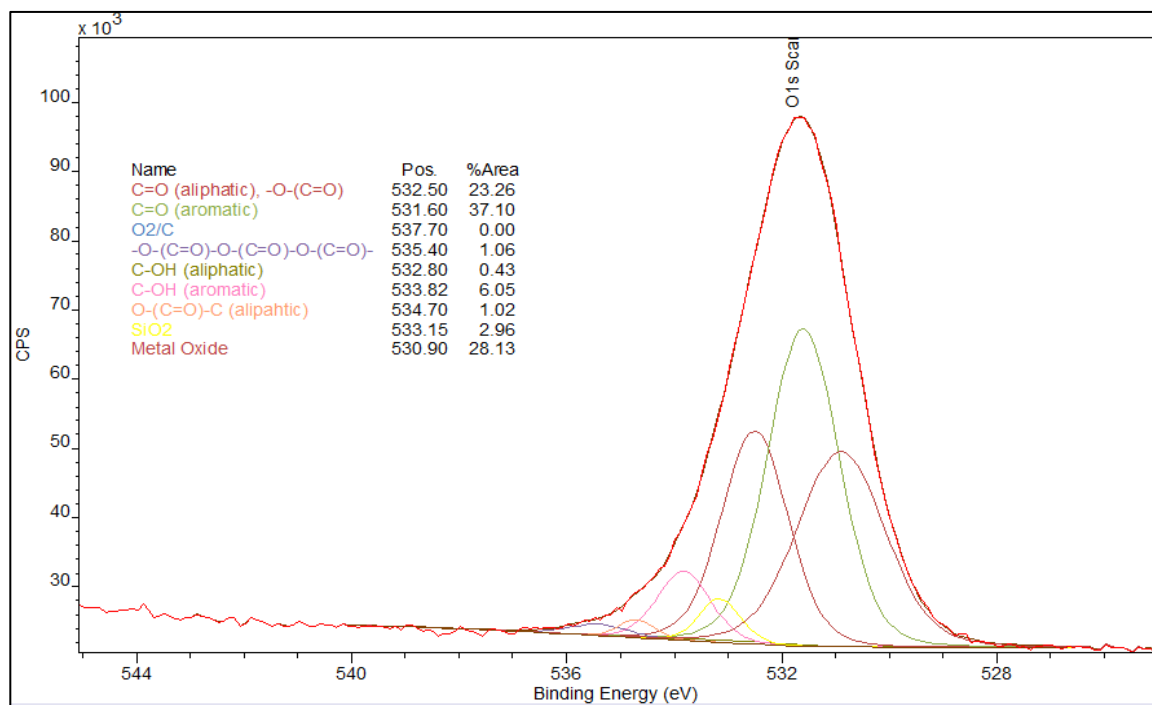


**Figure 36:** XPS deconvolution of the O1s peak for the activated carbon after chromium-only adsorption [67].

The XPS deconvolution of the Cr2p peak shows that the predominant species of chromium adsorbed onto the surface of the activated carbon is chromium hydroxide ( $\text{Cr}(\text{OH})_3$ ). Chromium hydroxide makes up 86.6% of the chromium on the surface while chromium (III) oxide ( $\text{Cr}_2\text{O}_3$ ) makes up 10% of the chromium on the surface and Cr (VI) species makes up 3.4% of the chromium on the surface. This indicates that the majority of the chromium being adsorbed onto the surface of the activated carbon is being reduced from chromium (VI) to chromium (III) during the adsorption process. This is discussed further in section 5.3.13..

### 5.3.12. XPS Characterization: Post-Adsorption of As:Cr Mixed Metal Samples

The XPS deconvolution of the O1s peak after exposure to the mixed arsenic:chromium solutions show a similar trend to the individual metal solutions. The carbonyl speciation is significantly increased as a result of the activated carbon's exposure to the mixed metal solutions while the hydroxyl functional groups are significantly decreased. As a result of the adsorption of chromium and arsenic, the metal oxide species are also significantly increased on the AC surface. The XPS deconvolution of the As2p and Cr2p peaks after exposure to the mixed arsenic:chromium solutions is similar to the XPS of the individual solutions where a reduction from arsenic (V) to arsenic (III) is observed and a reduction of chromium (VI) to chromium (III) is observed. As such, the predominant species of arsenic on the AC surface is As (III) and the predominant species of chromium is Cr(OH)<sub>3</sub> (Table 19).

**Table 19:** XPS deconvolution summary of the relevant species in the O1s, Cr2p, and As2p peaks post-exposure to the mixed metal solution [67,71,93].

Arsenic:Chromium Sample (ppm:ppm)	O1s Peak Deconvolution %			As2p Peak Deconvolution %		Cr2p Peak Deconvolution %
	C=O aliphatic, C=O aromatic	C-OH aliphatic, C-OH aromatic	Metal Oxide	Arsenate (As(V))	Arsenite (As(III))	Cr(OH) <sub>3</sub>
Standard AC	27.49	30.08	13.12	-----	-----	-----
50:0	34.82	11.91	38.87	31.84	68.16	-----
50:1	53.37	0.69	34.11	13.98	86.02	73.15
50:5	54.57	0.64	33.99	12.72	87.28	89.63
50:10	53.95	0.16	37.12	20.14	79.86	69.40
50:25	53.38	0.42	36.90	19.83	80.17	91.69
50:50	54.88	0.06	40.46	13.77	86.23	85.88
50:100	50.02	1.37	46.16	10.08	89.92	82.97
50:150	45.69	0.53	51.42	10.18	89.82	82.93
50:200	53.60	0.02	44.97	15.23	84.77	83.87
50:250	60.45	0.00	39.52	14.48	85.52	82.88

Figure 37 provides an example of the As2p and Cr 2p peak deconvolution. The binding energies for the species within the O1s peak can be found in Figure 34, Figure 35, Figure 36, above, and the binding energies for the species within the As1p and Cr2p peak can be found in Figure 37, below. However, it is important to note that the Cr<sub>2</sub>O<sub>3</sub> species identification is made more complex due to the well-known XPS multiplet splitting for this and other similar species. This is described by Surface Science Western's XPS Reference Page on Multiplet Splitting [92] and Biesinger et al. [72] in their XPS study of chromium compounds.

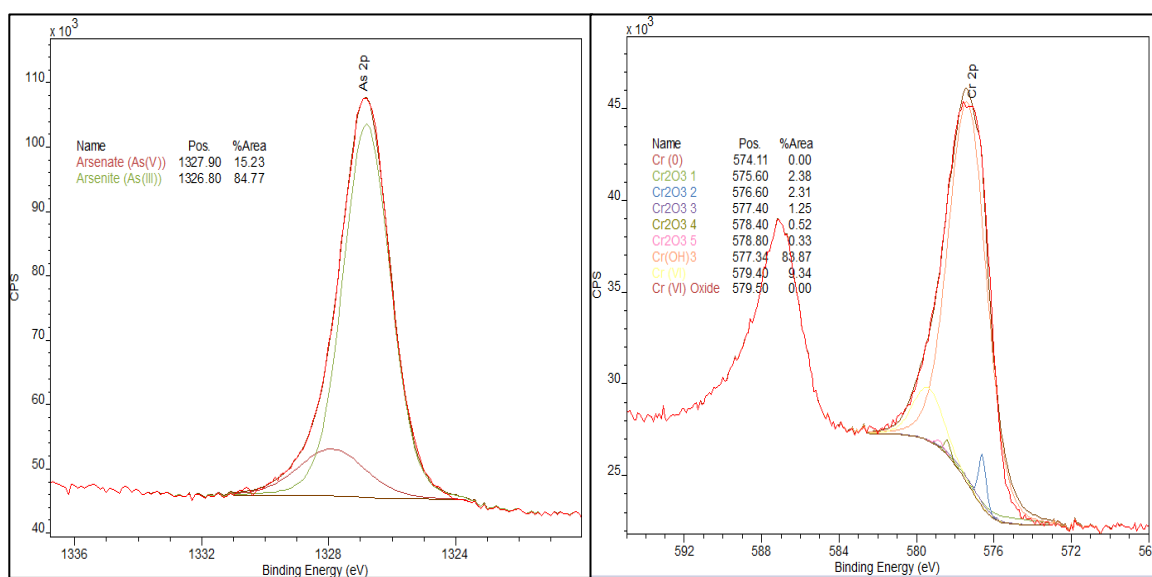


**Figure 37:** As2p peak deconvolution (left) and Cr2p peak deconvolution (right) for the AC exposed to the 50 ppm:200 ppm As:Cr solution [71,72,92,93].

### **5.3.13. Proposed Adsorption Mechanisms: Individual Adsorption Mechanisms**

Chromium is adsorbed onto the activated carbon surface through a similar process to the Jones Oxidation reaction as proposed by Fisher et al. 2022 [1]. Chromium (VI) reacts with a hydroxyl group on the AC surface to produce a carbonyl and an unstable chromium (VI) species ( $\text{H}_2\text{CrO}_3$ ) that gets reduced to Cr (III) and is adsorbed to the AC surface at the carbonyl site (See Figure 9).

Arsenic is adsorbed onto the activated carbon surface through redox reactions as proposed by Fisher et al. 2023 [2]. Arsenic when alone in solution is able to undergo redox reactions at the hydroxyl site, oxidizing the hydroxyl group to a carbonyl group while reducing the arsenic (V) to arsenic (III). The arsenic (III) is then physisorbed to the AC surface at the carbonyl site.

### **5.3.14. Proposed Adsorption Mechanisms: Chromium and Arsenic Co-Adsorption**

Several studies have shown arsenic acting as a ligand on other complexes. For example, an article by Sturala et al. [116] showed how layered gray arsenic and chromium hexacarbonyl would interact to form an  $\text{As}_3\text{Cr}(\text{CO}_3)$  complex. A 1989 paper by Dimaio and Rheingold [117] even investigates how hybrid transition-metal and main-group clusters form and that the group 15 elements are especially diverse due to donor capacities from group 15 elements such as phosphorus, arsenic, antimony, and bismuth; as well as the range of possible coordination geometries that these elements may have. The formation of a transition-metal, main-group complex, where chromium containing an

arsenic ligand, is likely what is occurring when the chromium and arsenic are mixed in solution. Figure 38 shows the formation and possible structure of a chromium complex with an arsenic ligand that would form in a mixed arsenic:chromium solution.

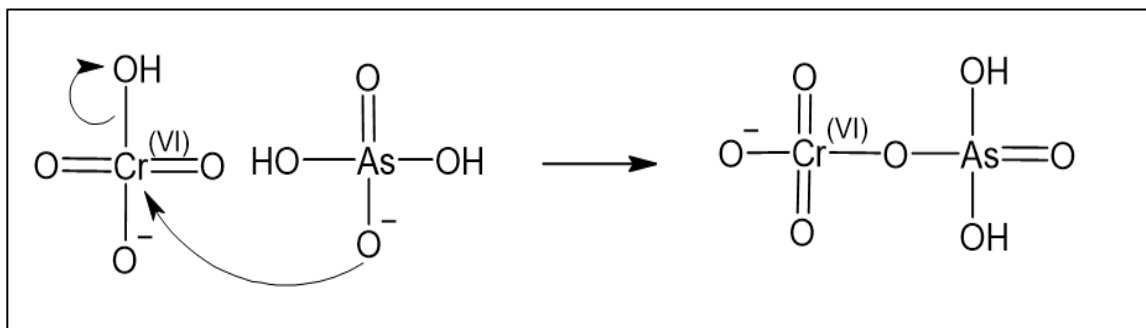


**Figure 38:** Possible formation and structure of a chromium complex containing an arsenic ligand in the mixed metal solution.

The formation of these chromium-arsenic complexes would also explain the enhancement of the arsenic adsorption observed in the mixed metal solutions and discussed in sections 5.3.2. to 5.3.5.. At low concentrations of chromium, where arsenic adsorption was significantly enhanced, the arsenic in solution is forming complexes with the available chromium in solution and is being pulled from solution as the chromium is being adsorbed onto the surface of the AC. The chromium follows the same mechanism as it does in an individual chromium solution (as shown in Figure 9), the only difference is rather than an anionic oxygen or hydroxide ligand, it has an arsenic ligand.

Sections 5.3.9. to 5.3.12. discussed the XPS results and showed that the predominant species of chromium on the surface of the AC was  $\text{Cr}(\text{OH})_3$  and that the predominant species of arsenic on the surface is arsenite. It is important to note that in the Cr2p XPS, there would be no differentiation between an O-H ligand and an O-AsX (where X is the remainder of the species bound to the arsenic) ligand as the Cr2p XPS

would identify the elements bound only to the chromium, thus the XPS showing  $\text{Cr}(\text{OH})_3$  is consistent with this proposed theory that arsenic is bound to the chromium as a ligand. Similarly, the  $\text{As}2p$  peak would show no differentiation between the O-H and O-CrX bonds and would also be consistent. It is important to note that the O1s peak would show no differentiation between an oxygen-arsenic (O-As) and an oxygen-chromium (O-Cr) species as they will both show up in the O1s peak deconvolution as a metal oxide at a binding energy of 530.70 eV.

In section 5.3.3., Figure 26 shows the arsenic adsorption in the pH 3 samples increases significantly at the lower concentrations of chromium and at the higher concentrations of chromium, the enhancement of arsenic adsorption drastically decreases. The maximum arsenic adsorption occurs when there is almost no leftover chromium in solution. This is consistent with the proposed mechanism because when more chromium is added, more chromium-arsenic complexes can form and therefore more arsenic is pulled onto the surface with the chromium. However, at the higher concentrations of chromium where some chromium is leftover in solution, we see the arsenic adsorption enhancement decrease. This is due to the increase in the amount of chromium in solution; the likelihood of the chromium-arsenic species being adsorbed becomes lower. For example, if there is excess chromium in solution to where there is one to one ratio of chromium-arsenic complexes to excess chromium molecules in solution, there is a 50:50 split on which species is adsorbed. As we increase the amount of excess chromium, we are decreasing the likelihood of the chromium-arsenic complex being adsorbed onto the surface and thus seeing a decrease in the arsenic adsorption enhancement. This is consistent with the isotherm modelling of the pH 3 solutions as the isotherms follow the

Langmuir model, indicating that once an adsorbate molecule occupies a binding site, that binding site is no longer accessible to any other adsorbate molecules.

It is interesting to note that while this is true for the pH 3 solutions, it is not true for the pH 8 solutions. Similar to the pH 3 solutions, the maximum adsorption of arsenic occurs when there is no excess chromium in solution, as shown in section 5.3.3., Figure 26. However, it is important to note that the decrease in the arsenic adsorption enhancement is not nearly as drastic in the pH 8 samples as it is in the pH 3 samples when there is excess chromium in solution. This is consistent with the isotherm modelling of the pH 8 data which indicates that the adsorption isotherms follow the Freundlich modelling, indicating that multilayer adsorption is occurring. This means that when there is excess chromium in solution, the competition for the binding sites between the chromium-arsenic complex and the individual chromium species is not as high as there can be more than one adsorbate for each of the binding sites available on the surface. This is also consistent in the isotherm comparisons between the mixed metal solutions and the individual chromium solutions. At pH 3 we see that the mixed metal solutions results in lower amounts of chromium adsorption as there is competition between the individual arsenic species, chromium-arsenic complexes, and individual chromium species in solution at the higher concentrations levels. At pH 8, we see that the mixed metal solutions results in higher amounts of chromium adsorbed compared to the individual solutions as the chromium is able to bind in a multilayer fashion with the chromium-arsenic complexes on the surface.

When applying these findings to actual tailings ponds environments, there is much to consider. One sample of oil sands process water (OSPW) that was received contained

extremely low concentrations of chromium and arsenic. A chromium concentration of  $2.66 \pm 0.73$  and an arsenic concentration of  $2.67 \pm 0.27$  was determined. As such, the conclusions of this study would imply that since arsenic and chromium are present in an approximately 1:1 ratio, the presence of both contaminants in solution at this ratio would increase the amount of chromium and arsenic that could be adsorbed onto the AC surface. In hard rock tailings, the ratio of chromium to arsenic is very different. A study by Okewale and Grobler [114] showed that in three different iron tailings, chromium was present in concentrations of 145, 230, and 118 mg of chromium per kg of tailings while arsenic was present in these tailings at concentrations of 7.0, 15.0, and 22.0 mg/kg. This implies that in these iron tailings, chromium is in significant excess compared to arsenic and, based on the results from this study, will then affect the enhancement phenomenon in a negative way due to the fact that excess chromium will be competing with the arsenic and the chromium-arsenic complexes for binding sites on the AC surface. This, again, differs in gold mine tailings where arsenic is much more prominent than chromium in the tailings. Akoto et al. [115] have shown that gold mine tailings in Obuasi have arsenic concentrations reaching up to  $598 \pm 132$  mg/kg and while they did not explicitly state the concentration of chromium, they ranked the mean concentration of metals in the tailings in decreasing order with chromium being lower than arsenic in the list. As such, the research presented in this thesis would imply that since arsenic is in excess compared to the chromium, the ratio of arsenic to chromium is below the maximum arsenic adsorption observed in Figure X and the adsorption of arsenic would therefore be slightly increased due to the presence of lower concentrations of chromium. All of the examples presented above, however, do not take into account the competition or affect that other species in the complicated matrices would pose.

## ***5.4. Conclusion***

In this study, the adsorption of arsenic and chromium were investigated to determine if a co-adsorptive or competitive relationship was present. At low starting concentration of chromium in solution, where all of the chromium can be adsorbed onto the surface, enhancement of the arsenic adsorption is observed. In the pH 3 solutions, once excess chromium is present, the enhancement phenomenon observed for the arsenic adsorption turns to a competitive relationship between the chromium-arsenic complexes that are formed and the excess chromium that is present in solution due to monolayer adsorption; while in the pH 8 solutions, once excess chromium is present, the enhancement phenomenon observed for the arsenic adsorption does not change significantly because multilayer adsorption can occur. Since these metals adsorb to the same binding site, this study was looking to investigate the competitive nature between the species; however, we found that by changing the concentration of one adsorbate, we can have a drastic effect on the adsorption of the opposing analyte. Indicating that while competition is generally observed between adsorbing species, co-adsorptive relationships between the species can cause enhancement of the adsorption for both species. This is important to note when dealing with complex mixtures, such as oil sands processed waters, where an enhancement phenomenon could aid in the removal of certain difficult to remove species.

## Chapter 6 – Conclusions and Future Works

### *6.1. Conclusions*

The main goals of this thesis were to produce an effective adsorbate that can be used for environmental remediation of heavy metals using a petroleum coke feedstock and to determine the mechanisms through which the adsorption of these heavy metals are adsorbed onto the AC surface by investigating how the heavy metals change the functionality of the AC surface. The works presented in this thesis have shown that specific heavy metals can be targeted for adsorption through surface modification of the petroleum coke activated carbon materials.

Chromium adsorption is significantly enhanced through modification of the oxygen functionality on the surface, specifically increasing the amount of hydroxyl functional groups on the AC surface. Chromium adsorption was found to follow a modified Jones Oxidation mechanism where hydroxyl functional groups on the surface of the AC are oxidized to a ketone and the chromium (VI) species in solution is reduced to chromium (III) before physisorption to the AC surface at the newly formed ketone site. Arsenic adsorption is significantly enhanced through the loading of metals onto the AC surface that will allow for oxidation-reduction reactions to occur between the AC itself or the loaded metal modifier and the arsenic in solution.

Similarly, arsenic adsorption occurs through oxidation-reduction reactions with the hydroxyl functional groups on the AC surface or with metal-loaded species on the AC surface where arsenic is reduced from arsenic (V) to arsenic (III) before physisorption to

the AC surface at the newly oxidized sites. It is important to note that arsenic adsorption is also significantly enhanced when present in solution with chromium due to the arsenic's ability to act as a ligand and to form hybrid transition-metal-main-group clusters with the chromium in solution [116,117]. The chromium can then be adsorbed onto the surface of the AC, effectively pulling the arsenic with it to increase the amount of arsenic that is capable of being adsorbed. Therefore, goals one, two, and three of this thesis were achieved as a petroleum coke sourced activated carbon was produced and has been shown to be an effective adsorbate for the removal of the heavy metal species that were investigated, the adsorption mechanisms through which the heavy metals are effectively adsorbed onto the AC surface were determined, and oxygen surface functionality (specifically the hydroxyl and carbonyl groups) of the AC surface was shown through XPS to change as a result of the AC's exposure to the heavy metals in solution.

Goal four of this thesis was to determine the forces which drive the adsorption of the heavy metals onto the AC surface and this was done through modelling of the kinetic data. Kinetic data presented in this work has shown that the driving forces of adsorption tend to be intermolecular forces such as van der Waals, dipole-dipole moments, or hydrogen bonding as opposed to intramolecular forces such as ionic or covalent bonding. In other words, the adsorption of the heavy metals species onto the activated carbon materials generally occurs through physical adsorption to the surface (i.e. physisorption) rather than through chemical adsorption to the surface (i.e. chemisorption).

Finally, goal five of this work was to determine how the behaviour of the chromium and arsenic species change when present in solution together as competition of the species for the hydroxyl functionality was expected. Instead of competition for the

adsorption sites, the results of this study found that co-adsorption of the chromium and arsenic species occurs. At low concentrations of chromium in solution, the arsenic adsorption is significantly enhanced while the chromium adsorption is unchanged. At high concentrations of chromium, the adsorption of arsenic is still enhanced, however to a lesser extent. The adsorption of chromium at the higher concentrations of chromium present in solution is also enhanced at a pH of 8 in the mixed solution compared to the individual chromium solutions due to the fact that multilayer adsorption with the arsenic is occurring. This, however, is not the case at pH 3, where the adsorption of chromium at the higher concentration of chromium present in solution is competing with the arsenic adsorption in the mixed solution, showing a lower adsorption of chromium in the mixed solution compared to the individual chromium solution. This is due to the fact that at pH 3, monolayer adsorption is occurring and the chromium and arsenic in the mixed solution are competing for the binding sites on the AC surface.

## ***6.2. Future Studies***

While this thesis focuses on the individual adsorption mechanisms of chromium and arsenic, and the behaviour of these metals in a mixed solution, hard rock mine tailings and oil sands tailings contain a complex mixture of heavy metals far beyond the two metals investigated in this thesis. As such, future research should include the individual adsorption of other metal species present in these contaminated waters such as aluminium, copper, iron, magnesium, manganese, molybdenum, nickel, lead, selenium, strontium, vanadium, and zinc. Determination of the model adsorption of these metal species onto the petroleum coke sourced activated carbon would provide information regarding the surface modification needed for their removal. Following individual

modelling of the adsorption of these metals, mixed solutions containing these metals can also be investigated to determine competition and/or enhancement behaviour occurring between the metal species in solution. This future work would provide valuable information on the adsorbent material required for the environmental remediation of contaminated wastewater and whether the metal contaminants should be specifically targeted with a specially designed activated carbon or whether a solve-all activated carbon can be produced to target all of the metal species in contaminated water supplies.

## Reference List

1. Fisher, Kyle S.; Vreugdenhil, Andrew J.. Adsorption of Chromium (VI) Using an Activated Carbon Derived from Petroleum Coke Feedstock. *Int. J. Mol. Sci.* 2022, 23, 19172. DOI: <https://doi.org/10.3390/ijms232416172>
2. Fisher, Kyle S.; Vreugdenhil, Andrew J.. Metal-Impregnated Petroleum Coke-Derived Activated Carbon for the Adsorption of Arsenic in Acidic Waters. *ACS Omega*. 8, 32, 29083-29100. 31 Jul. 2023. DOI: <https://doi.org/10.1021/acsomega.3c02078>
3. Fisher, Kyle S.; Vreugdenhil, Andrew J.. Investigation of the Co-Adsorptive Relationship between Arsenic (V) and Chromium (VI) Using a Petroleum Coke Sourced Activated Carbon. *Pending Publication*.
4. United States Environmental Protection Agency. Potential Well Water Contaminants and Their Impacts. *EPA*. Available Online: <https://www.epa.gov/privatewells/potential-well-water-contaminants-and-their-impacts#:~:text=Heavy%20metals%20can%20leach%20into,plants%2C%20and%20natural%20mineral%20deposits>. (last accessed on: Nov. 15, 2023)
5. The Mining Association of Canada. Economic Impacts and Drivers for the Global Energy Transition Report Highlights State of Canada's Mining Industry. *The Mining Association of Canada*. May 10, 2023. Available Online: <https://mining.ca/resources/press-releases/economic-impacts-and-drivers-for-the-global-energy-transition-report-highlights-state-of-canadas-mining-industry/> (last accessed Nov. 16, 2023)
6. Government of Canada. What are the oil sands? Government of Canada. Available Online: <https://www.nrcan.gc.ca/our-natural-resources/energy-sources-distribution/fossil-fuels/crude-oil/what-are-oil-sands/18089> (last accessed on: Nov. 15, 2023)
7. Government of Canada. Oil Resources. Government of Canada. Available Online: <https://www.nrcan.gc.ca/our-natural-resources/energy-sources-distribution/fossil-fuels/crude-oil/oil-resources/18085> (last accessed on: Nov. 15, 2023)
8. Alberta Energy Regulator. Oil Sands Mining. Nov. 2022. Available Online: [https://www.aer.ca/protecting-what-matters/holding-industry-accountable/industry-performance/water-use-performance/oil-sands-mining-water-use#:~:text=Water%2DUse%20Intensity&text=In%202021%2C%20oil%20sands%20mining,\(see%20the%20following%20figure\)](https://www.aer.ca/protecting-what-matters/holding-industry-accountable/industry-performance/water-use-performance/oil-sands-mining-water-use#:~:text=Water%2DUse%20Intensity&text=In%202021%2C%20oil%20sands%20mining,(see%20the%20following%20figure)). (last accessed on: Nov. 15, 2023)

9. Mining for Bitumen. Oil Sands Magazine. Mar. 3, 2021. Available Online: <https://www.oilsandsmagazine.com/technical/mining> (last accessed on: Nov. 15, 2023)
10. Oodith, Yajna; Mohammadi, Amir H.. An Overview of Oil Sand (Tar Sand) Extraction and Processing. Oct. 23, 2018. DOI: 10.13140/RG.2.2.30533.70889
11. Commission for Environmental Cooperation (CEC). Alberta Tailings Ponds II, Factual Record Regarding Submission SEM-17-001. North America Environmental Law and Policy. Sept. 2020. Available Online through Download at: <http://www.cec.org/publications/alberta-tailings-ponds-ii-factual-record/> (last accessed on: Nov. 15, 2023)
12. Kelly, Erin N.; et al.. Oil sands development contributes elements toxic at low concentrations to the Athabasca River and its tributaries. PNAS. Vol. 107: No. 37. Sept. 14, 2010. DOI: [www.pnas.org/cgi/doi/10.1073/pnas.1008754107](http://www.pnas.org/cgi/doi/10.1073/pnas.1008754107)
13. Kavanagh, Richard J.; et al.. Detecting oil sands process-affected waters in the Alberta oil sands region using synchronous fluorescence spectroscopy. Chemosphere. 120-126. Mar. 9, 2009. DOI: <https://doi.org/10.1016/j.chemosphere.2009.02.007>
14. Ahas, Jason M. E.; et al.. Characterization and Quantification of Mining-Related “Naphthenic Acids” in Groundwater near a Major Oil Sands Tailings Pond. Environ. Sci. Technol. 47, 5023-5030. Spr. 22, 2013. DOI: [dx.doi.org/10.1021/es3051313](http://dx.doi.org/10.1021/es3051313)
15. Roy, James W., Bickerton, Greg. Proactive Screening Approach for Detecting Groundwater Contaminants along Urban Streams at the Reach-Scale. Environ. Sci. Technol. 44, 6088-6094. June 30, 2010. DOI: 10.1021/es101492x
16. Li, C., A. Singh, N. Klameth, K. McPhedran, P. Chelme-Ayala, M. Belosevic and M. Gamal ElDin, 2014. Synthesis of Toxicological Behavior of Oil Sands Process-Affected Water Constituents. Oil Sands Research and Information Network, University of Alberta, School of Energy and the Environment, Edmonton, Alberta. OSRIN Report No. TR-50. 101 pp. Available Online: <https://era.library.ualberta.ca/items/5676110f-0176-4e24-934f-bac38d9123b7> (last accessed on: Nov. 15, 2023)
17. Toxics Use Reduction Institute. Hexavalent Chromium: Summary of Health and Environmental Effects. *TURI*. Available Online: <https://www.turi.org/content/download/8867/159153/file/Fact+Sheet+Hexavalent+Chromium+2013.pdf> (last accessed Nov. 16, 2023)
18. Environmental Health and Medicine Education. What are the Physiologic Effects of Arsenic Exposure? *Agency for Toxic Substances and Disease Registry (ATSDR)*. Available Online: [https://www.atsdr.cdc.gov/csem/arsenic/physiologic\\_effects.html](https://www.atsdr.cdc.gov/csem/arsenic/physiologic_effects.html) (last accessed on: Nov. 15, 2023)
19. Office of Wastewater Management. Hardrock Mining Overview. *U.S. Environmental Protection Agency*. Available Online:

- <https://www3.epa.gov/npdes/pubs/overview.htm> (last accessed on: Nov. 15, 2023)
20. Government of Canada, Environmental Code. Environmental Code of Practice for Metal Mines. *Government of Canada*. Mar. 3, 2017. Available Online: <https://www.ec.gc.ca/lcpe-cepa/default.asp?lang=En&n=CBE3CD59-1&offset=4> (last accessed on: Nov. 15, 2023)
  21. Office of Wastewater Management. Hardrock Mining Wastes. *U.S. Environmental Protection Agency*. Available Online: <https://www3.epa.gov/npdes/pubs/wastes.htm> (last accessed on: Nov. 15, 2023)
  22. Fashola, Muibat Omotola; Ngole-Jeme, Veronica Mpode; Babalola, Olubukola Oluranti. Heavy Metal Pollution from Gold Mines: Environmental Effects and Bacterial Strategies for Resistance. *Int. J. Environ. Res. Public Health*. 2016. 13(11), 1047. DOI: <https://doi.org/10.3390/ijerph13111047>
  23. Khulbe, K. C.; Matsuura, T. Removal of heavy metals and pollutants by membrane adsorption techniques. *Appl. Water Sci.* 2018, 8, 19. DOI: <https://doi.org/10.1007/s13201-018-0661-6>
  24. Gomase, V.; Jugade, R.; Doondani, P.; Saravanan, D.; Pandey, S. Sequential modifications of chitosan biopolymer for enhanced confiscation of Cr (VI). *Inorg. Chem. Commun.* 2022, 145, 110009. DOI: <https://doi.org/10.1016/j.inoche.2022.110009>
  25. Agboola, Omowumi D.; Benson, Nsikak U.. Physisorption and Chemisorption Mechanisms Influencing Micro (Nano) Plastics-Organic Chemical Contaminants Interactions: A Review. *Front. Environ. Sci.*. Vol. 9. May 28 2021. DOI: <https://doi.org/10.3389/fenvs.2021.678574>
  26. Tolkou, Athanasia, K.; Katsoyiannis, Ioannis A.; Zouboulis, Anastasios I.. Removal of Arsenic, Chromium and Uranium from Water Sources by Novel Nanostructured Materials Including Graphene-Based Modified Adsorbents: A Mini Review of Recent Developments. *Appl. Sci.* 10, 3241. May 7 2020. DOI: 10.3390/app10093241
  27. Zhang, K.; Dwivedi, V.; Chi, C.; Wu, J. Graphene oxide/ferric hydroxide composites for efficient arsenate removal from drinking water. *J. Hazard. Mater.* 2010, 182, 162–168. DOI: 10.1016/j.jhazmat.2010.06.010
  28. Jacukowicz-Sobala, I.; Ocinski, D.; Mazur, P.; Stanisławska, E.; Kociołek-Balawejder, E. Cu(II)-Fe(III) oxide doped anion exchangers—Multifunctional composites for arsenite removal from water via As(III) adsorption and oxidation. *J. Hazard. Mater.* 2020. DOI: <https://doi.org/10.1016/j.jhazmat.2020.122527>
  29. Xu, W.; Wang, J.; Wang, L.; Sheng, G.; Liu, J.; Yu, H.; Huang, X.-J. Enhanced arsenic removal from water by hierarchically porous CeO<sub>2</sub>-ZrO<sub>2</sub> nanospheres: Role of surface- and structure-dependent properties. *J. Hazard. Mater.* 2013, 260, 498–507. DOI: <https://doi.org/10.1016/j.jhazmat.2013.06.010>
  30. Mahato, Birendra Nath; Krithiga, T.. Efficient removal of arsenic and chromium from waste water by solvent free synthesized Fe<sub>2</sub>O<sub>3</sub>/AISBA-15 adsorbent. *Materials Today: Proceedings*. 17; 303-312. (2019) DOI: <https://doi.org/j.matpr.2019.06.434>
  31. Setshedi, K.Z.; Bhaumik, M.; Onyango, M.S.; & Maity, A. High-performance towards Cr (VI) removal using multi-active sites of polypyrrole-graphene oxide

- nanocomposites: Batch and column studies. *Chem. Eng. J.* 2015, 262, 921–931. DOI: <https://doi.org/10.1016/j.cej.2014.10.034>
32. Neisan, Roya Sadat et al. Arsenic Removal by Adsorbents from Water for Small Communities' Decentralized Systems : Performance, Characterization, and Effective Parameters. *Clean Technol.* 5(1), 352-402. Mar. 6, 2023. DOI: <https://doi.org/10.3390/cleantechnol5010019>
  33. Karnib, Mona; Kabbani, Ahmad; Holail, Hanafy; Olama, Zakia. Heavy Metals Removal using Activated Carbon, Silica, and Silica Activated Carbon Composite. *Energy Procedia.* 50, 113-120. 2014. DOI: <https://doi.org/10.1016/j.egypro.2014.06.014>
  34. Chatzimichailidou, Stella; Xanthopoulou, Maria; Tolkou, Athanasia K.; Katsoyiannis, Ioannis A.. Biochar Derived from Rice by-Products for Arsenic and Chromium Removal by Adsorption: A Review. *J. Compos. Sci.* 7, 59. Feb. 4, 2023. DOI: <https://doi.org/10.3390/jcs7020059>
  35. Pinedo-Torres, Laura Alejandra; et al.. Adsorption of Arsenic, Lead, Cadmium, and Chromium Ions from Aqueous Solution Using a Protonated Chabazite: Preparation, Characterization, and Removal Mechanism. *Adsorp. Sci. Technol.* Jan. 25, 2023. DOI: <https://doi.org/10.1155/2023/2018121>
  36. Alslaibi, Tamer M.; Abustan, Ismail; Ahmad, Mohd Azmier; Foul, Ahmad Abu. A review: production of activated carbon from agricultural by-products via conventional and microwave heating. *J. Chem. Technol. Biotechnol.* 88: 1183-1190. Feb. 11 2013. DOI: 10.1002/jctb.4028
  37. Tadda MA, Ahsan A, Shitu A, ElSergany M, Arunkumar T, Jose B, Razzaque MA, Daud NNN. A review on activated carbon: process, application and prospects. *Journal of Advanced Civil Engineering Practice and Research.* 2016; 2(1):7-13. <http://ababilpub.com/download/jacepr2-1-3/> (last accessed on: Nov. 15, 2023)
  38. Kuraray Co. LTD. Raw Materials. Available Online: <http://www.kuraray-c.co.jp/en/activecarbon/about/03.html> (last accessed on: Nov. 15, 2023)
  39. Cho, Dong-Wan et al.. Adsorption of nitrate and Cr (VI) by cationic polymer-modified granular activated carbon. *J. Chem. Eng.* 175, 295-305. Sept. 23, 2011. DOI: 10.1016/j.cej.2011.09.108
  40. Narayanan, N. Vivek; Ganesan, Mahesh. Use of adsorption using granular activated carbon (GAC) for the enhancement of removal of chromium from synthetic wastewater by electrocoagulation. *J. Hazard. Mater.* 161, 575-580. Apr. 3, 2008. DOI: 10.1016/j.jhazmat.2008.03.113
  41. Taiwo, Ademiluyi Falilat; Chinyere, Nze Jane. Sorption Characteristics for Multiple Adsorption of Heavy Metal Ions Using Activated Carbon from Nigerian Bamboo. *J. Mater. Sci. Chem. Eng.* 4, 39-48. Apr. 28 2016. DOI: <http://dx.doi.org/10.4236/msce.2016.44005>
  42. Gong, Xu-Jin; Li, Wei-Guang; Zhang, Duo-Ying; Fan, Wen-Biao; Zhang, Xin-Ran. Adsorption of arsenic from micro-polluted water by an innovative coal-based mesoporous activated carbon in the presence of co-existing ions. *Int. Biodeterior. Biodegrad.* 102, 256-264. Feb. 3, 2015. DOI:

- <http://dx.doi.org/10.1016/j.ibiod.2015.01.007>
43. Phonphuak, N.; Chindaprasirt, P.. Eco-Efficient Masonry Bricks and Blocks, Chapter 6 – Types of waste, properties, and durability of pore-forming waste-based fired masonry bricks. Subsection 6.3.3 Sawdust. Pages 103-127, 2015. DOI: <https://doi.org/10.1016/B978-1-78242-305-8.00006-1>
  44. Wood Energy. List and values of wood fuel parameters – Part 3. *Wood Energy*. Available Online: [http://www.woodenergy.ie/woodasafuel/listandvaluesofwoodfuelparameters-part3/#:~:text=The%20structural%20elements%20\(ultimate%20analysis,the%20small%20amount%20of%20sulphur.](http://www.woodenergy.ie/woodasafuel/listandvaluesofwoodfuelparameters-part3/#:~:text=The%20structural%20elements%20(ultimate%20analysis,the%20small%20amount%20of%20sulphur.) (last accessed on: Nov. 15, 2023)
  45. Celzard, A.; Fierro, V.; Marêché, J.F.; Furdin, G.. Advanced Preparative Strategies for Activated Carbons Designed for the Adsorptive Storage of Hydrogen. *Adsorb. Sci. Technol.* Vol. 25 No. 3/4. Apr. 2007. DOI: 10.1260/026361707782398254
  46. Rouzaud, J.N.; Oberlin, A.. Structure, microtexture, and optical properties of anthracene and saccharose-based carbons. *Carbon*. Vol. 27 Issue 4. 517-529. 1989. DOI: [https://doi.org/10.1016/0008-6223\(89\)90002-X](https://doi.org/10.1016/0008-6223(89)90002-X)
  47. Encyclopaedia Britannica. Charcoal. *1911 Encyclopaedia Britannica*. June 1. 2016. Available Online: [https://en.wikisource.org/wiki/1911\\_Encyclop%C3%A6dia\\_Britannica/Charcoal](https://en.wikisource.org/wiki/1911_Encyclop%C3%A6dia_Britannica/Charcoal) (last accessed on: Nov. 15, 2023)
  48. Agico Cement. Carbonization. Available Online: [https://agicokiln.com/activated-carbon-production-line/?gclid=Cj0KCQiA54KfBhCKARIsAJzSrdoZEBh5CB25XivRVi7odjUN1ou3\\_aLmokTKj5S7i7oDZue8BBejEsaAsZaEALw\\_wcB](https://agicokiln.com/activated-carbon-production-line/?gclid=Cj0KCQiA54KfBhCKARIsAJzSrdoZEBh5CB25XivRVi7odjUN1ou3_aLmokTKj5S7i7oDZue8BBejEsaAsZaEALw_wcB) (last accessed on: Nov. 15, 2023)
  49. Sinopec. Petroleum Coke. *Sinopec*. Available Online: <http://www.sinopecgroup.com/group/en/ProductsServices/sycp3.shtml#:~:text=The%20composition%20of%20petroleum%20coke,catalytic%20cracking%2C%20etc> (last accessed on: Nov. 15, 2023)
  50. OilChange International, Petroleum Coke: The Coal Hiding in the Tar Sands Report. January 2013. Available Online: <https://priceofoil.org/content/uploads/2013/01/OCI.Petcoke.FINALSCREEN.pdf> (last accessed on: Nov. 15, 2023)
  51. McKinsey. Coker. *Energy Insights*. Available Online: [https://www.mckinseyenergyinsights.com/resources/refinery-reference-desk/coker/#:~:text=In%20a%20refinery%2C%20the%20coker,solid%20carbon%20\(pet%20coke\)](https://www.mckinseyenergyinsights.com/resources/refinery-reference-desk/coker/#:~:text=In%20a%20refinery%2C%20the%20coker,solid%20carbon%20(pet%20coke)) (last accessed on: Nov. 15, 2023)
  52. Tripathi, Nimisha; Singh, Raj S.; Hills, Colin D.. Microbial removal of sulfur from petroleum coke (petcoke). *Fuel*. 235, 1501-1505. 14 Aug. 2018. DOI: <https://doi.org/10.1016/j.fuel.2018.08.072>
  53. Strem Chemicals. Safety Data Sheet : Activated Carbon Item 06-0050. Available Online: [https://www.strem.com/uploads/sds/sd06-0050\\_US.pdf](https://www.strem.com/uploads/sds/sd06-0050_US.pdf) (last accessed on: Nov. 16, 2023)

54. Strong, O.K.L.; Nazari, E.; Roy, T.; Scotland, K.M.; Pede, P.R.; Vreugdenhil, A.J.. Transforming micropores and mesopores by heat cycling KOH activated petcoke for improved kinetics of adsorption of naphthenic acids. *Heliyon*. 9 (2) e13500, 2023. DOI: <https://doi.org/10.1016/j.heliyon.2023.e13500>
55. Revellame, E.D.; Fortela, D.L.; Sharp, W.; Hernandez, R.; Zappi, M.E. Adsorption kinetic modelling using pseudo-first order and pseudo-second order rate laws: A review. *Clean. Eng. Technol.* 2020, 1, 100032. DOI: <https://doi.org/10.1016/j.clet.2020.100032>
56. Government of Alberta. Annual Report: Energy 2020–2021. June 2021. Available Online: <https://open.alberta.ca/dataset/cbd7147b-d304-4e3e-af28-78970c71232c/resource/4da34006-a913-46e7-b7cc-eb8d66e2e999/download/energy-annual-report-2020-2021.pdf> (last accessed on: Nov. 16, 2023)
57. Allen, W. E.. Process water treatment in Canada’s oil sands industry: I. Target pollutants and treatment objectives. *J. Environ. Eng. Sci.* 2008, 7, 123–138. DOI: <https://doi.org/10.1139/S07-038>
58. Health Canada. Federal-Provincial-Territorial Committee on Drinking Water. Chromium in Drinking Water—Document for Public Consultation. Government of Canada. Available Online: <https://www.canada.ca/en/health-canada/programs/chromium-drinking-water/chromium-drinking-water.html> (last accessed on: Nov. 16, 2023)
59. Leghouchi, E.; Laib, E.; Guerbet, M. Evaluation of chromium contamination in water, sediment and vegetation caused by the tannery of Jijel (Algeria): a case study. *Environ. Monit. Assess.* 2008, 153, 111–117. DOI: <https://doi.org/10.1007/s10661-008-0341-3>
60. MiningWatch Canada, Potential Toxic Effects of Chromium, Chromite Mining, and Ferrochrome Production: A Literature Review, May 2012. Available Online: [https://miningwatch.ca/sites/default/files/chromite\\_review.pdf](https://miningwatch.ca/sites/default/files/chromite_review.pdf) (last accessed on: Nov. 16, 2023)
61. Mohan, D.; Pittman, C. U., Jr. Activated carbons and low cost adsorbents for remediation of tri- and hexavalent chromium from water. *J. Hazard. Mater.* 2006, B137, 762–811. DOI: <https://doi.org/10.1016/j.jhazmat.2006.06.060>
62. Yang, J.; Li, C.; Yang, B.; Kang, S.; Zhang, Z. Study on Adsorption of Chromium (VI) by Activated Carbon from Cassava Sludge. *IOP Conf. Ser. Earth Environ. Sci.* 2018, 128, 012017. DOI: <https://doi.org/10.1088/1755-1315/128/1/012017>
63. Wang, Y.; Peng, C.; Padilla-Ortega, E.; Robledo-Cabrera, A.; López-Valdivieso, A. Cr(VI) adsorption on activated carbon: Mechanisms, modelling and limitations in water treatment. *J. Environ. Chem. Eng.* 2020, 8, 104031. DOI: <https://doi.org/10.1016/j.jece.2020.104031>
64. Alvarez-Galvan, Y.; Minofar, B.; Futera, Z.; Francoeur, M.; Jean-Marius, C.; Brehm, N.; Yacou, C.; Jauregui-Haza, U. J.; Gaspard, S. Adsorption of Hexavalent Chromium Using Activated Carbon Produced from *Sargassum* ssp.: Comparison between Lab

- Experiments and Molecular Dynamics Simulations. *Molecules*. 2022, 27, 6040. DOI: <https://doi.org/10.3390/molecules27186040>.
65. Guo, S.; Gao, Y.; Wang, Y.; Liu, Z.; Wei, X.; Peng, P.; Xiao, B.; Yang, Y.. Urea/ZnCl<sub>2</sub> in situ hydrothermal carbonization of *Camellia sinensis* waste to prepare N-doped biochar for heavy metal removal. *Environ. Sci. Pollut. Res.* 2019, 26, 30365–30373. DOI: <https://doi.org/10.1007/s11356-019-06194-8>.
66. Chu, B.; Amano, Y.; Machida, M. Preparation of bean dreg derived N-doped activated carbon with high adsorption for Cr(VI). *Colloids Surf. A* 2019, 586, 124262. DOI: <https://doi.org/10.1016/j.colsurfa.2019.124262>.
67. Surface Science Western X-ray Photoelectron Spectroscopy (XPS) Reference Pages. Oxygen. Available Online: <http://www.xpsfitting.com/search/label/Oxygen> (last accessed on: Nov. 16, 2023)
68. Naumkin, A.V.; Kraut-Vass, A.; Gaarenstroom, S.W.; Powel, C.J. NIST X-ray Photoelectron Spectroscopy Database. 2012. Available Online: <https://srdata.nist.gov/xps/> (last accessed on: Nov. 16, 2023)
69. Moulder, J.F.; Stickle, W.F.; Sobol, P.E.; Bomben, K.D. Handbook of X-ray Photoelectron Spectroscopy—A Reference Book of Standard Spectra for Identification and Interpretation of XPS Data. Perkin-Elmer Corporation. October 1992. Available Online: <https://www.hic.ch.ntu.edu.tw/PES/file/%E5%8F%83%E8%80%83%E8%B3%87%E6%96%99/XPS%20handbook.pdf> (last accessed on: Nov. 16, 2023)
70. Tran, Hai Nguyen; You, Sheng-Jie; Hosseini-Bandegharai, Ahmad; Chao, Huan-Ping. Mistakes and inconsistencies regarding adsorption of contaminants from aqueous solutions: A critical review. *Water Res.* 120, 88-116. 18 Apr. 2017. DOI: <http://dx.doi.org/10.1016/j.watres.2017.04.014>
71. Surface Science Western X-ray Photoelectron Spectroscopy (XPS) Reference Pages. Chromium. Available Online: <http://www.xpsfitting.com/search/label/Chromium> (last accessed on: Nov. 16, 2023)
72. Biesinger, M.C.; Brown, C.; Mycroft, J. R.; Davidson, R. D.; McIntyre, N. S.. R-Ray Photoelectron Spectroscopy Studies of Chromium Compounds. *Surf. Interface Anal.* 2004, 36, 1550–1563. DOI: <https://doi.org/10.1002/sia.1983>
73. Clayden, J.; Greeves, N.; Warren, S.. *Organic Chemistry*, 2nd ed.; Oxford University Press: Oxford, UK, 2012.
74. Rakhunde, R.; Deshpande, L.; Juneja, H.D. Chemical Speciation of Chromium in Water: A Review. *Environ. Sci. Technol.* 2012, 42, 776–810. DOI: <https://doi.org/10.1080/10643389.2010.534029>.
75. National Research Council. Arsenic: medical and biological effects of environmental pollutants. *National Academy of Sciences*. 1977. DOI: 10.17226/9003
76. de Andrade, Renato Pereira; Filho, Salomão Santana; de Mello, Jaime Wilson Vargas; de Figueiredo, Bernardino Ribeiro; Dussin, Tânia Mara. Arsenic Mobilization from Sulfuric Materials from Gold Mines in Minas Gerais State. *Quim. Nova*. Vol. 31, No. 5, 1127-1130. 15 May 2008. DOI: <https://doi.org/10.1590/S0100-40422008000500037>

77. Clark, Ian D.; Raven, Kenneth G.. Sources and Circulation of Water and Arsenic in the Giant Mine, Yellowknife, NWT, Canada. *Isotopes Environ. Health Stud.* 115-128. 26 Jan. 2007. DOI: <https://doi.org/10.1080/10256010410001671014>
78. Society for Mining, Metallurgy, and Exploration. The Role of Arsenic in the Mining Industry. Apr. 2015. Available Online: <https://me.smenet.org/docs/Publications/ME/Issue/TheRoleofArsenicintheMiningIndustry.pdf> (last accessed on: Nov. 16, 2023)
79. World Health Organization. Arsenic. Feb. 15, 2018. Available Online: <https://www.who.int/news-room/fact-sheets/detail/arsenic#:~:text=Arsenic%20is%20highly%20toxic%20in,cause%20cancer%20and%20skin%20lesions.> (last accessed on: Nov. 16, 2023)
80. World Health Organization. Drinking Water. Mar. 21, 2022. Available Online: <https://www.who.int/news-room/fact-sheets/detail/drinking-water> (last accessed on: Nov. 16, 2023)
81. Byambaa, Erdenechimeg; et al.. Arsenic (V) Removal by an Adsorbent Material Derived from Acid Mine Drainage Sludge. *Appl. Sci.* 11, 47. 23 Dec. 2020. DOI: <https://dx.doi.org/10.3390/app11010047>
82. Singh, Simranjeet; et al.. A systematic study of arsenic adsorption and removal from aqueous environments using novel graphene oxide functionalized UiO-66NDC nanocomposites. *Scientific Reports.* 12:15802. 2022. DOI: <https://doi.org/10.1038/s41598-022-18959-2>
83. Rahdar, Somayeh; Taghavi, Mahmoud; Khaksefidi, Razieh; Ahmadi, Shahin. Adsorption of arsenic (V) from aqueous solution using modified saxaul ash: isotherm and thermodynamic study. *Appl. Wat. Sci.* 9:87. 13 May 2019. DOI: <https://doi.org/10.1007/s13201-019-0974-0>
84. Liu, Cheng-Hua; et al.. Mechanism of Arsenic Adsorption on Magnetite Nanoparticles from Water: Thermodynamic and Spectroscopic Studies. *Environ. Sci. Technol.* 49, 7726-7734. 9 Jun. 2015. DOI: 10.1021/acs.est.5b00381
85. Zhang, Jianying; et al.. Enhanced Adsorption of Trivalent Arsenic from Water by Functionalized Diatom Silica Shells. *PLoS ONE.* 10(4): e0123395. DOI: 10.1371/journal.pone.0123395
86. Yao, Shuhua; Liu, Ziru; Shi, Zhongliang. Arsenic removal from aqueous solutions by adsorption onto iron oxide/activated carbon magnetic composite. *J. Environ. Health Sci. Eng.* 12:58. 2014. DOI: 10.1186/2052-336X-12-58
87. Pourrezaei, Parastoo; et al.. Removal of organic compounds and trace metals from oil sands process-affected water using zero valent iron enhanced by petroleum coke. *J. Environ. Manage.* 139. 26 Mar. 2014. DOI: <http://dx.doi.org/10.1016/j.jenvman.2014.03.001>
88. Karimi, Arash; Thinon, Olivier; Fournier, Joseph; Hill, Josephine M.. Activated Carbon Prepared from Canadian Oil Sands Coke by CO<sub>2</sub> Activation: II. Adsorption of Metallic Ions and Organic Constituents from Oil Sands Tailings Water. *Can. J. Chem. Eng.* 91. 24 Jan. 2013. DOI: 10.1002/cjce.21769
89. Mondal, Monoj Kumar; Garg, Ravi. A Comprehensive Review on Removal of Arsenic using Activated Carbon Prepared from Easily Available Waste Materials. *Environ. Sci. Pollut. Res.* Apr.11, 2017. DOI: <https://doi.org/10.1007/s11356-017-8842-7>
90. Nesbitt, H. W.; Banerjee, D.. Interpretation of XPS Mn(2p) spectra of Mn oxyhydroxides and constraints on the mechanism of MnO<sub>2</sub> precipitation. *Am. Min.* Vol. 83, 305-315. 1998. DOI: 0003-004X/98/0304-0305\$05.00

91. Grosvenor, A. P.; Kobe, B. A.; Biesinger, M. C.; McIntyre, N. S.. Investigation of multiplet splitting of Fe 2p XPS spectra and bonding in iron compounds. *Surf. Interface Anal.*. 36: 1564-1574. 7 Oct. 2004. DOI: 10.1002/sia.1984
92. Surface Science Western. X-Ray Photoelectron Spectroscopy (XPS) Reference Pages. Multiplet Splitting. Available Online: <http://www.xpsfitting.com/2008/09/multiplet-splitting.html> (last accessed on: Nov. 16, 2023)
93. Surface Science Western. X-Ray Photoelectron Spectroscopy (XPS) Reference Pages. Arsenic. Available Online: <http://www.xpsfitting.com/search/label/Arsenic> (last accessed on: Nov. 16, 2023)
94. Surface Science Western. X-Ray Photoelectron Spectroscopy (XPS) Reference Pages. Iron. Available Online: <http://www.xpsfitting.com/search/label/Iron> (last accessed on: Nov. 16, 2023)
95. Surface Science Western. X-Ray Photoelectron Spectroscopy (XPS) Reference Pages. Manganese. Available Online: <http://www.xpsfitting.com/search/label/Manganese> (last accessed on: Nov. 16, 2023)
96. Rahman, Md Musfiqur; Hafez, Islam; Tajvidi, Mehdi; Amirbahman, Aria. Highly Efficient Iron Oxide Nanoparticles Immobilized on Cellulose Nanofibril Aerogels for Arsenic Removal from Water. *Nanomaterials*. 23 Oct. 2021. DOI: <https://doi.org/10.3390/nano11112818>
97. Chiavola, Agostina; D'Amato, Emilio; Stoller, Marco; Chianese, Angelo; Boni, Mario Rosaria. Application of Iron Based Nanoparticles as Adsorbents for Arsenic Removal from Water. *The Italian Association of Chemical Engineering*. Vol. 47, 2016. DOI: <https://doi.org/10.3303/CET1647055>
98. Lagergren, S.. About the theory of so-called adsorption of soluble substances. *K. Sven. Vetensk. Handl.* 24 (4), 1e39. 1898. In press.
99. Blanchard, G.; Maunaye, M.; Martin, G.. Removal of heavy metals from waters by means of natural zeolites. *Water Res.*. 18 (12), 1501-1507. 1984. DOI: [https://doi.org/10.1016/0043-1354\(84\)90124-6](https://doi.org/10.1016/0043-1354(84)90124-6)
100. Tolkou, Athanasia, K.; Kyzas, George Z.; Katsoyiannis, Ioannis, A.. Arsenic (III) and Arsenic (V) Removal from Water Sources by Molecularly Imprinted Polymers (MIPs): A Mini Review of Recent Developments. *Sustainability*. 26 Apr. 2022. DOI: <https://doi.org/10.3390/su14095222>
101. Shakoor, Muhammad Bilal; et al.. Exploring the arsenic removal potential of various biosorbents from water. *Environ. Int.*. 123, 567-579. 07 Jan. 2019. DOI: <https://doi.org/10.1016/j.envint.2018.12.049>
102. The Business Research Company. Mining Global Market Report 2023. *Research and Markets*. April 2023. Available Online: <https://www.researchandmarkets.com/reports/5781216/mining-global-market-report#:~:text=The%20growth%20rate%20of%20the%20Global%20Mining%20Market%20is%206.7,of%20%242775.5%20billion%20by%202027.> (last accessed on: Nov. 16, 2023)
103. Hadzi, George Yaw. Effect of Mining on Heavy Metals Toxicity and Health Risk in Selected Rivers of Ghana. *IntechOpen*. June 23, 2022. DOI: 10.5772/intechopen.102093
104. Flora, Swaran Jeet Singh. *Handbook or Arsenic Toxicology*, 1<sup>st</sup> ed.; Academic Press: Dec. 26, 2014.
105. Little, Amanda J.; et al.. The impacts of century-old, arsenic-rich mine tailings on multi-trophic level biological assemblages in lakes from Cobalt (Ontario, Canada). *Sci. Total Environ.*. 709, 136212. Dec. 20, 2019. DOI:

- <https://doi.org/10.1016/j.scitotenv.2019.136212>
106. Smith, Allan H.; Steinmaus, Craig M.. Health Effects of Arsenic and Chromium in Drinking Water: Recent Human Findings. *Annu. Rev. Public Health.* 30: 107-122. Apr. 29 2009. DOI: 10.1146/annurev.publhealth.031308.100143
  107. Katz, S.A.; Salem, H.. The toxicology of chromium with respect to its chemical speciation: a review. *J. Appl. Toxicol.* 13(3):217-24. June 1993. DOI: 10.1001/jat.2550130314
  108. Suljević, Damir; et al.. Assessing hexavalent chromium tissue-specific accumulation patterns and induced physiological responses to probe chromium toxicity in *Coturnix japonica* quail. *Chemosphere.* 266, 129005. Mar. 2021. DOI: <https://doi.org/10.1016/j.chemosphere.2020.129005>
  109. Ding, Zecong; Fu, Fenglian; Dionysiou, Dionysios D.; Tang, Bing. Coadsorption and subsequent redox conversion behaviors of As (III) and Cr (VI) on Al-containing ferrihydrite. *Environ. Pollut.* 235; 660-669. Jan. 12 2018. DOI: <https://doi.org/10.1016/j.envpol.2017.12.118>
  110. Azzam, Ahmed M.; et al.. Nanospherical inorganic  $\alpha$ -Fe core-organic shell necklaces for the removal of arsenic (V) and chromium (VI) from aqueous solution. *J. Phys. Chem. Solids.* 109; 78-88. May 19 2017. DOI: <http://dx.doi.org/10.1016/j.jpcs.2017.05.017>
  111. Mahata, Birendra Nath; Krithiga, T.. Efficient removal of arsenic and chromium from waste water by solvent free synthesized  $\text{Fe}_2\text{O}_3/\text{AISBA-15}$  adsorbent. *Materials Today: Proceedings -ICAMEES2018.* 303-312. 2019. DOI: <https://doi.org/10.1016/j.matpr.2019.06.434>
  112. Sing, Kenneth S. W. and Williams, Ruth T.. Physisorption Hysteresis Loops and the Characterization of Nanoporous Materials. *Adsorp. Sci. Technol.* Vol. 22. No. 10. 15 Jun. 2004. DOI: <https://journals.sagepub.com/doi/pdf/10.1260/0263617053499032#:~:text=Type%20H4%20loops%20are%20given,multilayer%20physisorption%20and%20capillary%20condensation>
  113. Kalam, Shams; et al.. Surfactant Adsorption Isotherms: A Review. *ACS Omega.* 6: 32342-32348. 2021. DOI: <https://doi.org/10.1021/acsomega.1c04661>
  114. Okewale, Ismail Adeniyi; Grobler, Hendrik. Assessment of heavy metals in tailings and their implications on human health. *GeoGeo.* 20 Apr. 2023. DOI: <https://doi.org/10.1016/j.geogeo.2023.100203>
  115. Akoto, Osei; et al.. Characterization, Spatial Variation and Risk Assessment of Heavy Metals and a Metalloid in Surface Soils in Obuasi, Ghana. *J. Health Pollut.* 8(19), Sept. 2018. DOI: <https://doi.org/10.5696/2156-9614-8.19.180902>
  116. Sturala, Jiri; Sofer, Zdenek; Pumera, Martin. Coordination chemistry of 2D and layered gray arsenic: photochemical functionalization with chromium hexacarbonyl. *NPG Asia Materials.* 11:42. 2019. DOI: <https://doi.org/10.1038/s41427-019-0142-x>
  117. Dimairo, Anthony-Joseph; Rheingold, Arnold. Structural Chemistry of Transition-Metal Complexes Containing Arsenic-Arsenic Bonds. *Chem. Rev.* Vol. 90 No. 1: 169-190. Aug. 7, 1989. DOI: <https://pubs.acs.org/doi/10.1021/cr00099a006>

## Appendix A: Fe2p, Mn2p, and As2p Peak Deconvolution

This appendix provides the XPS spectra for the FeMn-Loaded AC pre-arsenic exposure, the Fe-Loaded AC post-arsenic exposure, and the Mn-Loaded AC post-arsenic exposure.

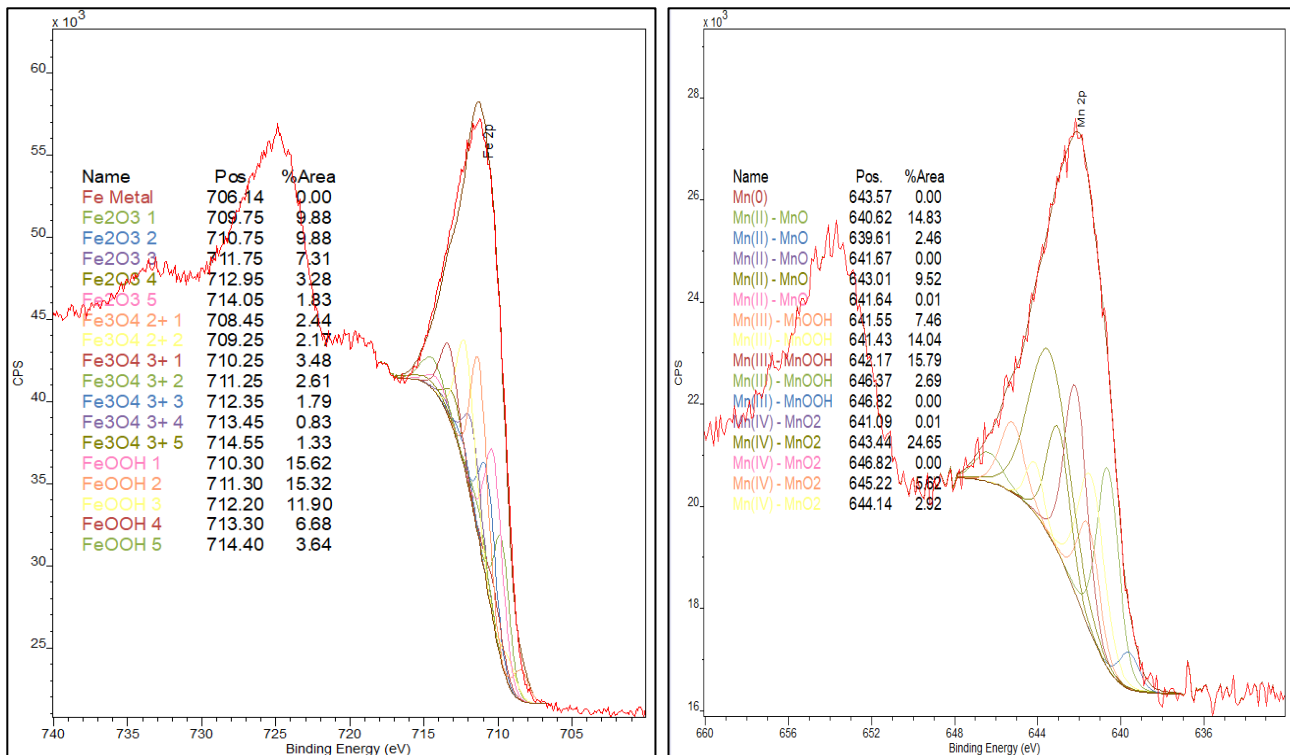


**Figure A1:** XPS deconvolution of the Fe2p (left) and Mn2p (right) peaks in the FeMn-Loaded AC pre-arsenic exposure.

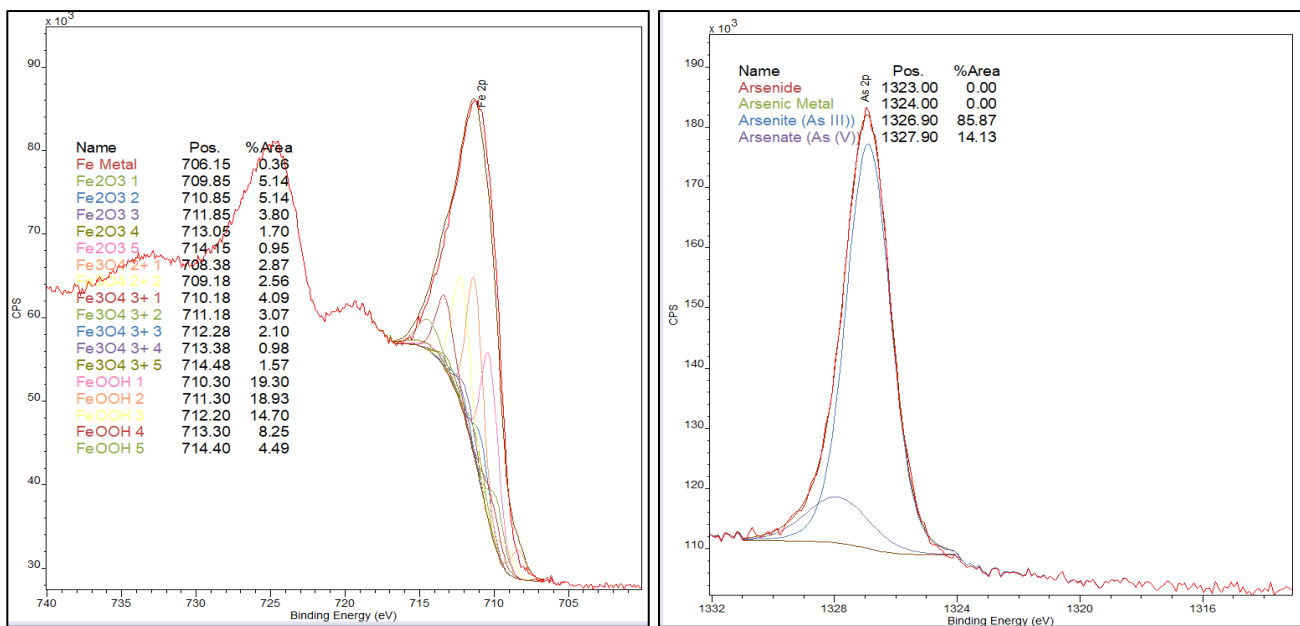


**Figure A2:** XPS deconvolution of the Fe2p (left) and As2p (right) peaks in the Fe-Loaded AC post-arsenic exposure.

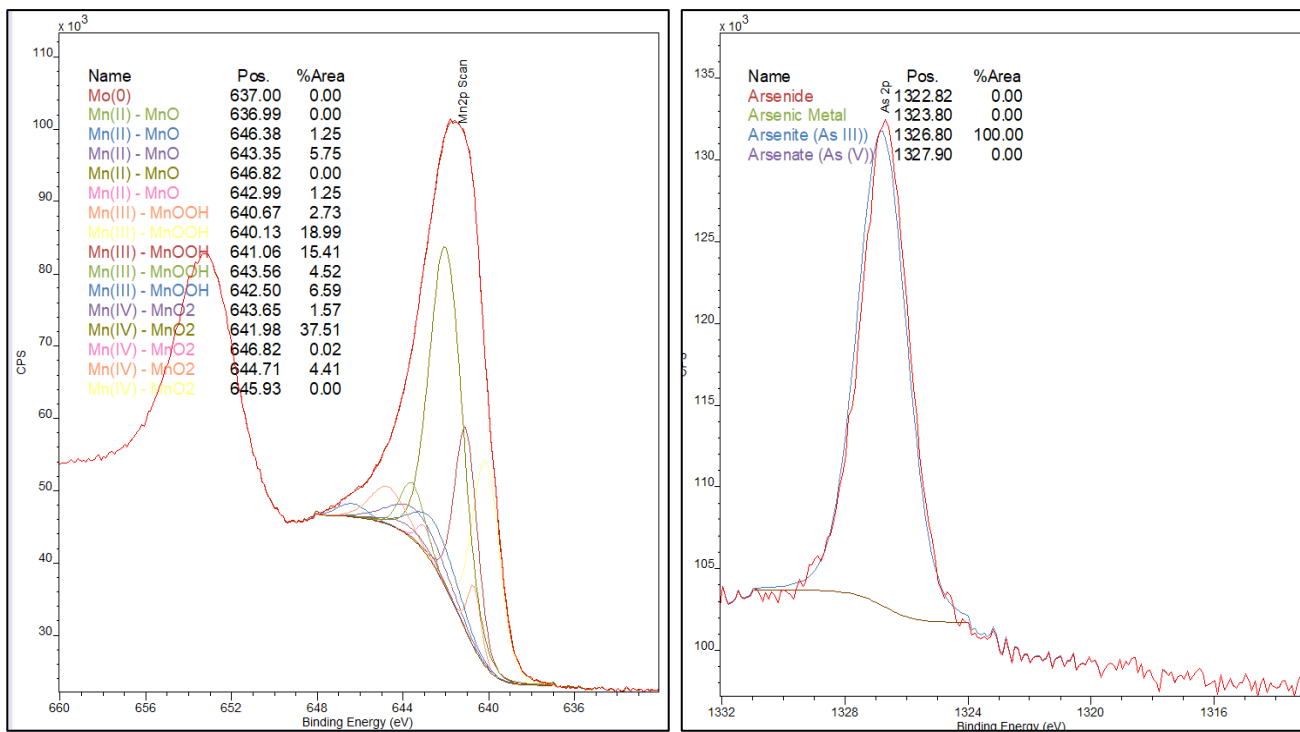


**Figure A3:** XPS deconvolution of the Mn2p (left) and As2p (right) peaks in the Mn-Loaded AC post-arsenic exposure.

## Appendix B: Elemental Distribution Mapping

This appendix provides the elemental distribution of carbon, oxygen, iron, and manganese in the Standard, Fe-Loaded, and Mn-Loaded activated carbons. This appendix also includes a layered distribution map of each of the surface's elemental composition.

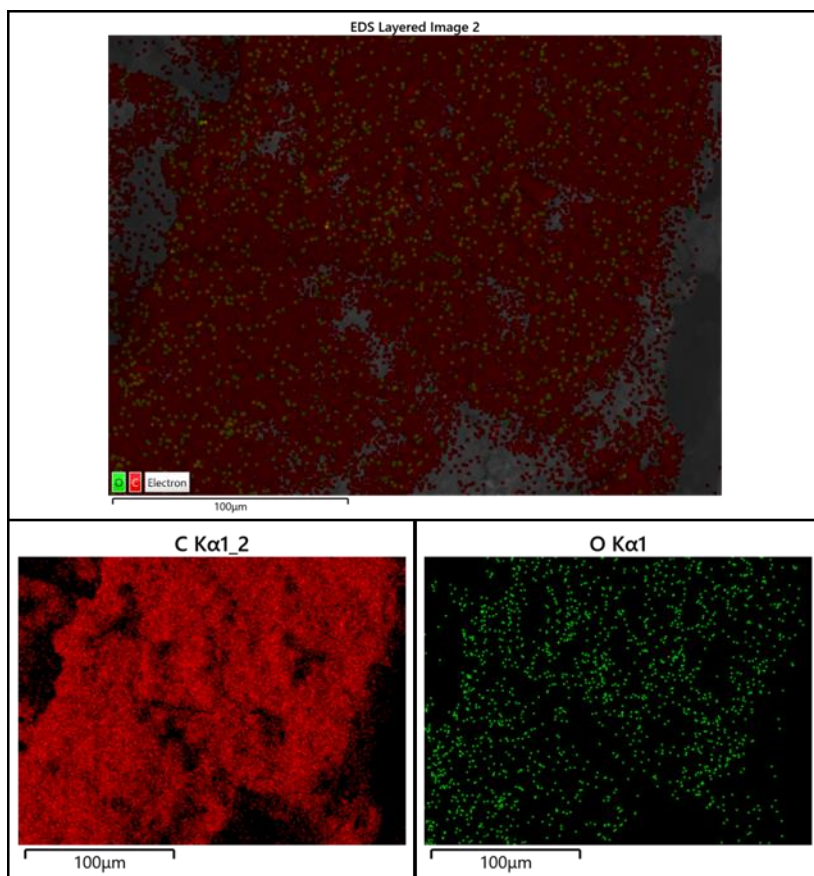


**Figure B1:** Elemental distribution mapping of the carbon (bottom left), and oxygen (bottom right) present within the Standard AC at 500x magnification. A layered distribution map of the surface's elemental composition is shown at the top.

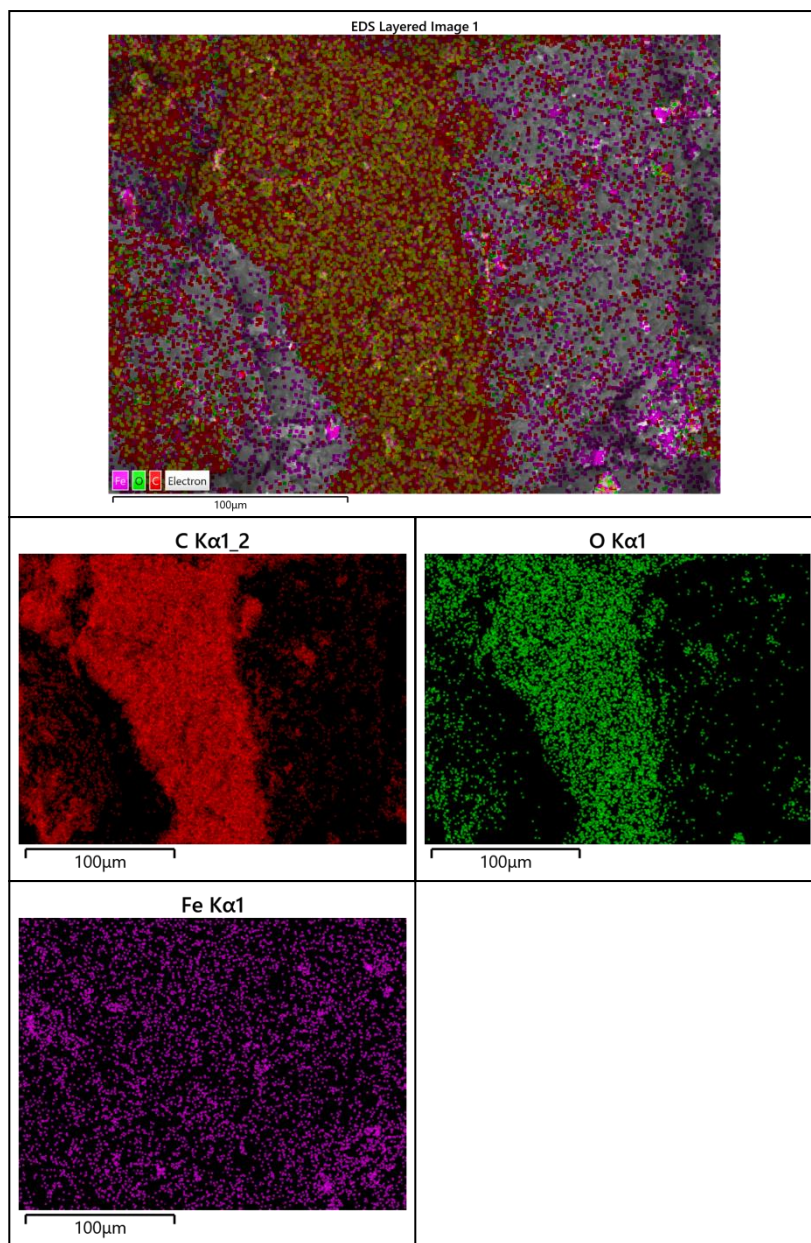


**Figure B2:** Elemental distribution mapping of carbon (middle left), oxygen (middle right), and iron (bottom) present within the Fe-Loaded activated carbon at 500x magnification. A layered distribution map of the surface's elemental composition is shown at the top.

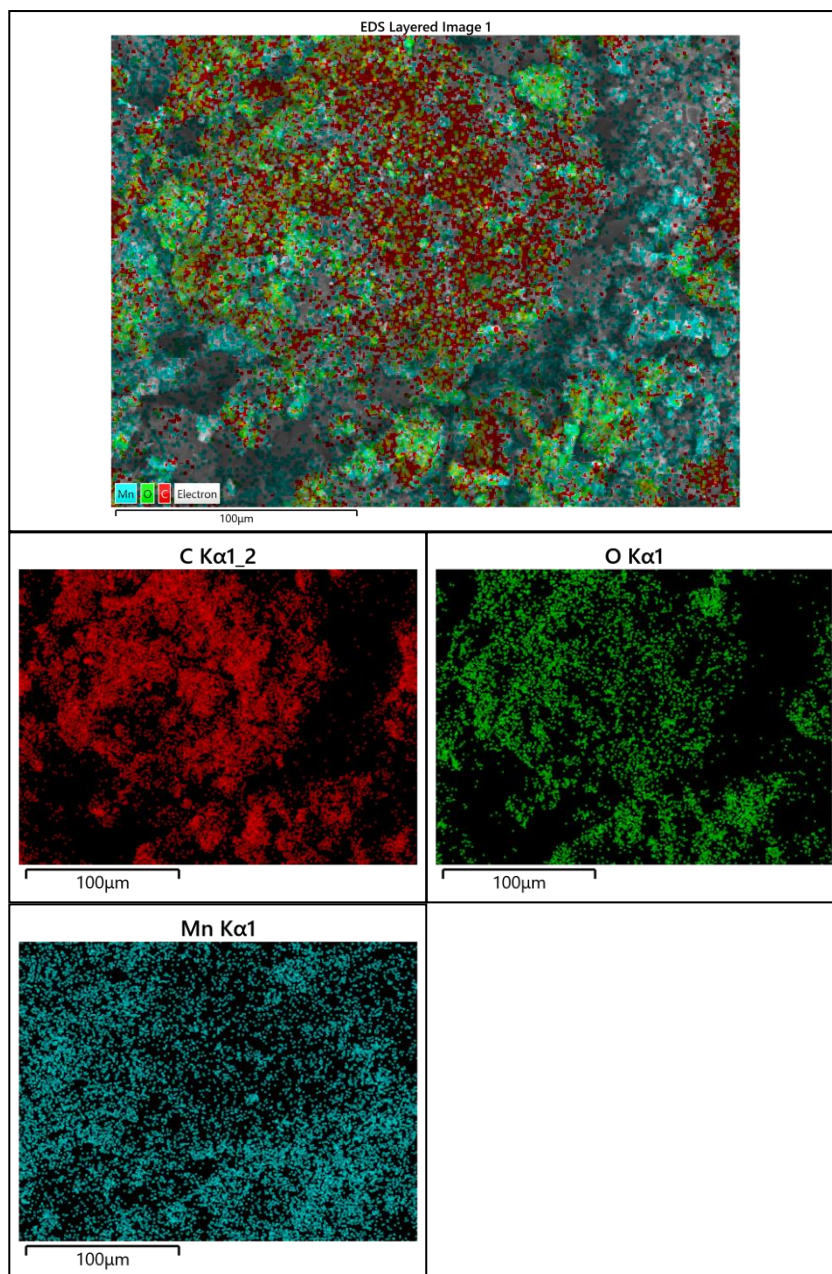


**Figure B3:** Elemental distribution mapping of carbon (middle left), oxygen (middle right), and manganese (bottom) present within the Mn-loaded activated carbon at 500x magnification. A layered distribution map of the surface's elemental composition is shown at the top.

## Appendix C: O1s Peak Deconvolution

This appendix provides the O1s peak deconvolution of the Fe-, Mn-, and FeMn-Loaded ACs pre-arsenic exposure.

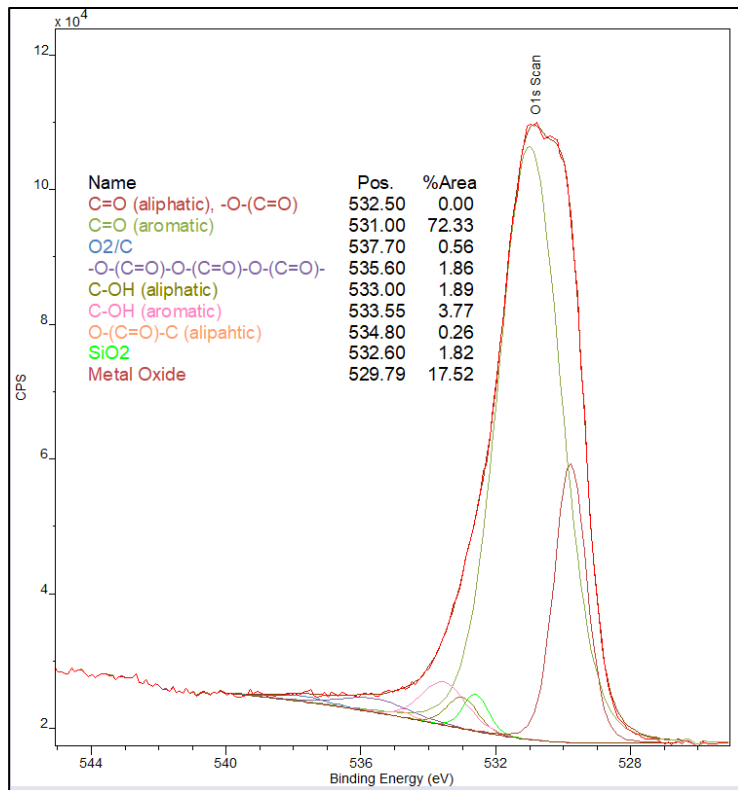


**Figure C1:** XPS deconvolution of the O1s peak for the Fe-Loaded AC.

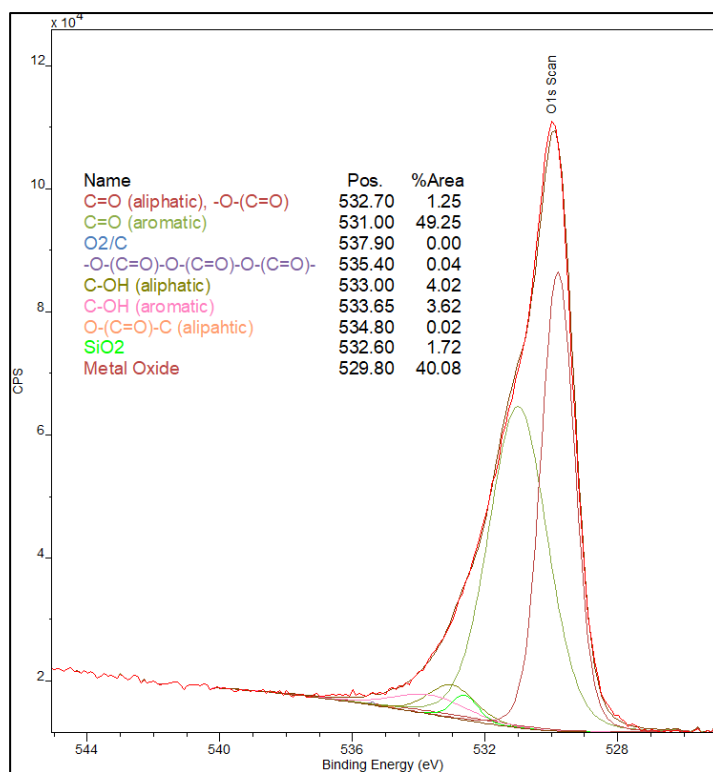


**Figure C2:** XPS deconvolution of the O1s peak for the Mn-Loaded AC.

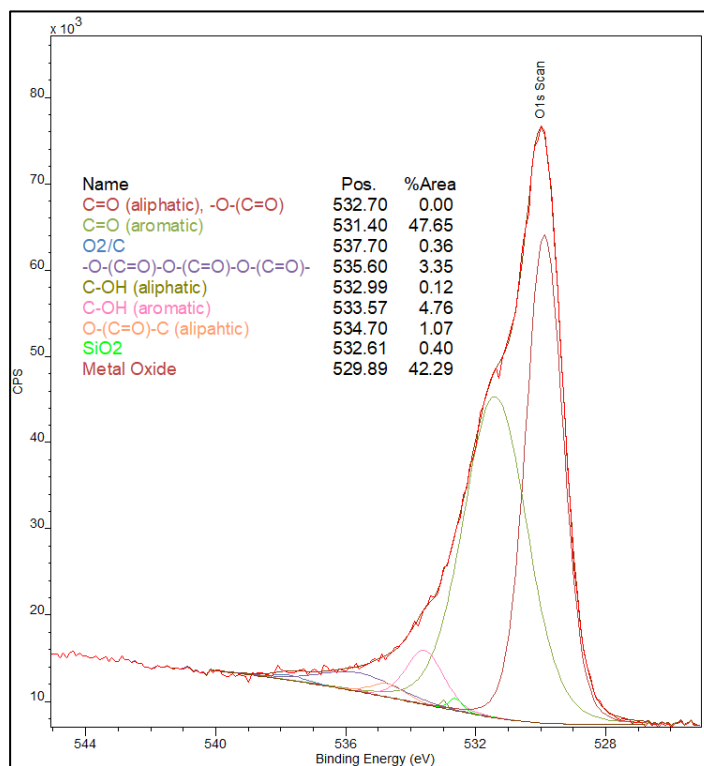


**Figure C3:** XPS deconvolution of the O1s peak for the FeMn-Loaded AC.

### Appendix D: Kinetic Modelling for the Adsorption of As (V)

This appendix provides the pseudo first-order and pseudo second-order kinetic modelling for the adsorption of arsenic (V) using the Standard AC, Commercial AC, Fe-Loaded AC, and Mn-Loaded AC.

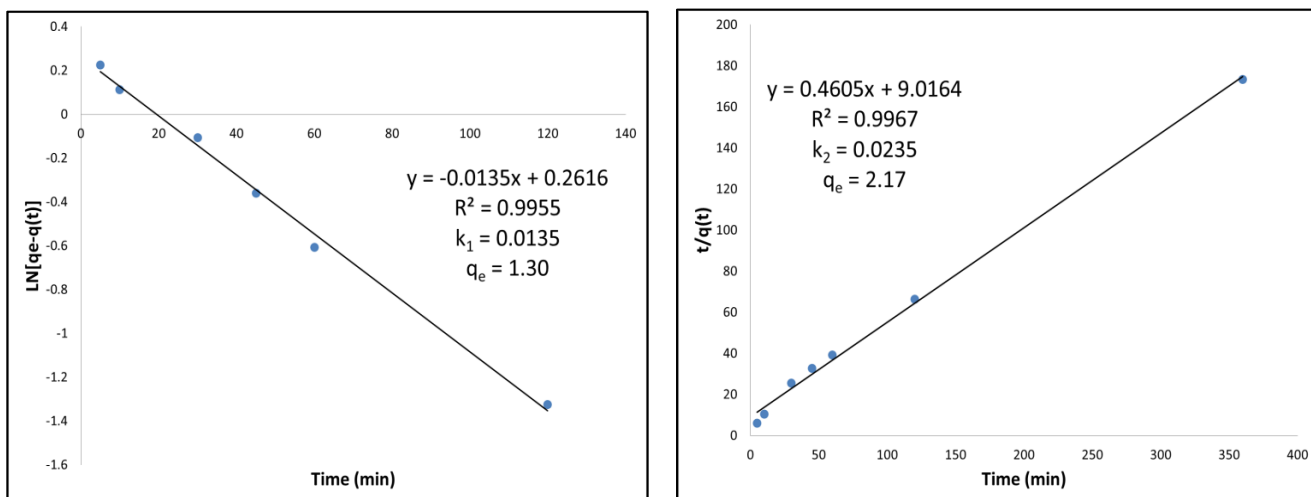


**Figure D1:** Pseudo First- (left) and Pseudo Second- (right) Order kinetic models for the adsorption of As (V) using the Standard AC.

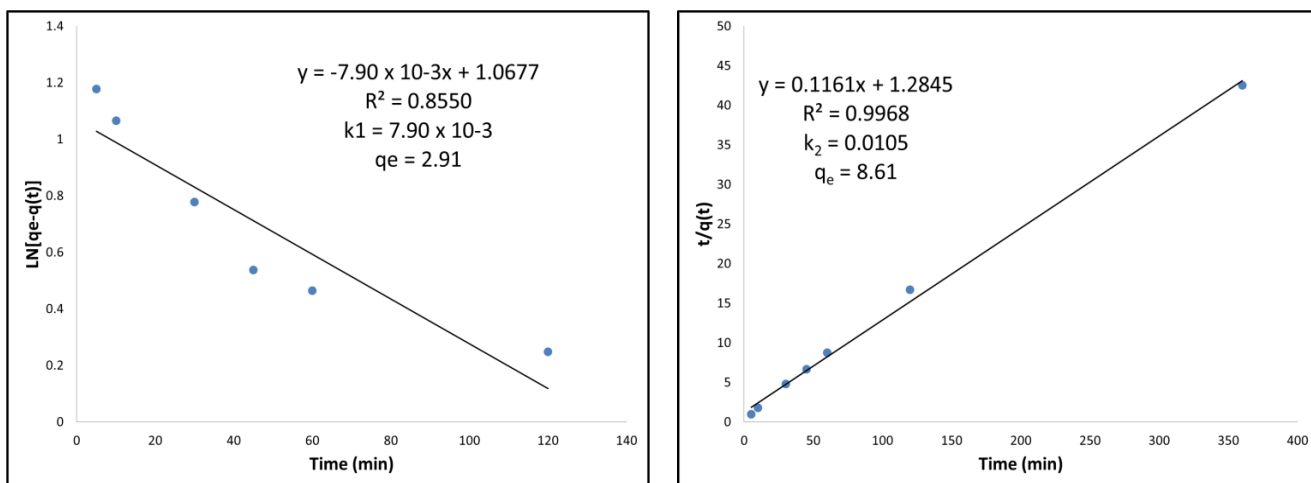


**Figure D2:** Pseudo First- (left) and Pseudo Second- (right) Order kinetic models for the adsorption of As (V) using the Commercial AC.

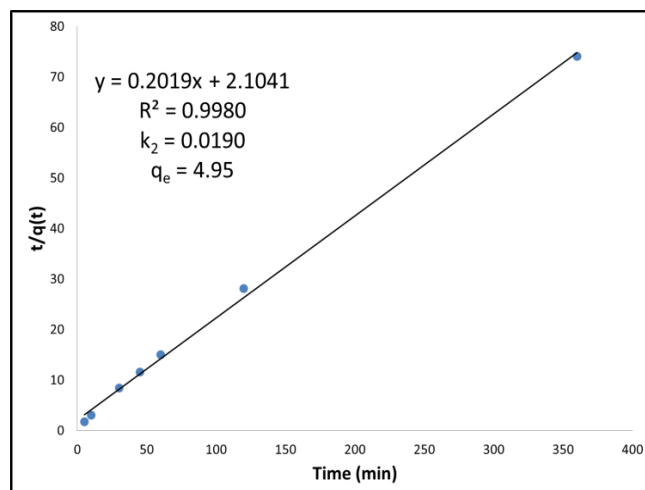
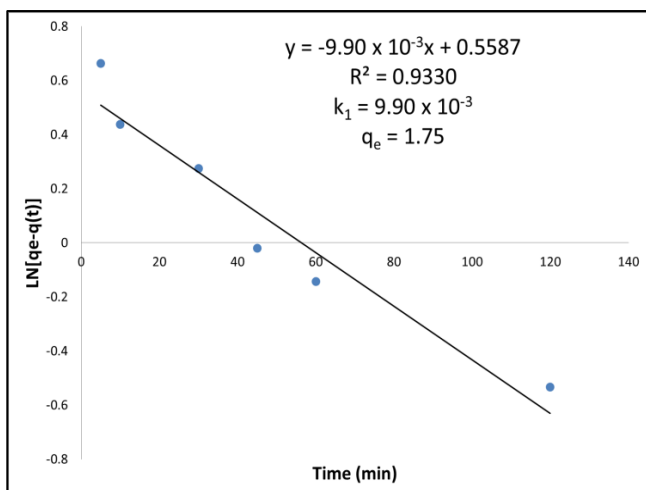


**Figure D3:** Pseudo First- (left) and Pseudo Second- (right) Order kinetic models for the adsorption of As (V) using the Fe-Loaded AC.

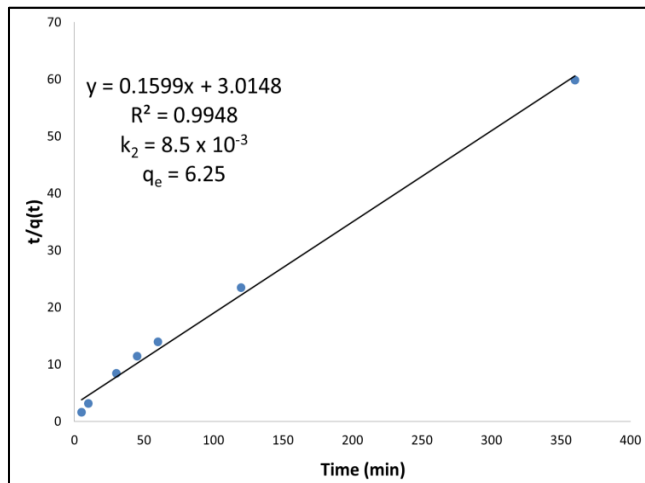
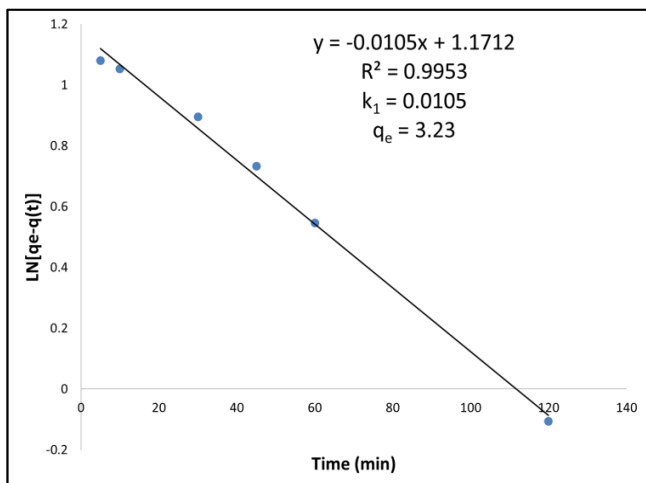


**Figure D4:** Pseudo First- (left) and Pseudo Second- (right) Order kinetic models for the adsorption of As (V) using the Mn-Loaded AC.

### Appendix E: Kinetic Modelling for the Adsorption of As (III)

This appendix provides the pseudo first-order and pseudo second-order kinetic modelling for the adsorption of arsenic (III) using the Standard AC, Commercial AC, and FeMn-Loaded AC.

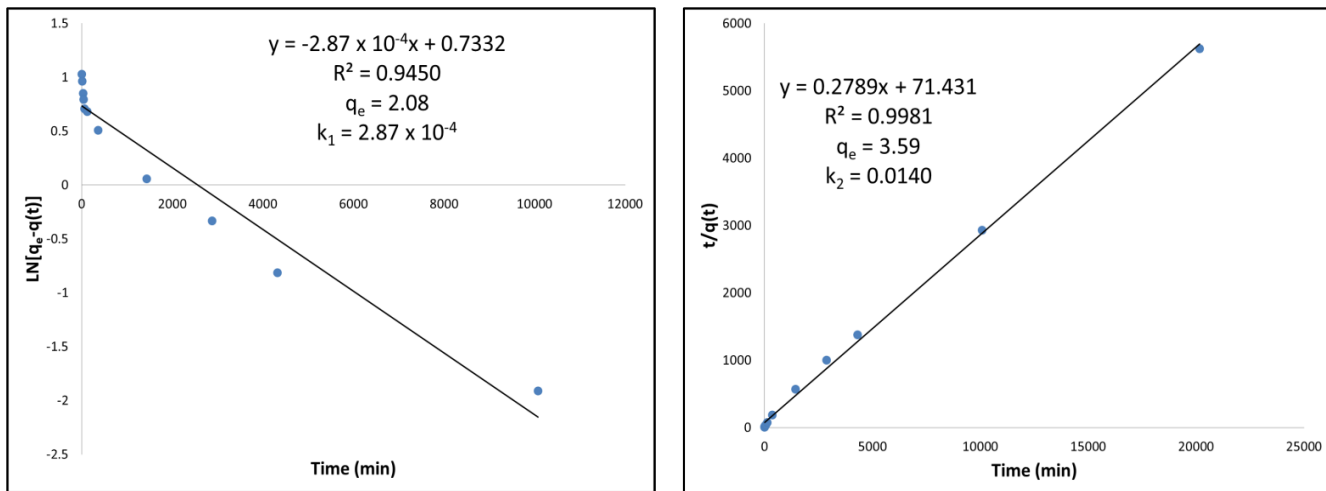


**Figure E1:** Pseudo First- (left) and Pseudo Second- (right) Order kinetic models for the adsorption of As (III) using the Standard AC.

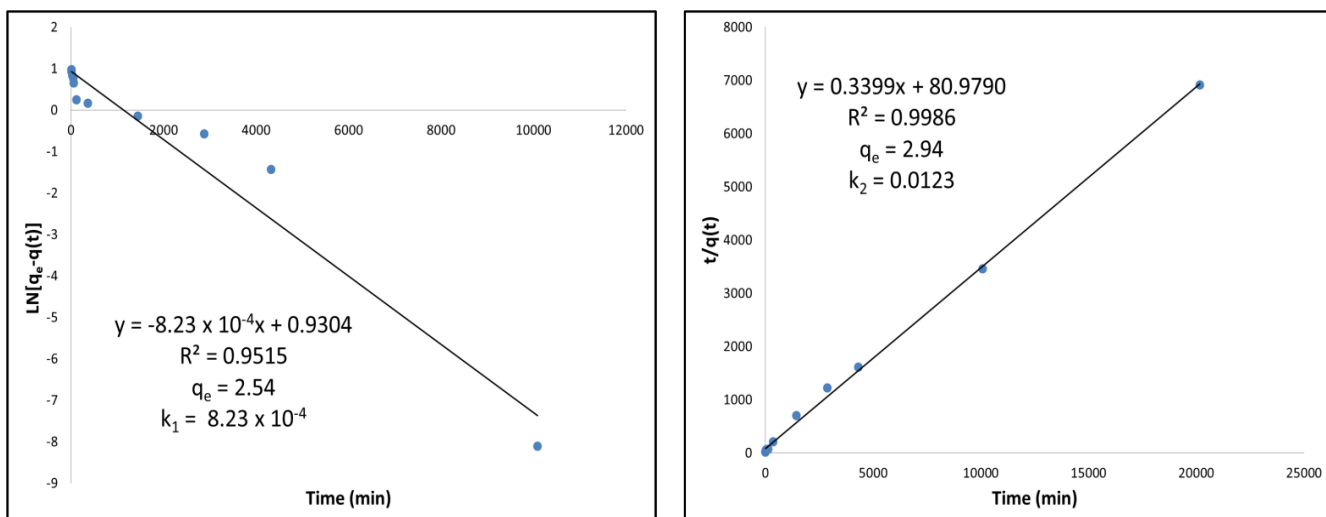


**Figure E2:** Pseudo First- (left) and Pseudo Second- (right) Order kinetic models for the adsorption of As (III) using the Commercial AC.

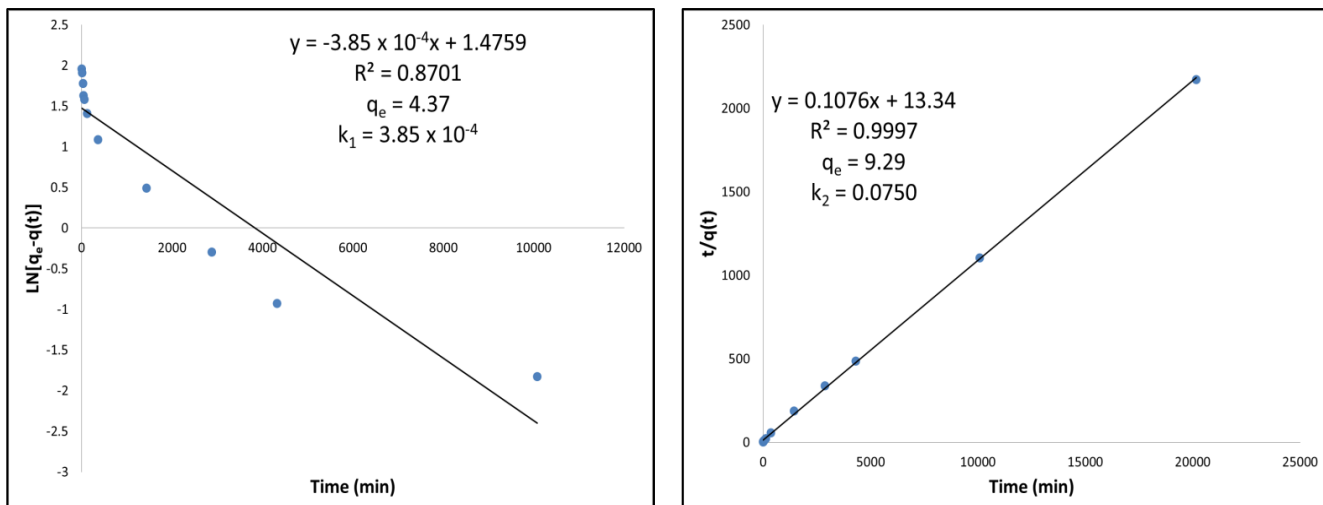


**Figure E3:** Pseudo First- (left) and Pseudo Second- (right) Order kinetic models for the adsorption of As (III) using the FeMn-Loaded AC.

## Appendix F: Freundlich Isotherm Modelling for pH 3 Chromium Adsorption

This appendix provides the Freundlich isotherm modelling for the pH 3 chromium in the mixed metal solutions and in the individual chromium solutions.

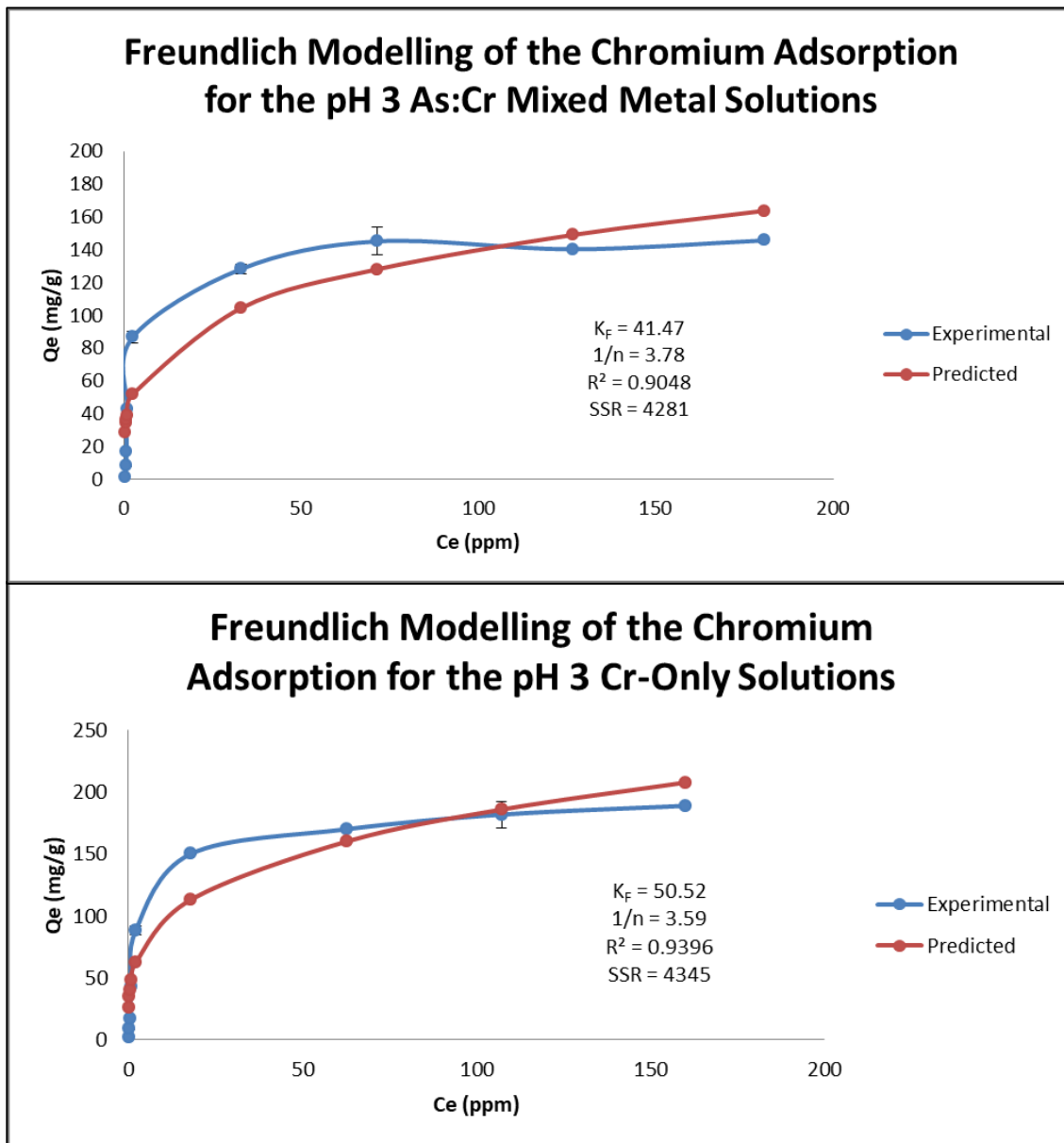


**Figure F1:** Freundlich isotherm modelling of the chromium adsorption for the pH 3 isotherm data.

### Appendix G: Langmuir Isotherm Modelling for pH 8 Chromium Adsorption

This appendix provides the Langmuir isotherm modelling for the pH 8 chromium in the mixed metal solutions and in the individual chromium solutions.

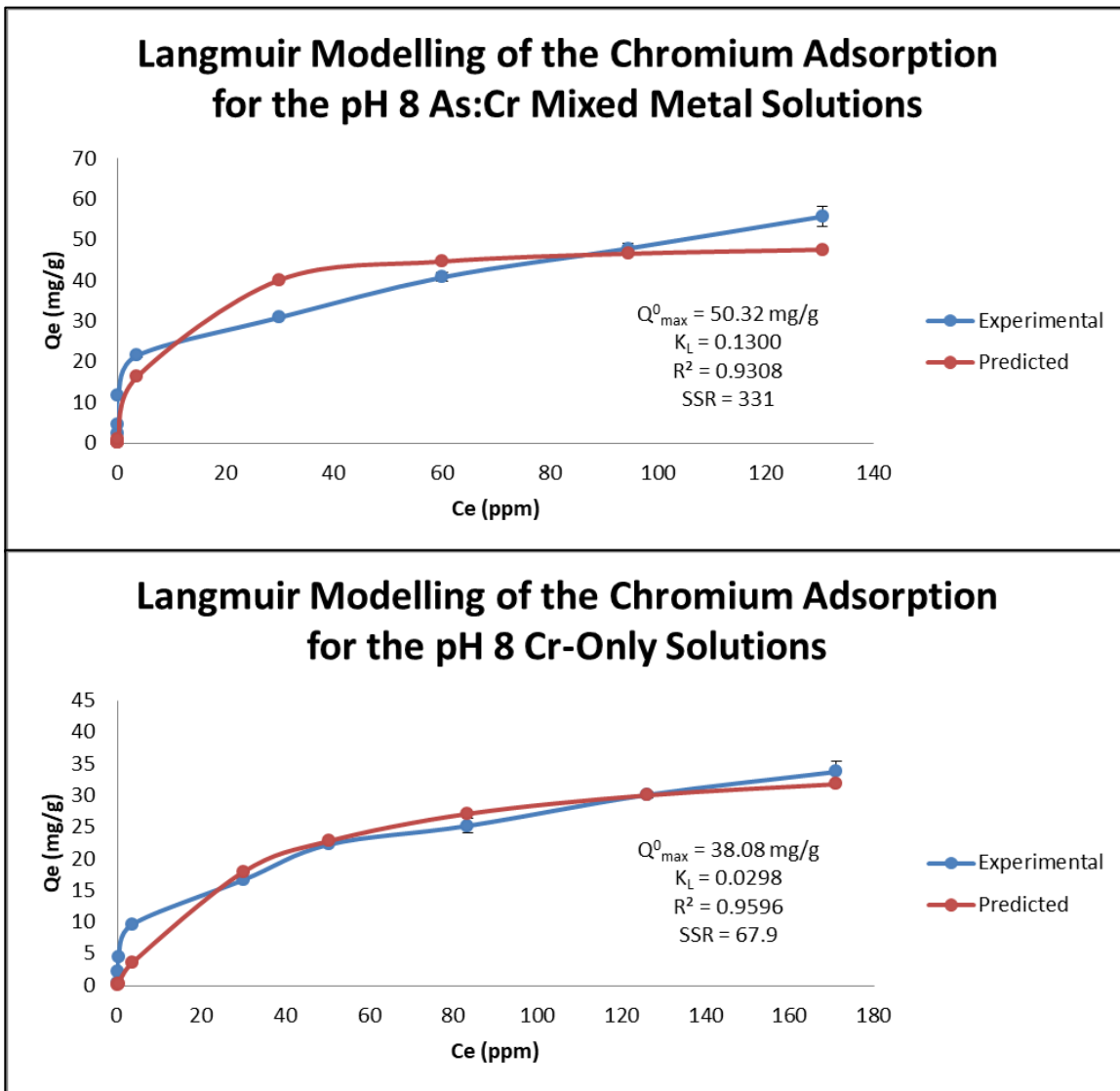


**Figure G1:** Langmuir isotherm modelling of the chromium adsorption for the pH 8 isotherm data.